Transport and mixing of passive scalars in geophysical flows

Bernard Legras

Laboratoire de Météorologie Dynamique
CNRS / Ecole Normale Supérieure, Paris

Introduction

Theories of the passive scalar transport

- Statistical theory
- Deterministic theory

Theories at work with real flows

Part I: Introduction

Why transport and mixing is important for the distribution of chemical and biological compounds in geophysical flows?

The 2D approximation and limits to its validity

Turbulence in 3D and 2D

Chlorophyll in the ocean

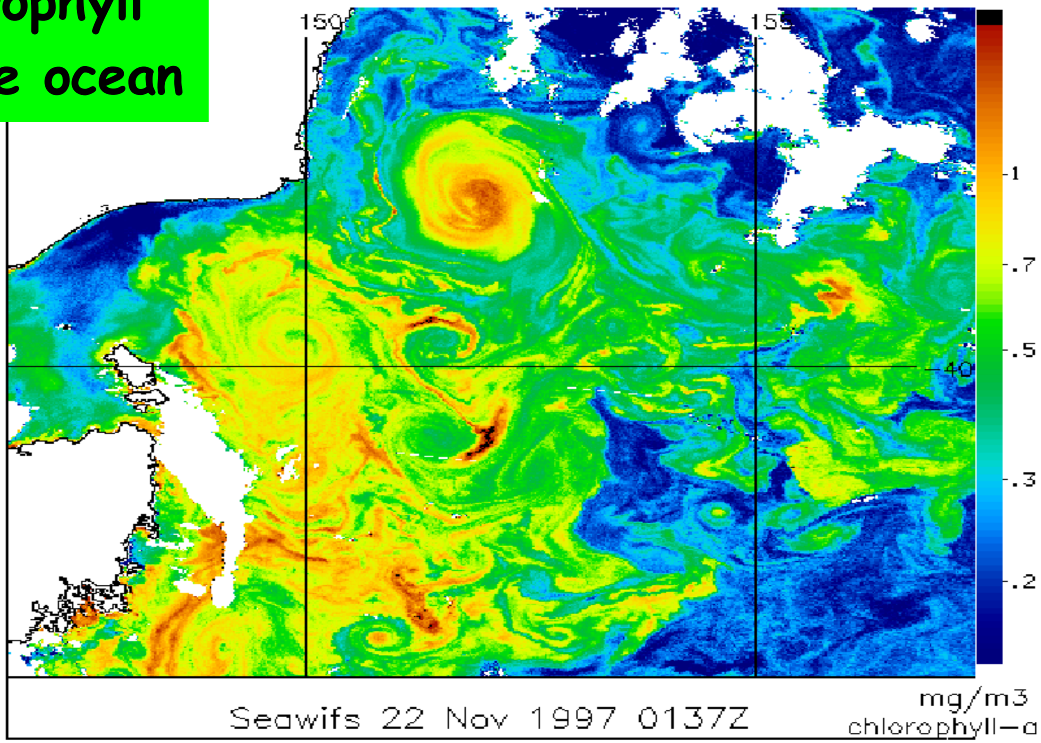

The atmosphere is filled with minor components (CO_2, ozone, H_2O, CO, CH_4, other greenhouse gases, N_2O, aerosols, ...), some of them controlling the climate, others like CO resulting from pollution.

The ocean carries nutrients on which depends the biologic production.

The distribution of long-live tracer depends to a large extend of transport and stirring by winds and oceanic currents.

Biological production in the ocean and chemical reactions in the atmosphere depend on mixing which is performed by the turbulent motion.

Huge Reynolds number $O(10^{10})$

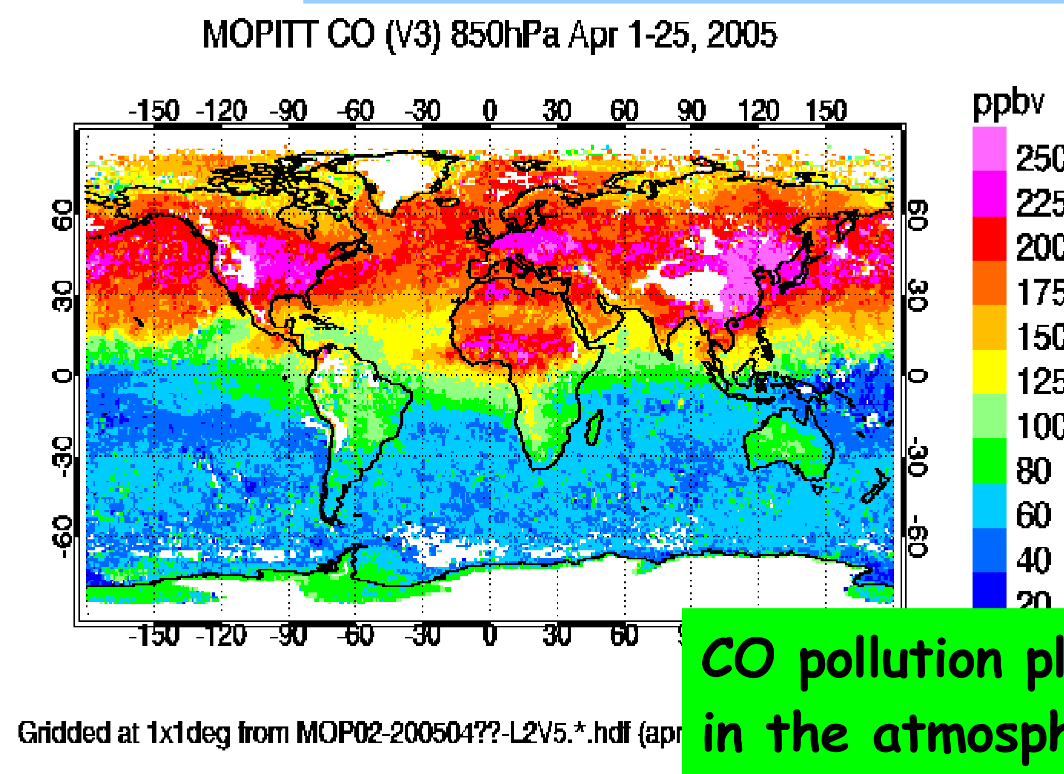

CO pollution plume in the atmosphere

Ozone is an essential UV filter for life on the surface of the Earth. 90% of ozone is in the stratosphere.

Under 25 km, in the stratosphere, life-time of ozone is of the order of several months, except in the winter polar vortex where it is depleted by anthropogenic chlorine.

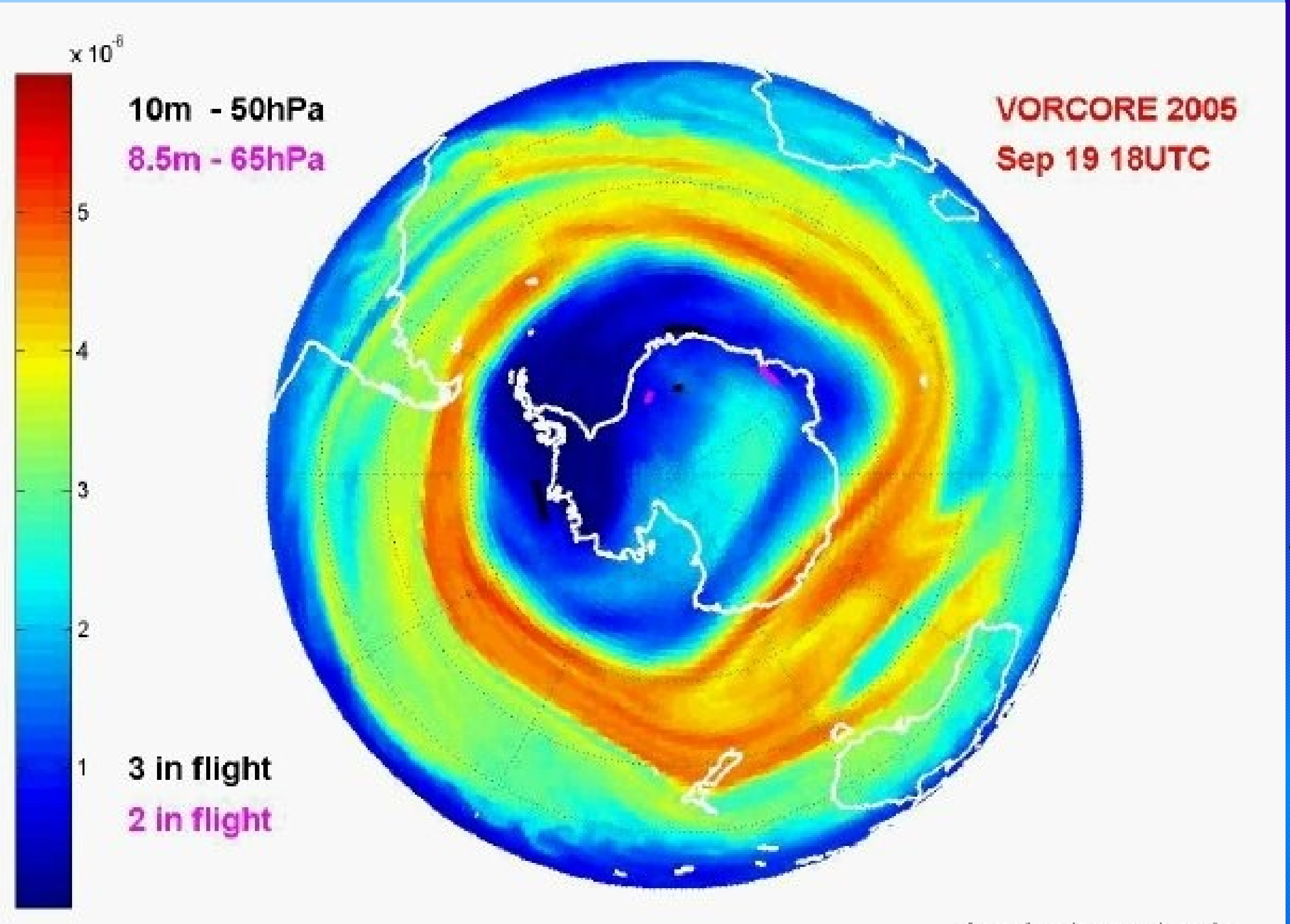

Courtesy of C. Basdevant

Even there, the distribution of ozone is largely determined by transport. The isolines of ozone tend to follow more or less closely the streaklines of the flow as made apparent by the movie featuring also real balloons from VORCORE experiment.

Large-scale motion (L>100 km in the atmosphere, L>10 km in the ocean) is dominated by layerwise quasi two-dimensional motion as a result of aspect-ratio, rotation and stratification

Numerically simulated two-dimensional turbulence

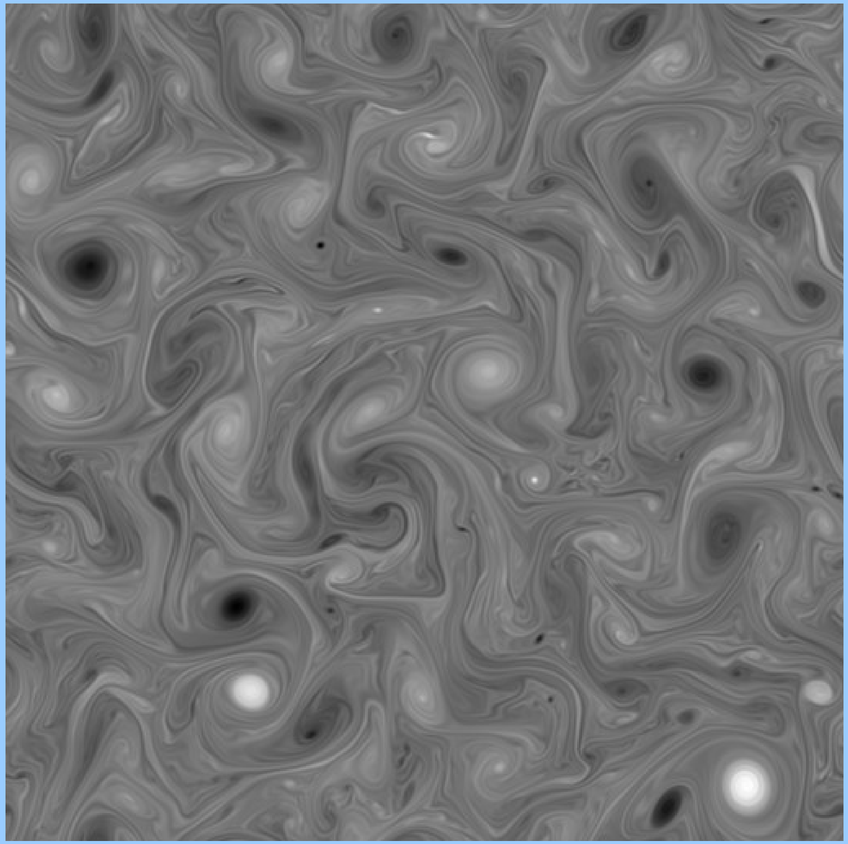

Chlorophyll in the ocean

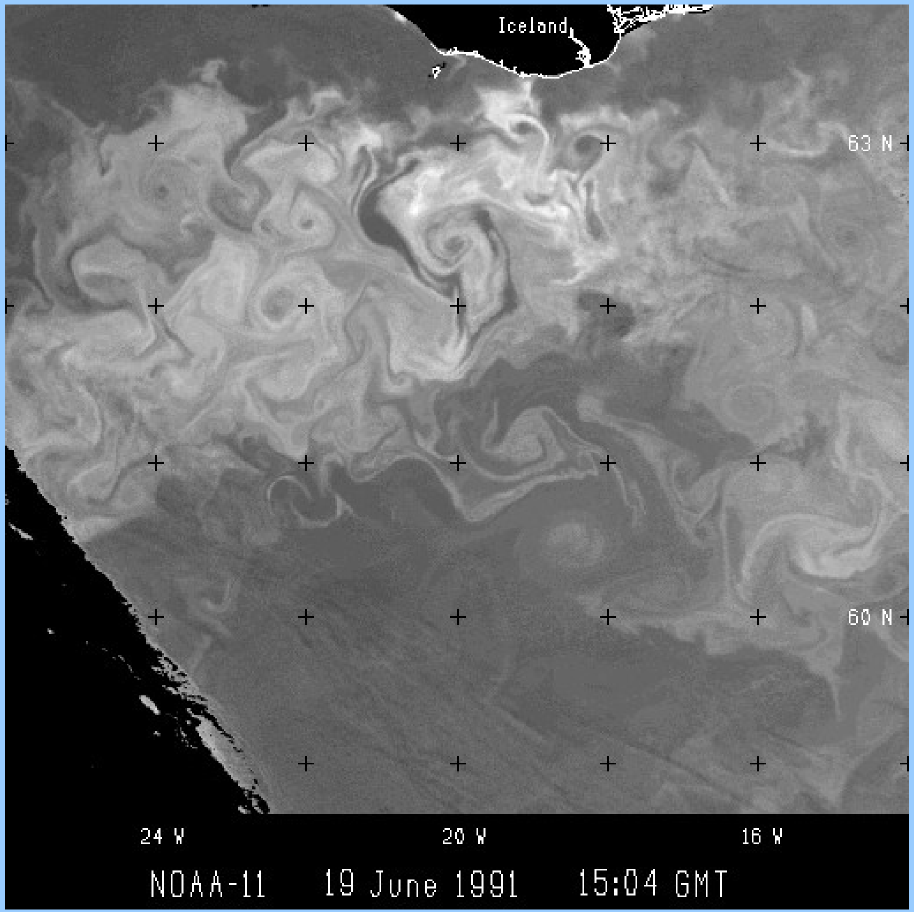

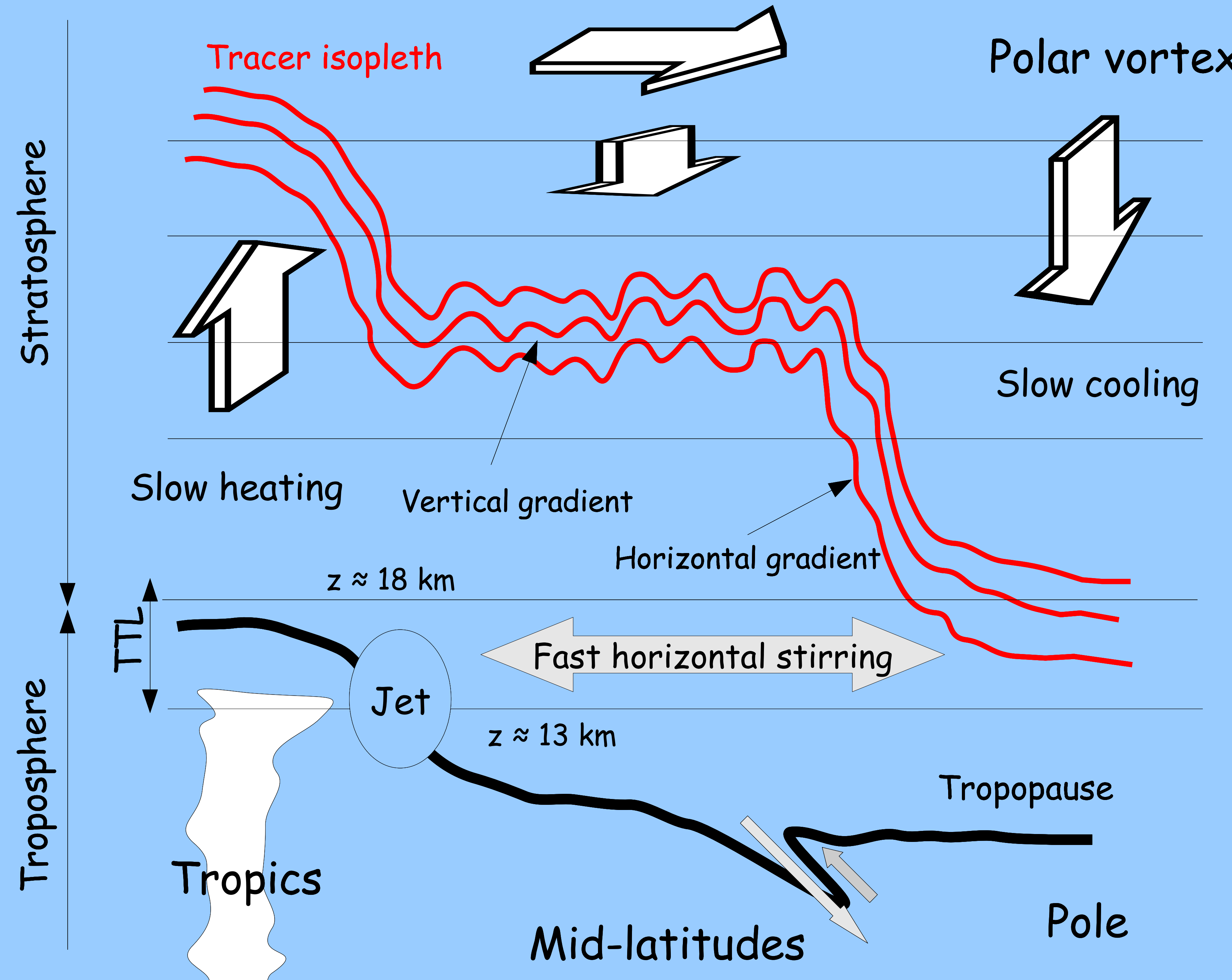

Motion in the stratosphere

Holton et al., Rev. Geophys., 33,403-440, 1995

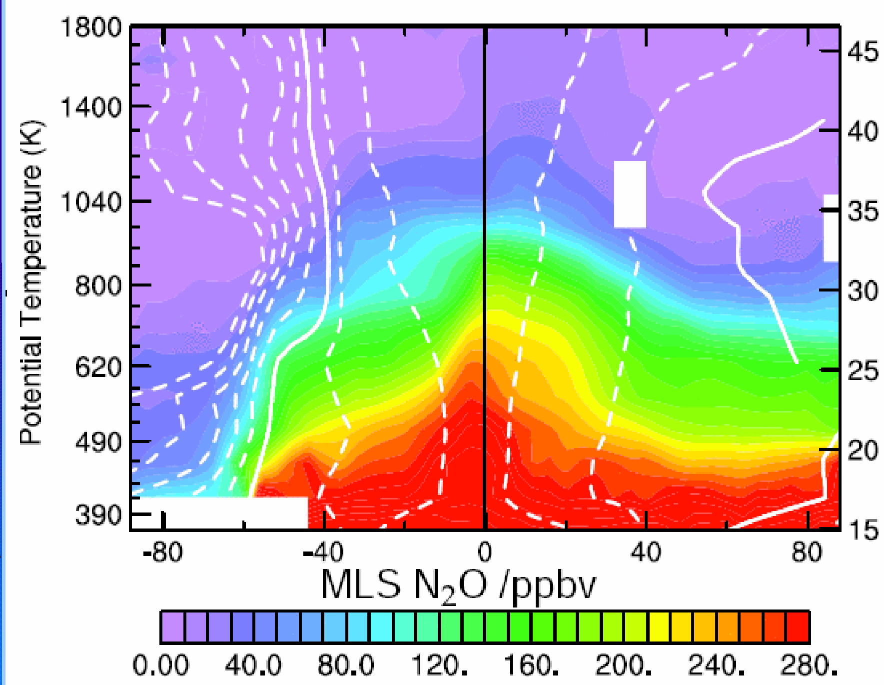

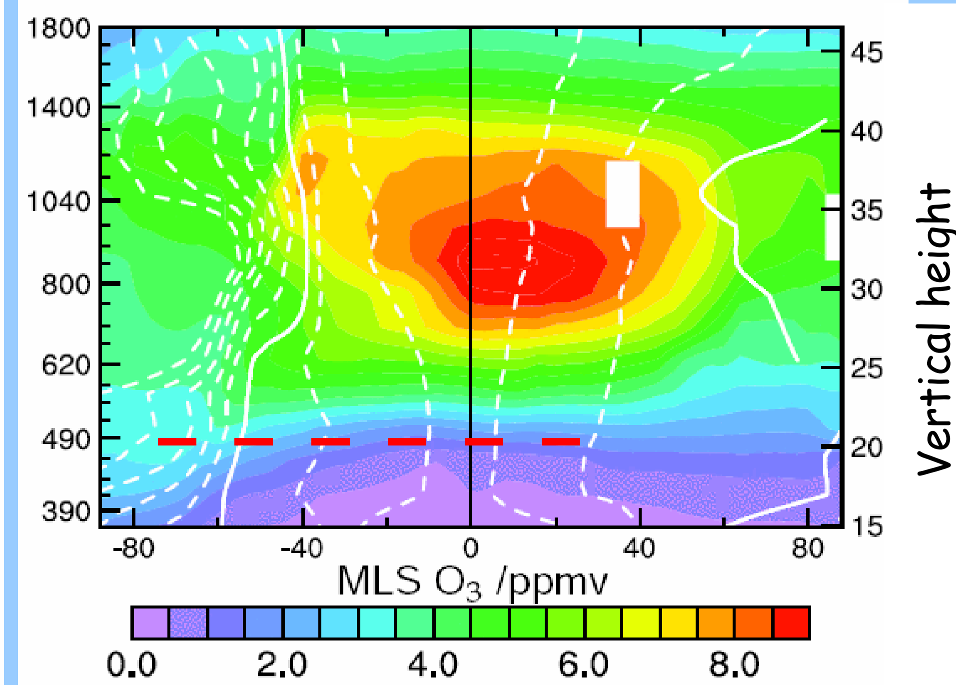

Gloria Manney, JPL, Caltech/NASA

Zonally averaged meridional sections of N_20 and O_3 from MLS-AURA.
3 August 2006

White contours: scaled PV

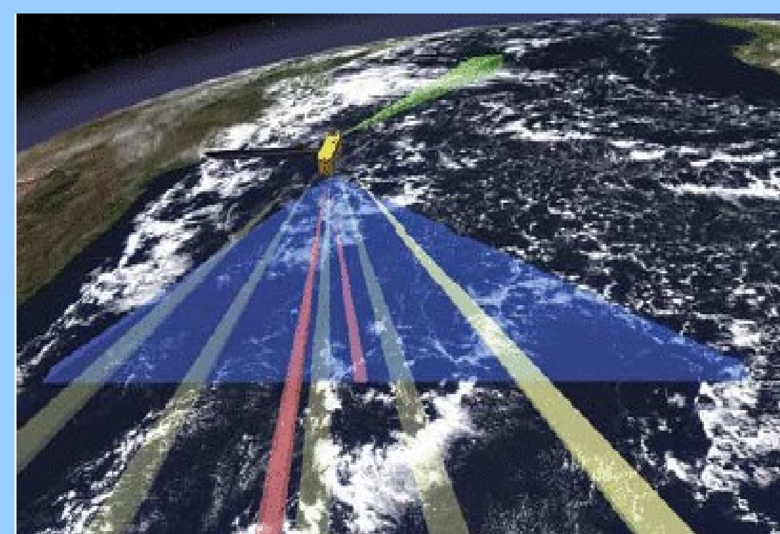

Artistic view of the MLS limb sounder in operation

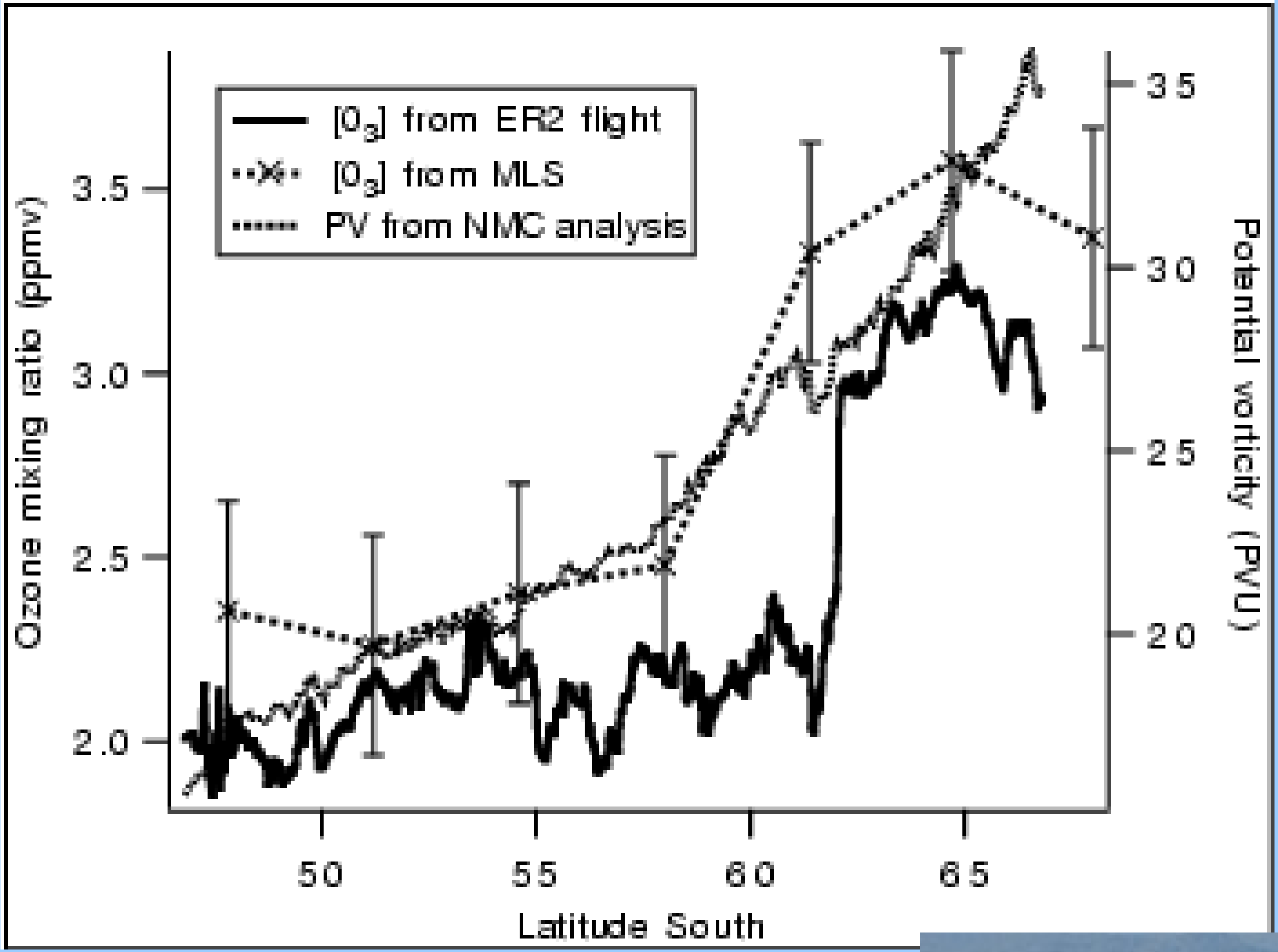

NASA ER-2 transect
across the edge of the
Antarctic polar vortex

sharp transition over a few km

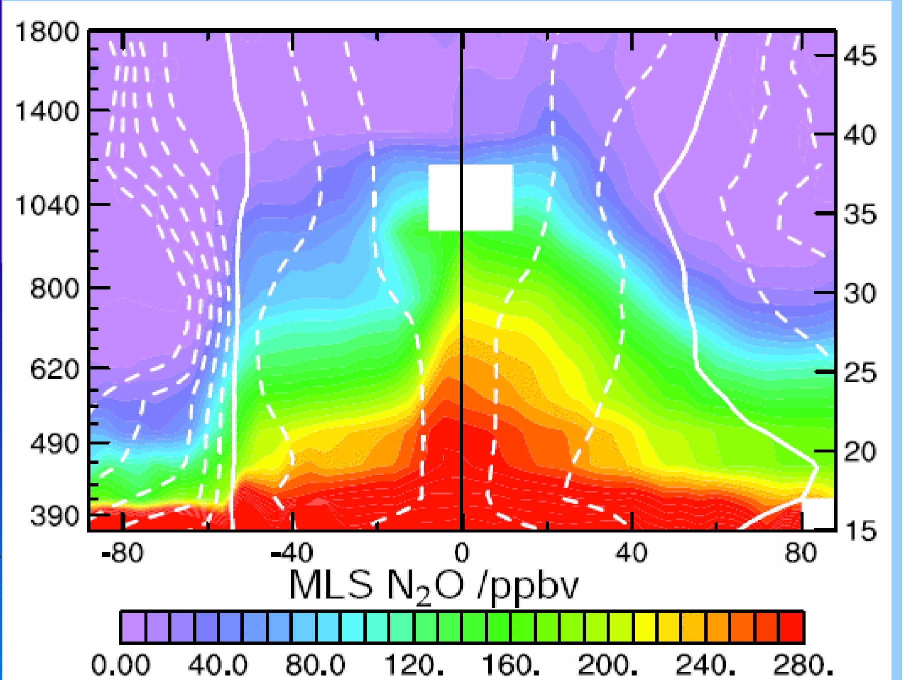

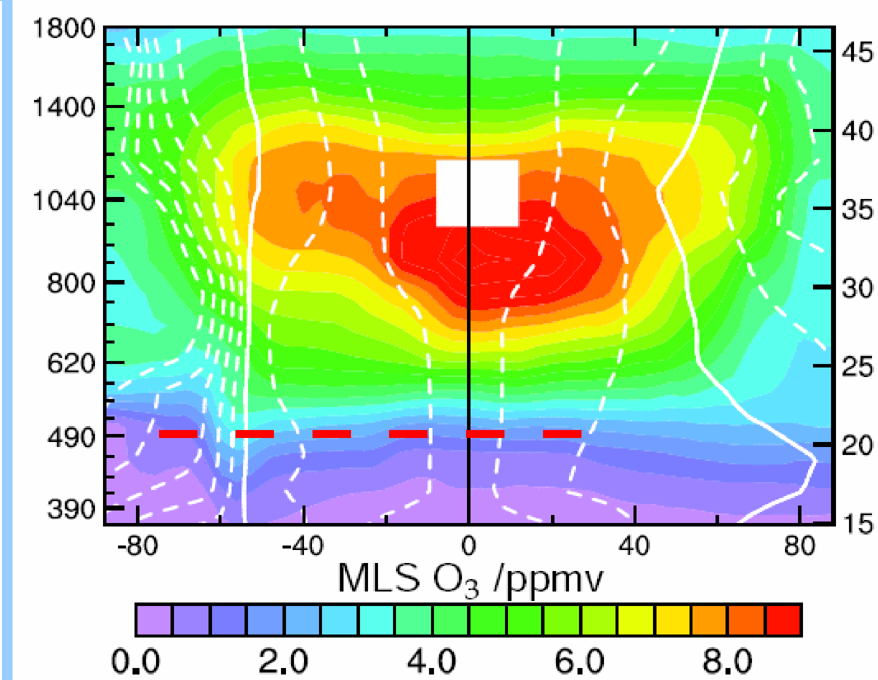

Vertical height

White contours: scaled PV

Black: temperature

MLS AURA

15 September 2006

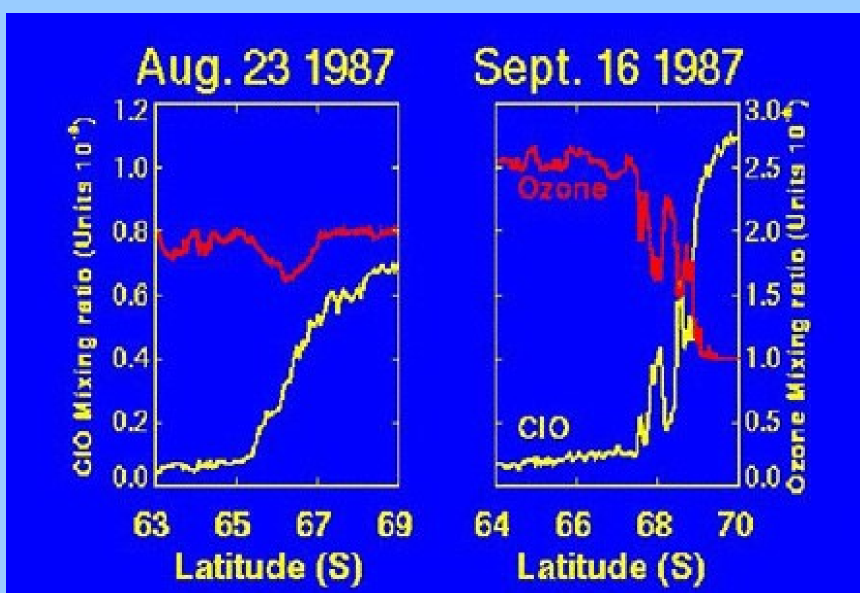

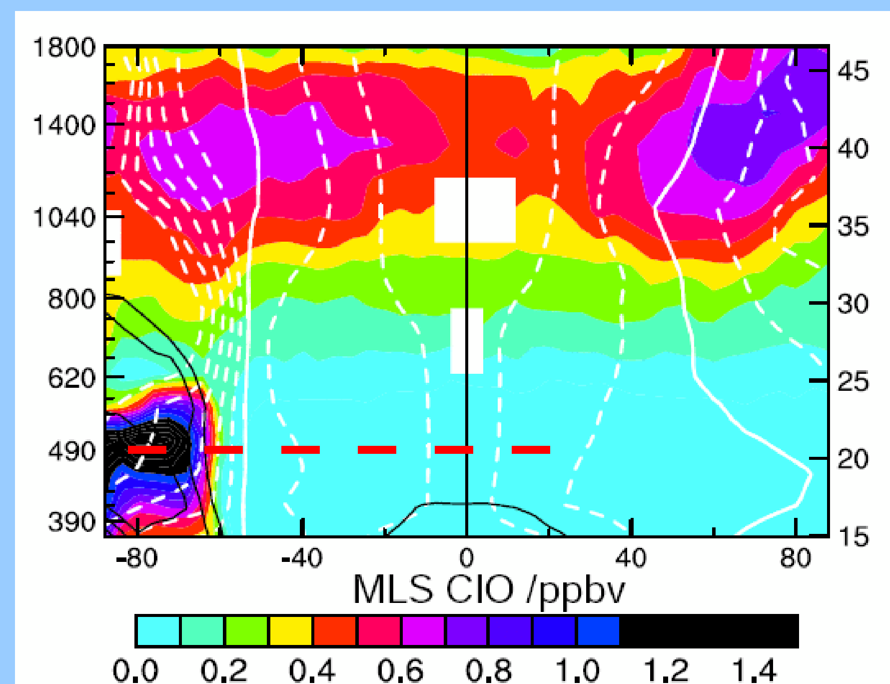

Gloria Manney, JPL, Caltech/NASA

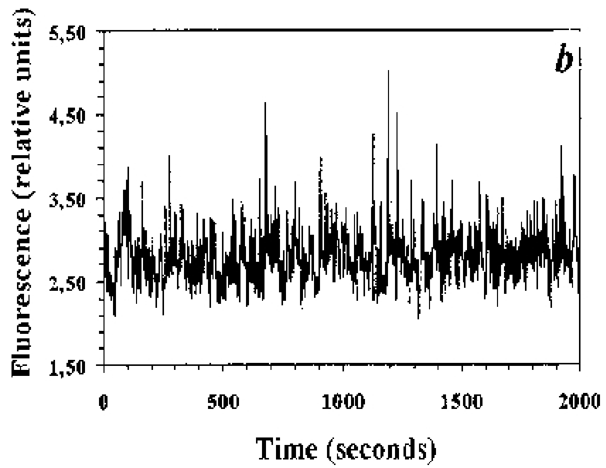

In vivo fluorescence at a fixed station in the English Channel.
Seuront et al., Nonlinear Proc. In Geophys. 3, 236 (1996).

In situ measurements exhibit a large amount of small-scale fluctuations, that are still poorly represented by models

N2O measured from aircraft in the stratosphere

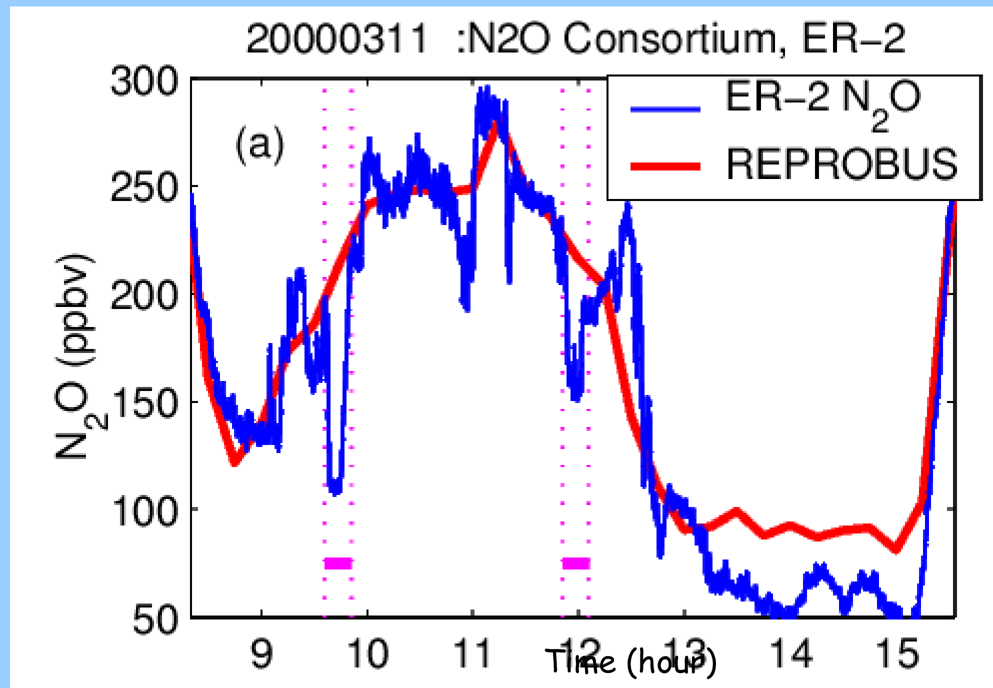

Hence, it is both interesting from the theoretical point of view and challenging from the practical point of view to understand the distribution of tracers in geophysical flows.

In summary,

2D approximation is relevant for geophysical flows because of aspect ratio, stratification and rotation.
Vertical velocities are small, motion is layerwise.

Large persistent tracer gradients are observed, indicating transport barriers.

Wide range of small-scale structures.

From thermodynamical point of view, outside active convective regions (<10% in the troposphere, none in the stratosphere), diabatic processes at any scale are slow with respect to dynamic processes
(in the stratosphere it takes 1 month to travel 1 km in the vertical)
Hence motion is mostly adiabatic on isentropic surfaces characterized by potential temperature $\Theta=T(p_0/p)^{R/C_p}$

Layerwise motion does not mean that the dynamics is strictly two-dimensional.
Actually, it is not: A multilayer framework (at least two layers) is necessary to provide the minimum description of atmospheric and oceanic dynamics driven by baroclinic instabilities in the mid and high-latitudes. In the tropical region, dynamics is driven by convection.

However, from the point of view of transported scalar, the two-dimensional approximation provides very useful insights and can even be used for real practice.
In the first approximation, one can consider the stratosphere and, to some extend the stratosphere, to be governed by layerwise quasi-2D isentropic motion.
In the second approximation, on must take into account both slow diabatic tendencies and fast mixing events due to convection, wind shear instabilities, and gravity-wave breaking.

The advecting winds span a much broader class than the solutions of the two-dimensional Navier-Stokes equation.

Ubiquity of quasi-horizontal layers in the troposphere

Reginald E. Newell*, Valerie Thouret*†, John Y. N. Cho*, Patrick Stoller*‡, Alain Marenco† & Herman G. Smit§

Nature, 25 March 1999

About 15% of the atmosphere is occupied by layers.

Mainly due to stratospheric intrusions

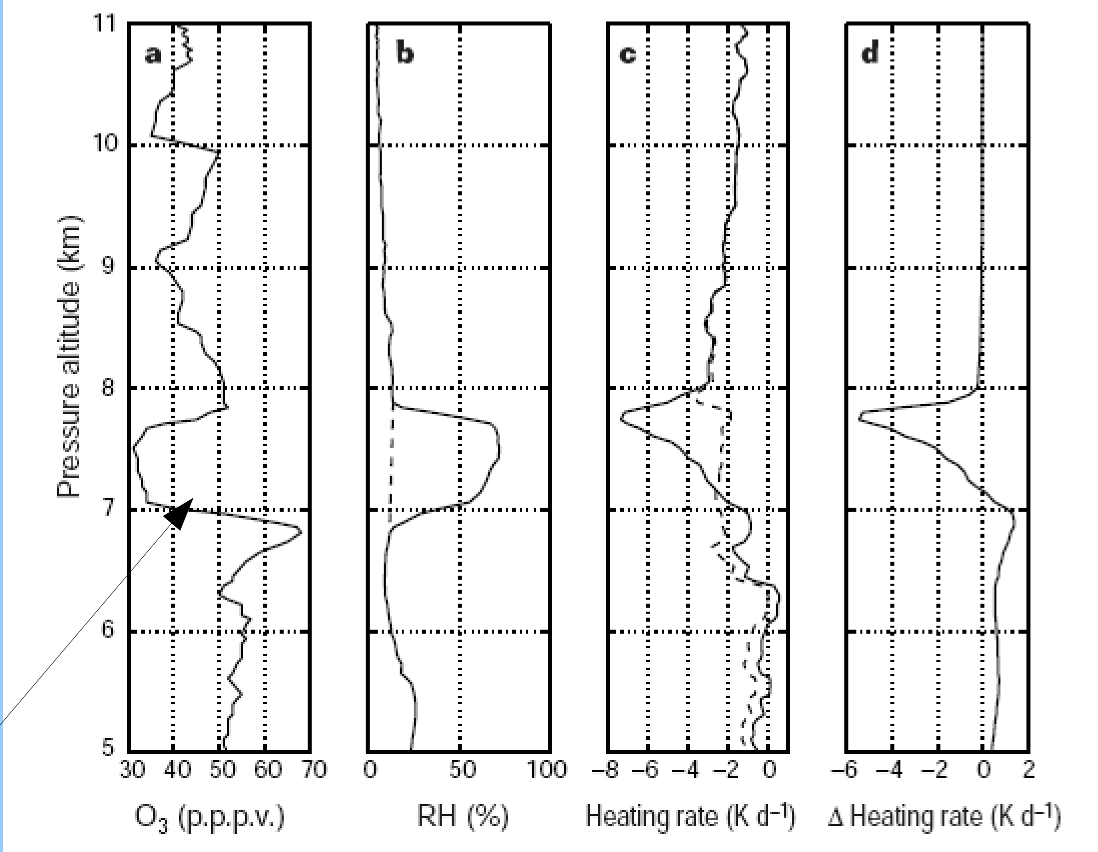

Ozone layer in the troposphere a few km under the tropopause

Example of layering in the free troposphere

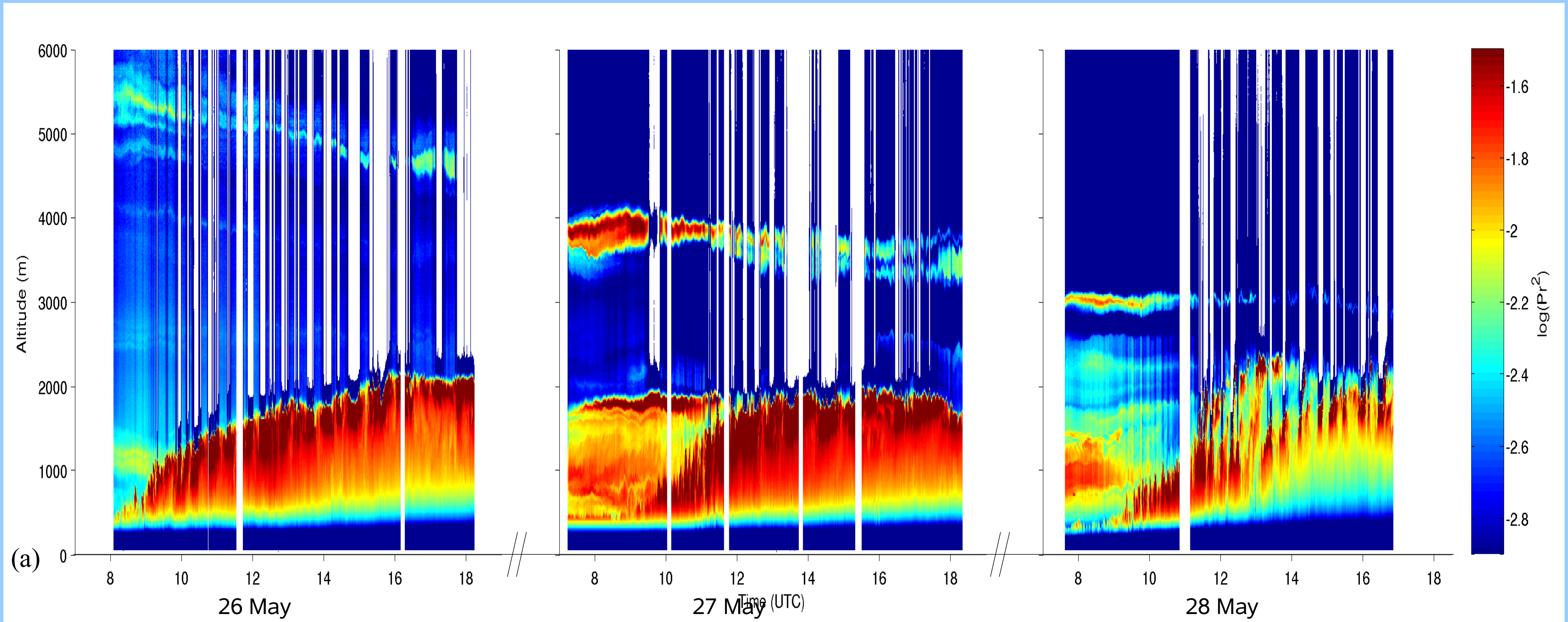

SIRTA aerosol lidar on 26-28 May 2003
Ecole Polytechnique / LMD

Turbulent stirring in 3D flows for large Reynolds with a large number of excited structures down to the Kolmogorov dissipative scale (of the order of 1mm in the atmosphere and ocean under standard conditions).

Ultimate mixing is performed by molecular forces under the Kolmogorov dissipative scale.
(let us assume as a simplification that diffusion = viscosity, e.g. Peclet=1)

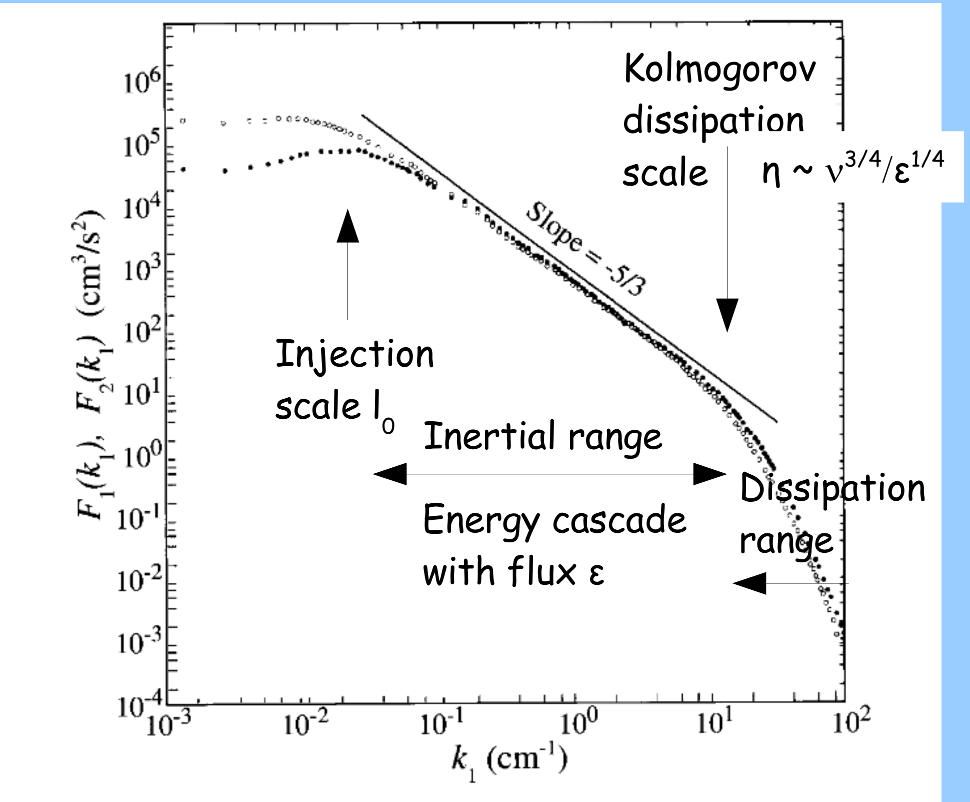

Fig. 5.7. log–log plot of the energy spectra of the streamwise component (white circles) and lateral component (black circles) of the velocity fluctuations in the time domain in a jet with $R_\lambda = 626$ (Champagne 1978).

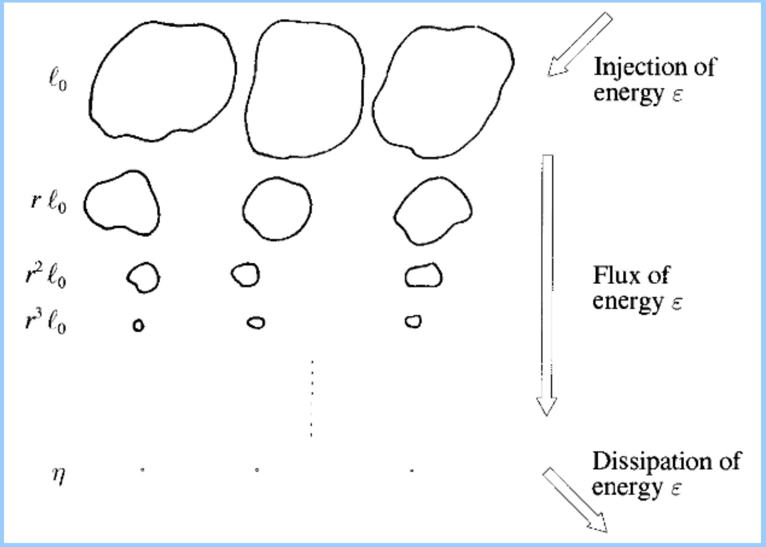

Integral scale provided by
$\int \langle v(0)v(r)\rangle dr = L \langle v^2\rangle$

3D TURBULENCE

Ref.: Frisch, Turbulence, CUP

Within the inertial range, the velocity fluctuations are non smooth.

The famous Kolmogorov law is
$\langle(\delta v(r))^3\rangle = -4/5\, \varepsilon r + O(\nu)$
Thus $\delta v(r) \sim r^{1/3}$

The velocity gradient is singular in the inviscid $\nu \to 0$ limit.

Intermittency of the velocity increment $\delta v(r)$: large fluctuations are, in proportion, more frequent as $r \to \eta$ (dissipation scale).

Non Gaussian distribution of the velocity increments.

In the dissipation range, $r < \eta$, the velocity is smooth.

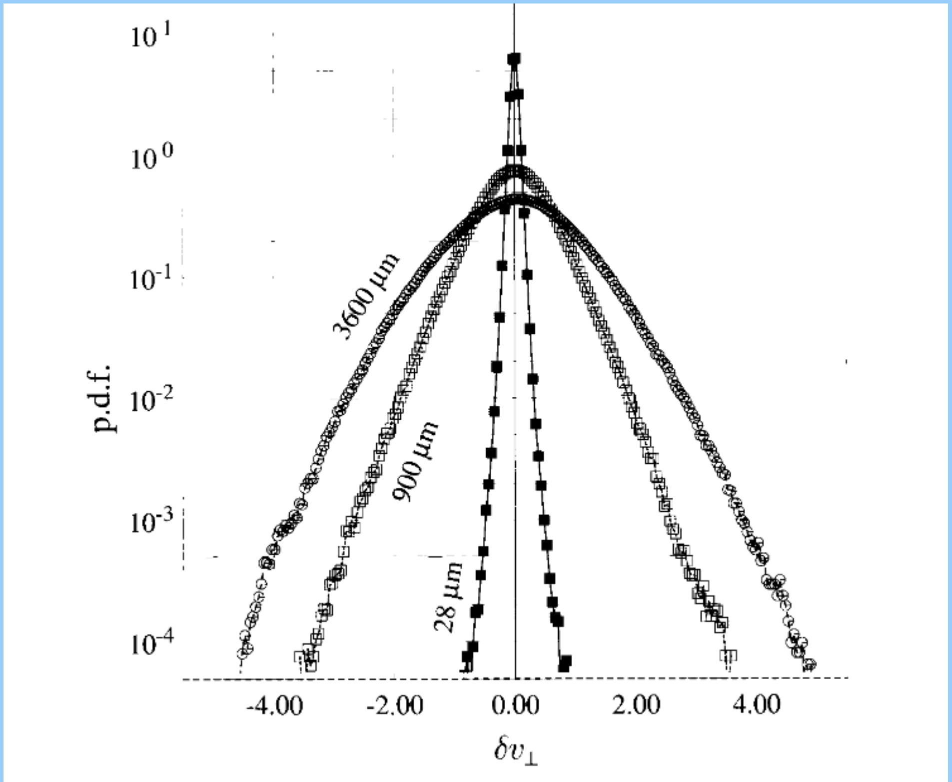

Fig. 8.23. Probability densities of transverse velocity increments obtained by the RELIEF flow tagging technique in a turbulent jet at $R_\lambda \approx 240$ for various separations ℓ, as labeled. The Kolmogorov dissipation scale is $\eta = 16\,\mu$m. The velocity increment scale is linear and in units of v_0, the r.m.s. transverse velocity fluctuation. Lower levels of p.d.f. (not shown) are too noisy to be significant (Noullez, Wallace, Lempert, Miles and Frisch 1996).

PDF of velocity increments at various separations within the inertial range

In 2D or quasi-2D flows, the vorticity or a generalization, the potential vorticity $P=((\mathrm{rot}(v)+2\Omega).\mathrm{grad}(\Theta))/\rho$ are Lagrangian invariant of motion.

Under the assumptions that stratification is large ($\partial\Theta/\partial z \gg \partial\Theta/\partial x, \partial\Theta/\partial y$) and/or Ω dominates the rotation, velocity gradient is bounded by initial conditions

-> motion is smooth at small scale $\delta v(r) \sim r$.

No intermittency

In 2D turbulence: two quadratic invariant of motion for the Euler equation, energy $\frac{1}{2}\int v^2\, dx\, dy$ and the enstrophy $\frac{1}{2}\int (\mathrm{rot}\ v)^2\, dx\, dy$, inducing two inertial ranges.

A direct (to small-scale) enstrophy cascade.

An inverse (to large-scale) energy cascade.

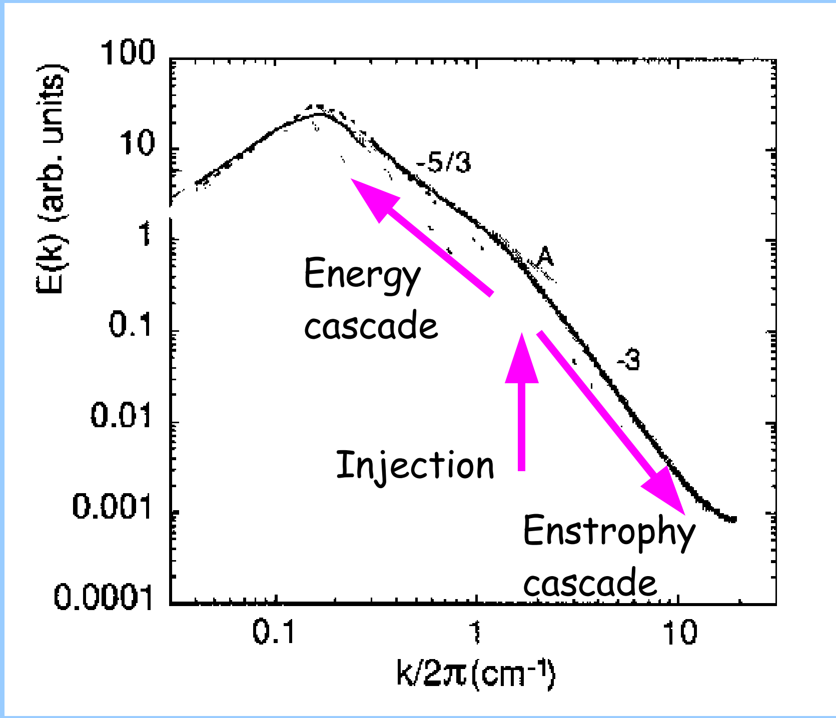

2D TURBULENCE

PDF of velocity increments in the inverse cascade

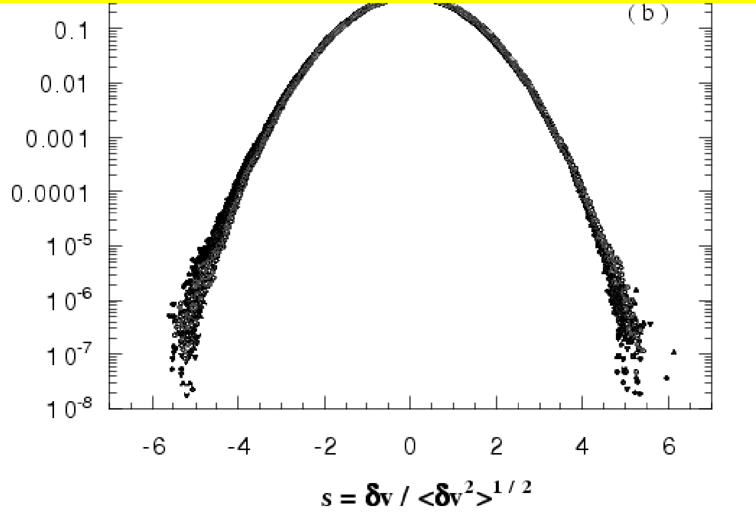

PDF of vorticity increments in the direct cascade

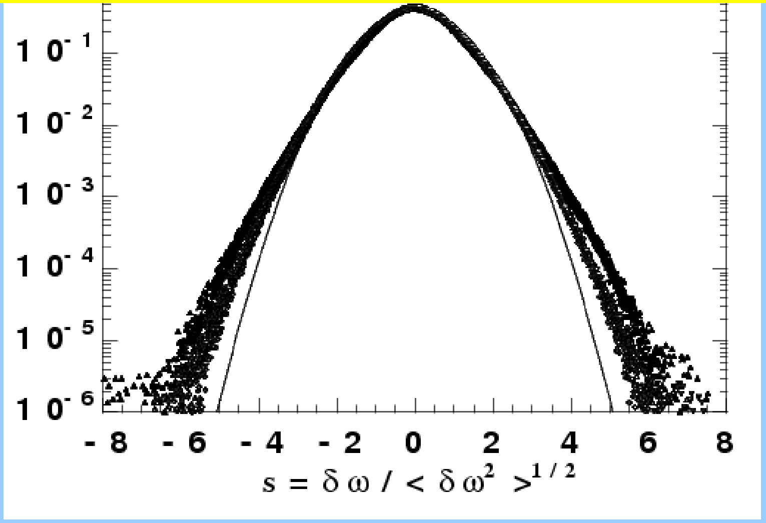

Velocity increments in the inverse cascade and vorticity increments in the direct cascade are essentially Gaussian.

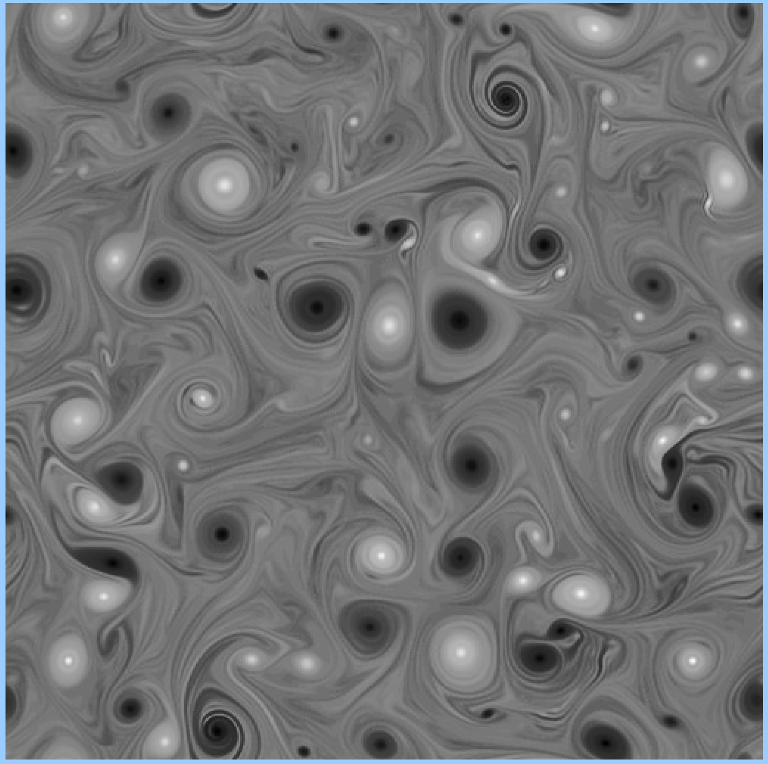

In forced dissipative 2D turbulence, coherent eddies are ubiquitous. They dominate the advection.

Chaotic stirring in layerwise (quasi-2D) flows is
- smooth $\delta U(r) \sim r$
- dominated by the large-scale advection

Ref on 2D turbulence: Tabeling

Part II: Theories of the passive scalar transport

- Mixing versus stirring

•II.A Spectral theory
- 1 Standard spectra of passive scalar
- 2 Verification of spectral theory in the lab
- 4 Observations apparently disagrees

II.B Large-scale limit
- 1 Random walk and diffusion
- 2 Taylor dispersion, diffusive limit

II.C Blob and wave-packet dynamics
- 1 Blob and wave-packet in fixed smooth flow
- 2 Selection of decaying modes
- 3 Lyapunov exponents
- 4 Stable and unstable Lyapunov eigenvectors
- 5 Lyapunov probability distribution
- 6 Wave packets under time varying smooth flow
- 7 Synthesis of blob evolution
- .8 Global modes
- 9 Prediction for the PDF of the tracer
- 10 Laboratory and atmospheric results
- 11 Variance spectrum

Stirring versus mixing

$$A+B \longrightarrow C$$

Reaction ⇐ reactants in the same fluid element (molecular diffusion and mixing) ⇐ spatial gradients, for example produced by stirring, will greatly favor this.

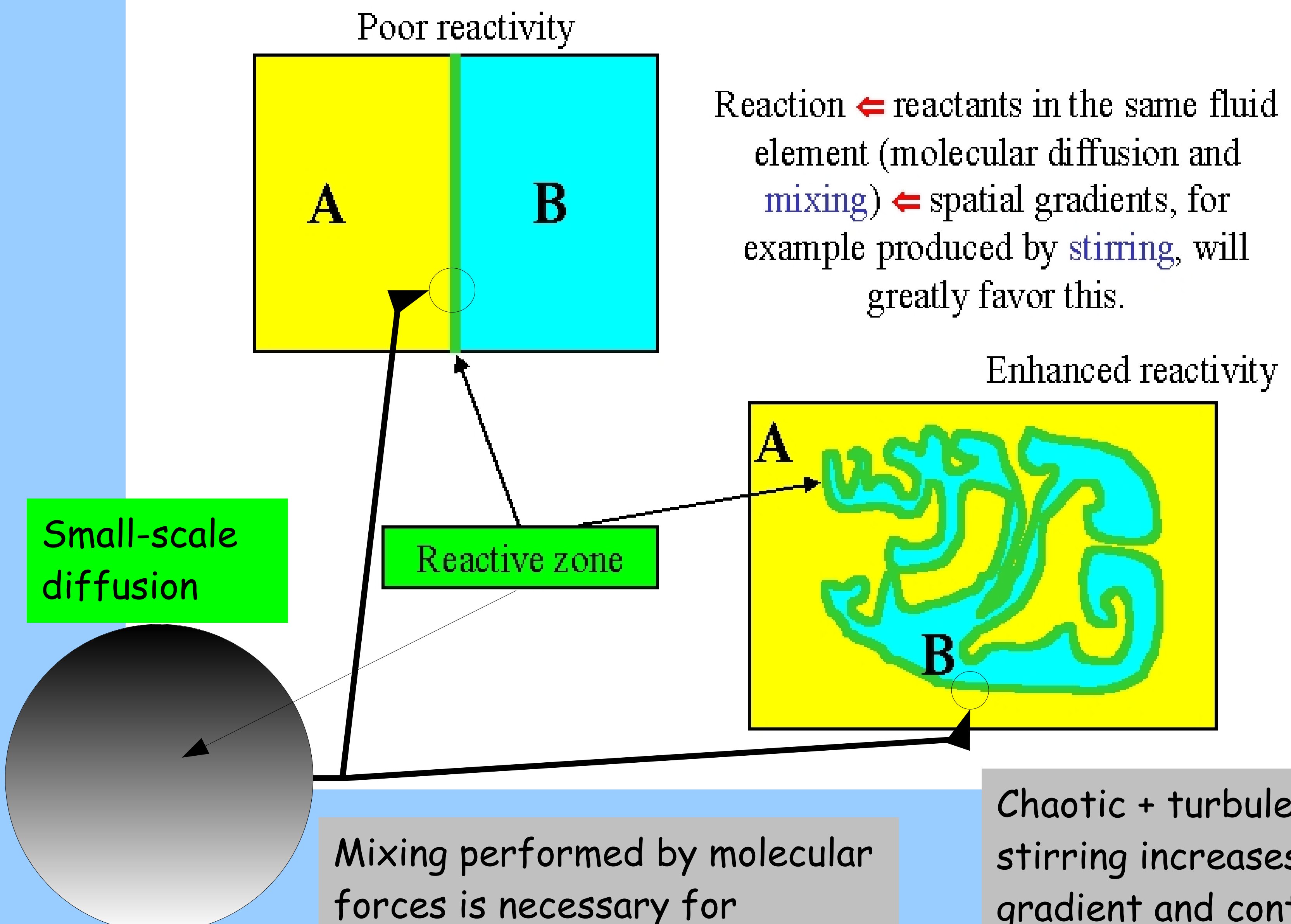

Mixing performed by molecular forces is necessary for chemical
reactions to occur

Chaotic + turbulent stirring increases gradient and contour length (or surfaces in 3D)

Batchelor and Obhukov-Corrsin passive scalar spectra

The spectral variance of the scalar is defined as

$$\theta(x,y)=\frac{1}{(2\pi)^2}\iint_{-\infty}^{\infty} dk\,dl\,\hat{\theta}(k,l)\,e^{i(kx+ly)}$$

and $C(K)=\dfrac{1}{(2\pi)^2\iint dx\,dy}\displaystyle\int_0^{2\pi} d\phi\left|\hat{\theta}(K,\phi)\right|^2$ where $(k,l)=K(\cos\phi,\sin\phi)$

If the velocity fluctuations at scale $r\sim 1/K$ are characterized by a time scale τ and if χ is the mean rate of the cascade (flux of variance across wavenumber par unit of time), then

$$C(K)\sim\chi\,\tau\,K^{-1}$$

If the flow is <u>smooth</u>, there is a unique time scale τ independent of K, hence $C(K)\sim K^{-1}$

If $\delta v(r)\sim r^h$ with $0<h<1$, then $\tau\sim\dfrac{r}{\delta v}\sim r^{1-h}\sim K^{h-1}$, that is $C(K)\sim K^{h-2}$

For $h=1/3$, corresponding to a $K^{-5/3}$ energy spectrum, $C(K)\sim K^{-5/3}$

A 2D laboratory experiment

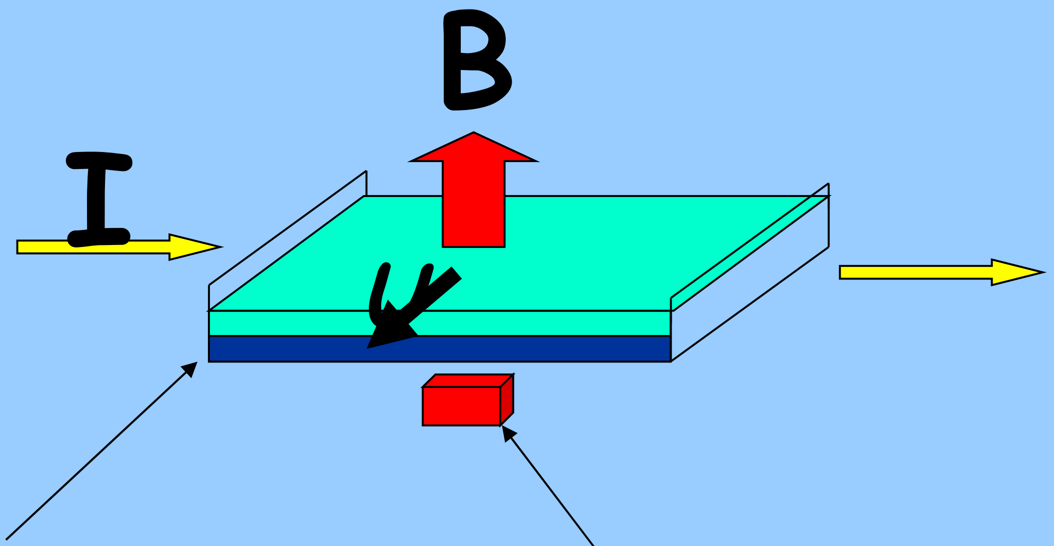

2 fluid layers, salt and
Clear water

Magnet

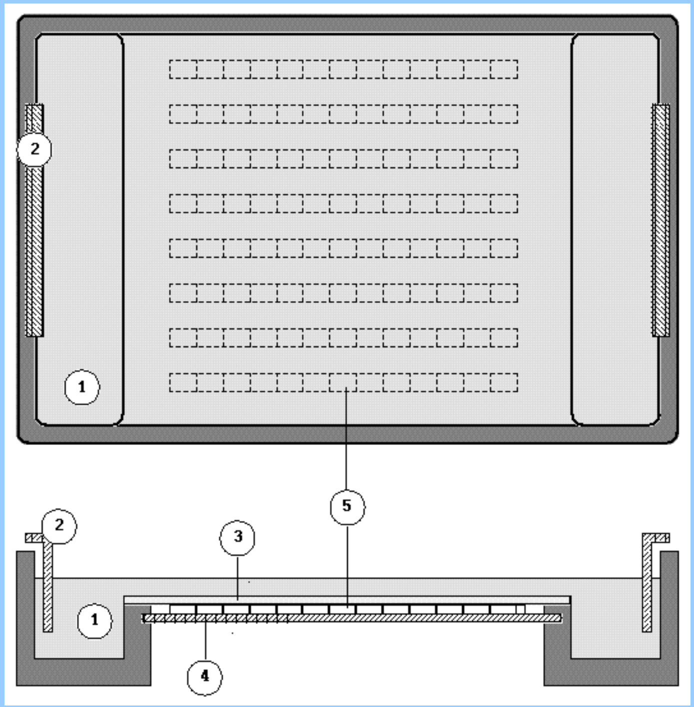

Tabeling, 2001, Experiments in a thin layer of electrolytic fluid

ref: Tabeling, Two-dimensional turbulence: a physicist approach, Physics Report, 362, pp. 1-62, 2002

CHARACTERISTICS OF THE VELOCITY FIELD (GIVING RISE TO BATCHELOR REGIME)

Energy Spectrum

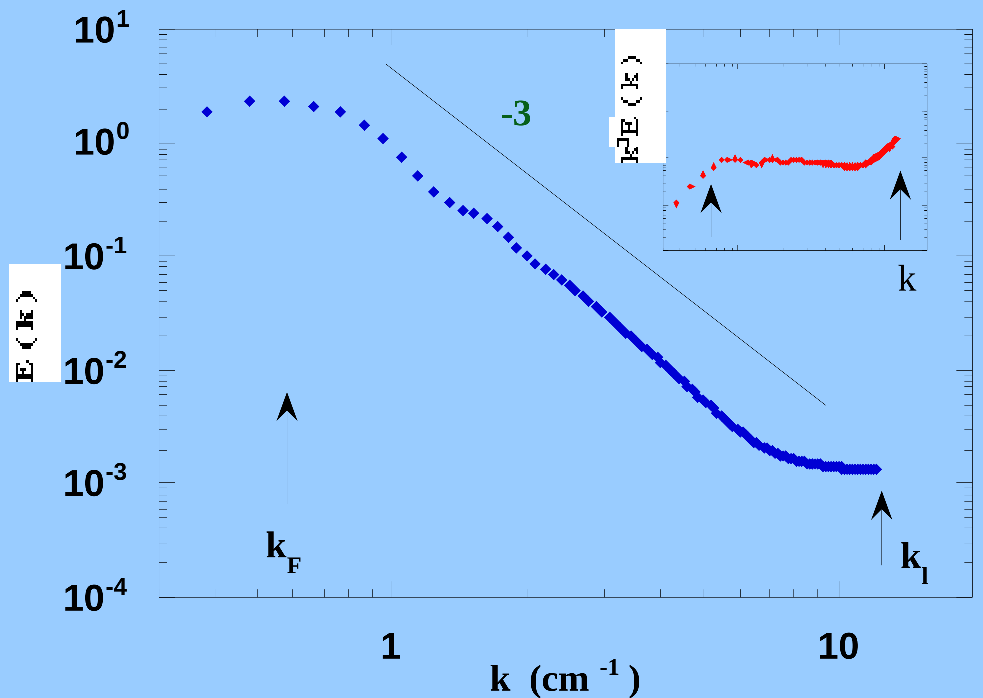

2D Energy spectrum

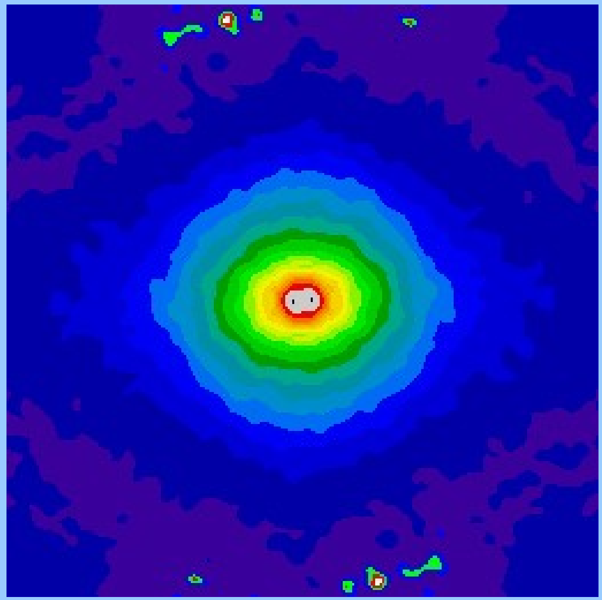

Tabeling, 2001

SPECTRUM OF THE CONCENTRATION FIELD

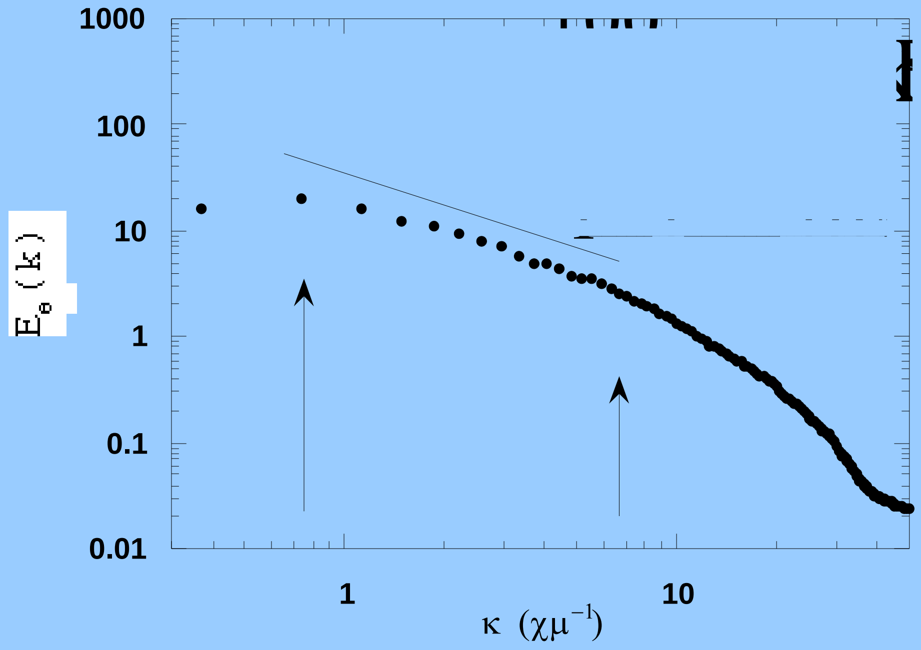

2D Spectrum

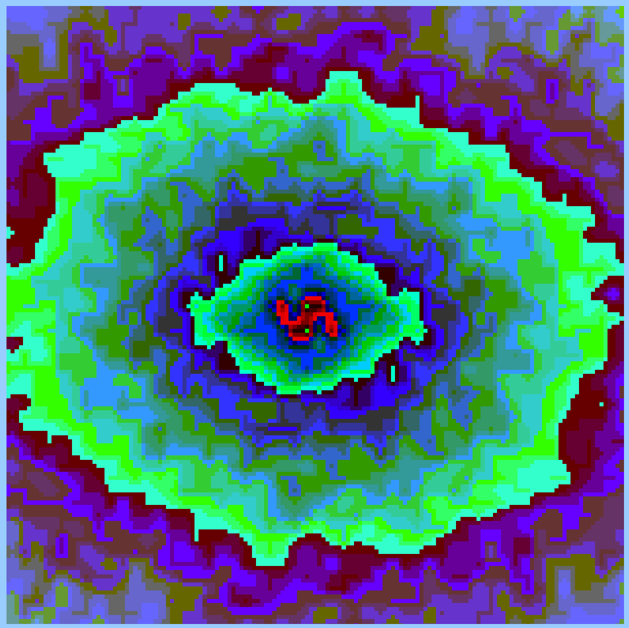

Tabeling, 2001

Evolution of a drop in the Batchelor regime

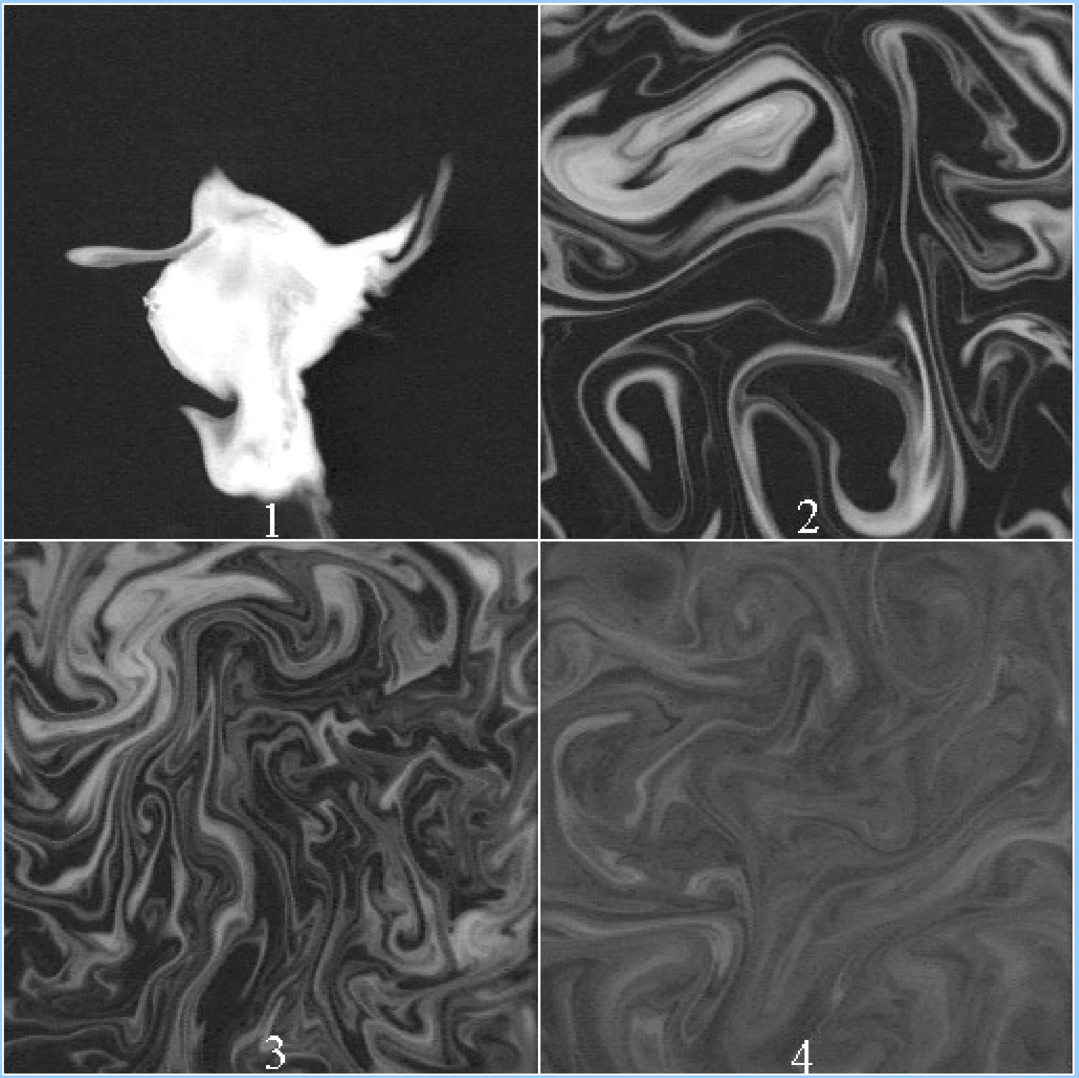

Energy spectrum for the inverse cascade

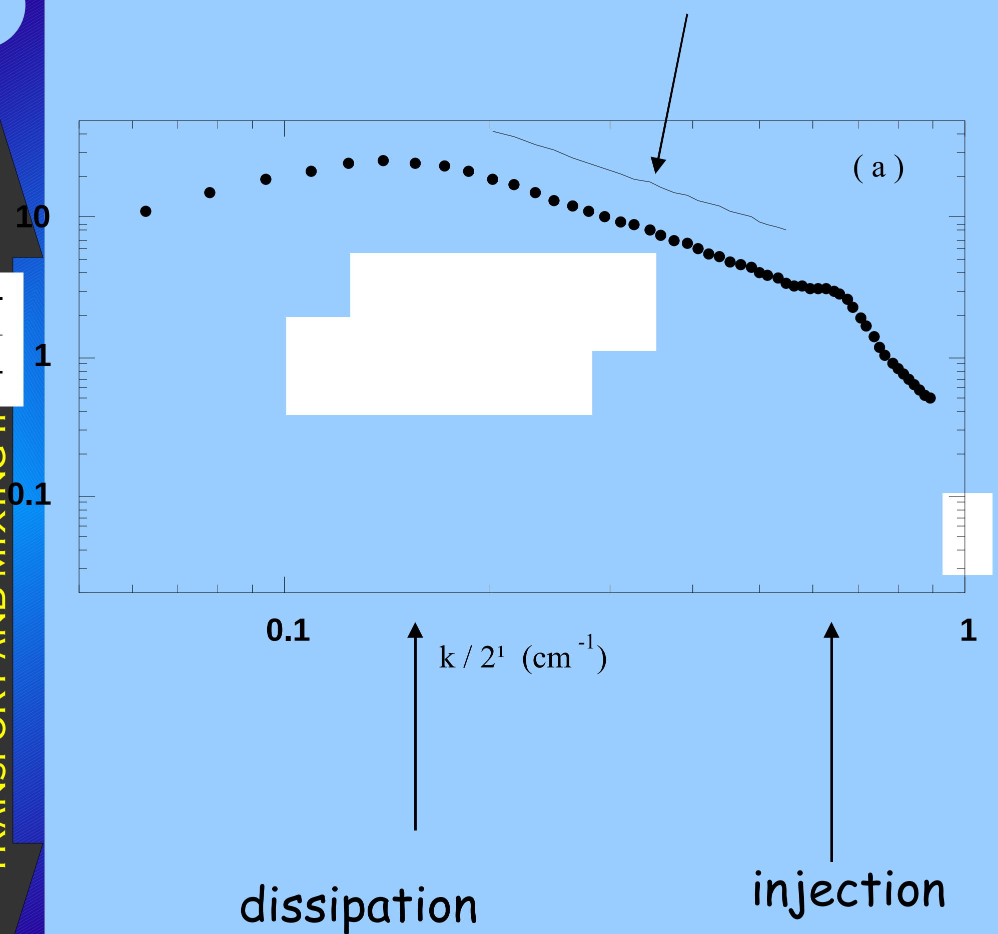

2D spectrum

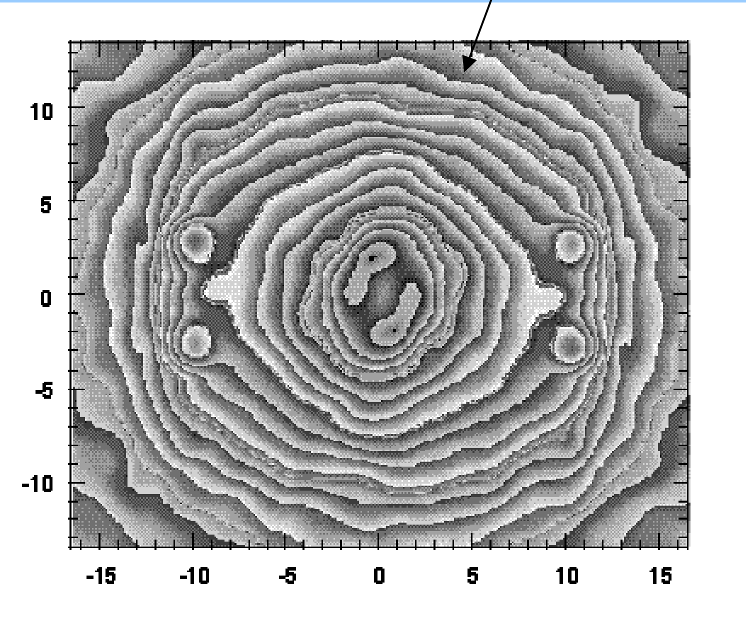

Snapshot of the flow

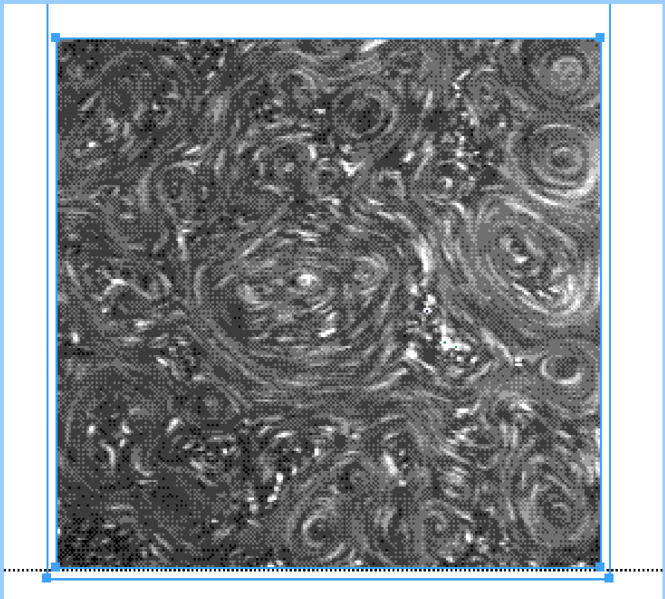

Spectrum of the concentration field

Spectrum

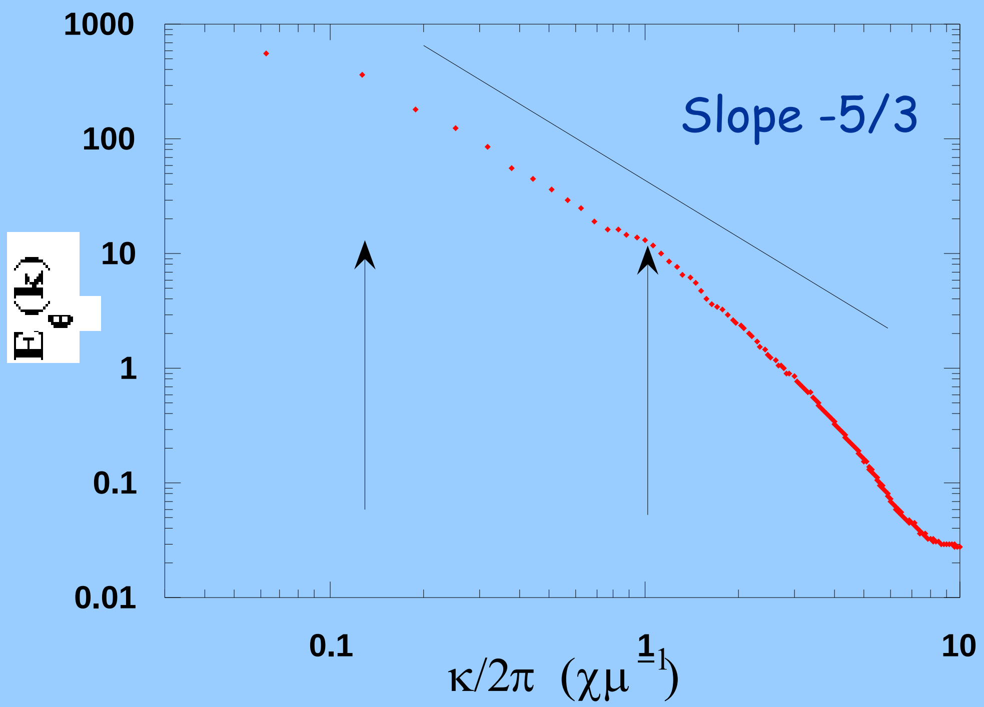

2D Spectrum

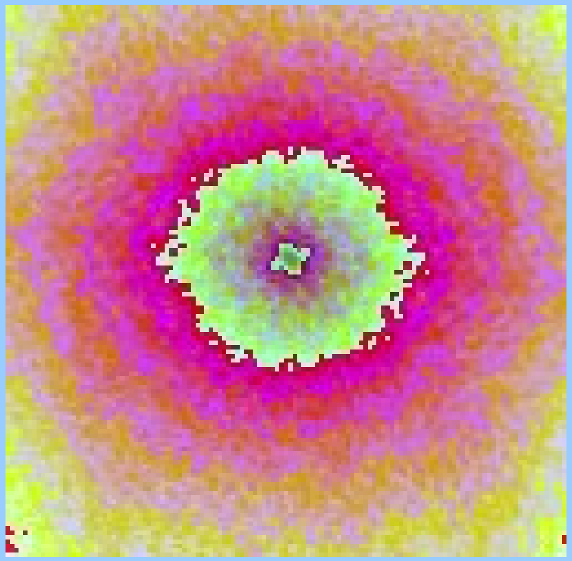

Evolution of a drop released in the inverse cascade

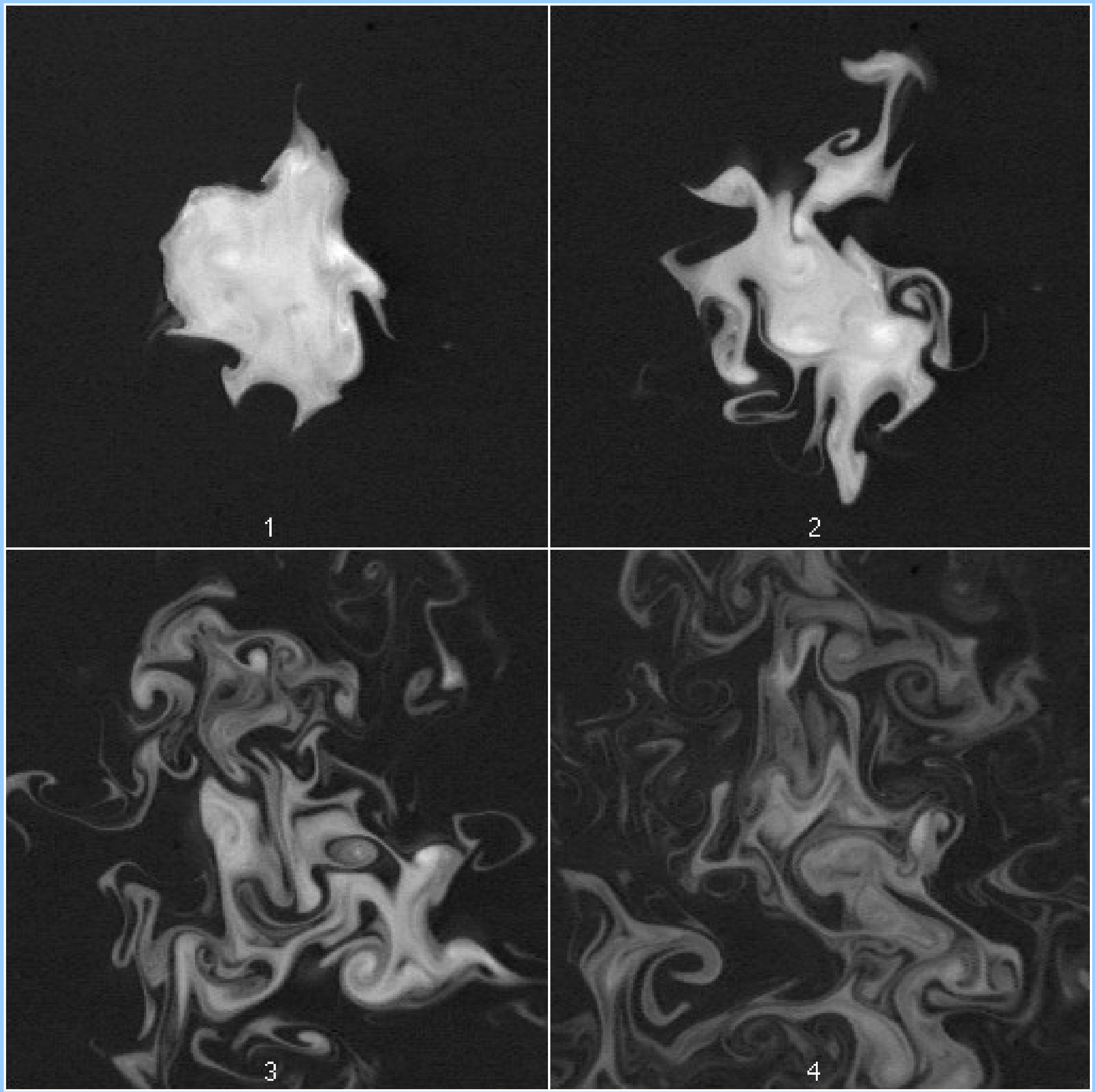

What about the atmosphere?

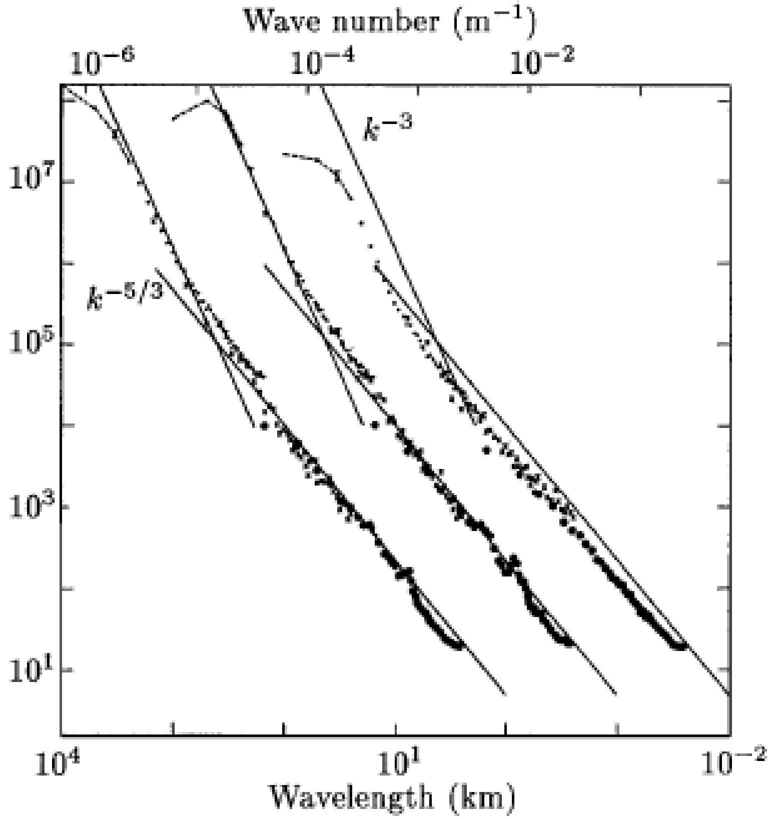

FIG. 1. From left to right: variance power spectra of zonal wind, meridional wind ($m^3\ s^{-2}$), and potential temperature (K^2 m) near the tropopause from Global Atmospheric Sampling Program aircraft data. The spectra for meridional wind and temperature are shifted one and two decades to the right, respectively. Reproduced from [7].

Nastrom & Gage, J. Atmos. Sci., 1985

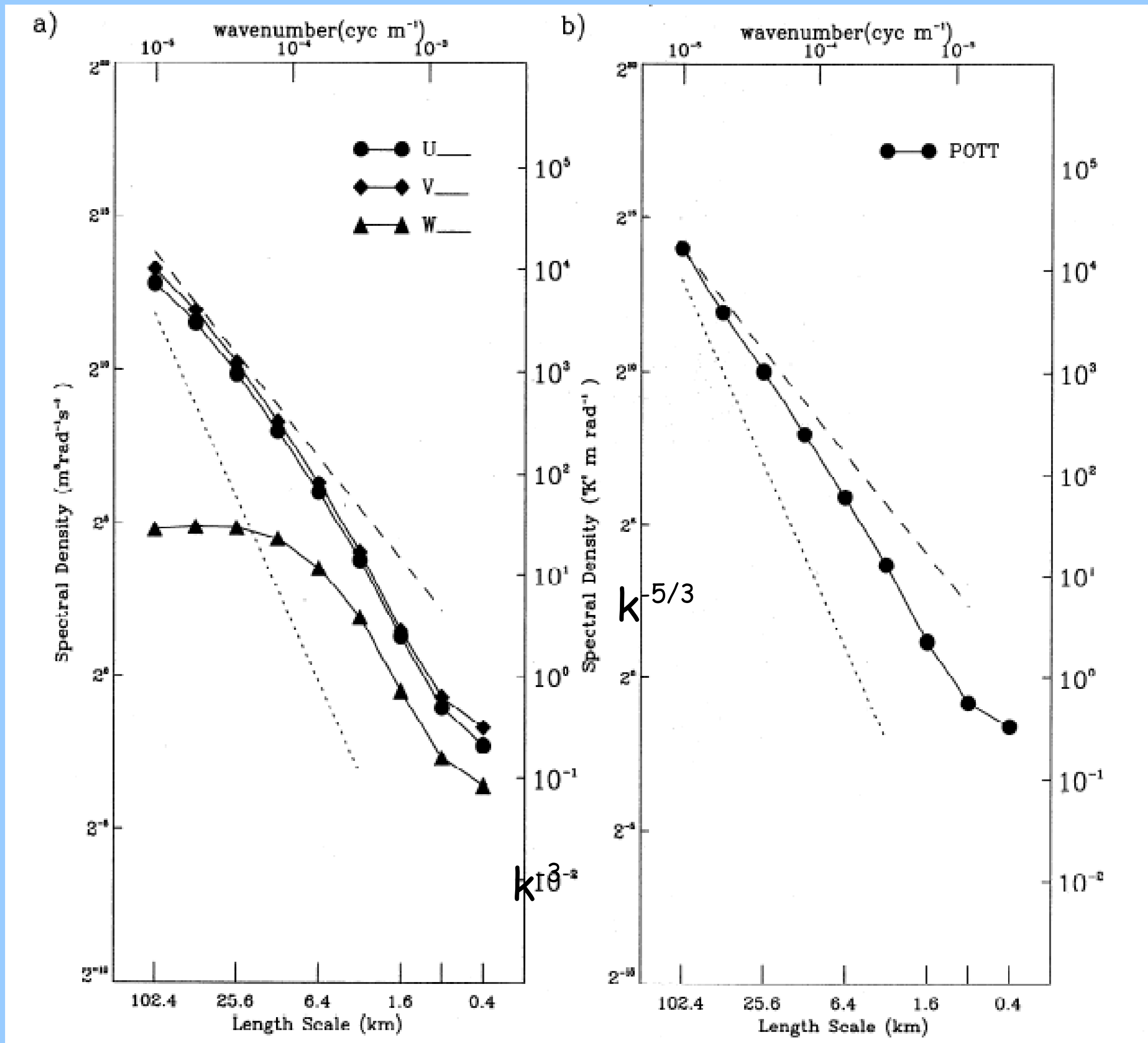

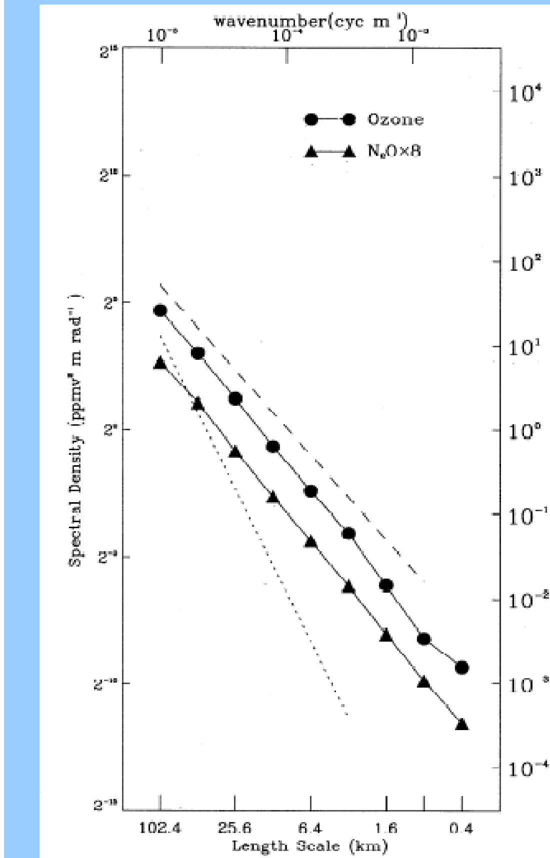

Bacmeister et al., J. Geophys. Res., 1996

Both velocities and temperature tend to show a $k^{-2.5}$ behaviour for the variance spectrum at scales smaller than about 25 km and $k^{-5/3}$ between 200 km and 25 km. Tracers show $k^{-5/3}$ slope down to small scales.

So what?

- Theory works well in the lab but less easily in the atmosphere
- Not easy to estimate isentropic spectra from airborne measurements

corrected structure function

uncorrected structure function

variance spectrum in $k^{-\beta}$

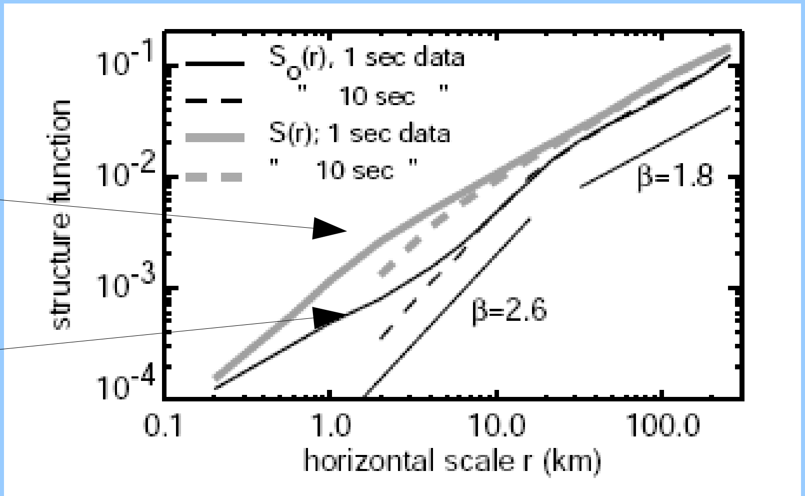

- The existence of direct and inverse 2D cascades is uncertain in the atmosphere.
- **Gravity waves** can generate a downscale energy cacascade (Dewan, J. Geophys. Res. 1997)
- Discrete jumps in the tracer field, due to barrier effects, generate $\sim k^{-2}$ contributions to the variance spectrum.
- Variance spectrum depends on the spatial distribution of stretching and dissipation.
- Let us try to understand better

Random walk and diffusion

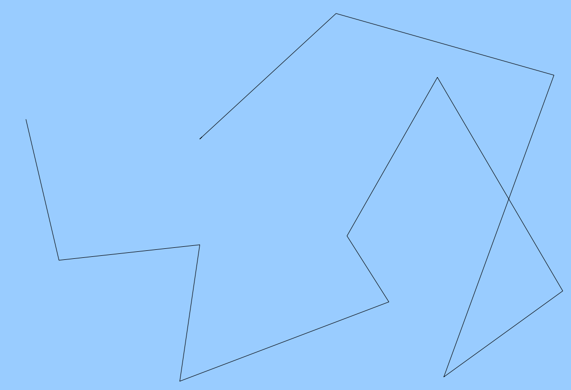

White noise, zero mean, variance σ

$$\langle \boldsymbol{w_i} \boldsymbol{w_j} \rangle = \sigma_w^2 \delta_{ij}$$

Displacement over N steps, or time $T = N \delta t$

$$\boldsymbol{X} = \sum_{i=1}^{N} \delta \boldsymbol{x_i} = \left(\sum_{i=1}^{N} \boldsymbol{w_i} \right) \delta t$$

By central limit theorem, $\boldsymbol{X}$ is a Gaussian random process with zero mean and variance

$$\langle \boldsymbol{X}^2 \rangle = N^2 \sigma_w^2 \delta t^2 = (\sigma_w^2 \delta t) T$$

Hence, the p.d.f. $P_{\boldsymbol{X}}(\boldsymbol{x}, t)$ satisfies

$$\frac{\partial P}{\partial t} = \kappa \Delta P_{\boldsymbol{X}}(x, t) \quad \text{with} \quad P_{\boldsymbol{X}}(\boldsymbol{x}, 0) = \delta(x),$$

which has solution $P_{\boldsymbol{X}}(x, t) = \dfrac{1}{(2 \kappa t)^{d/2}} \exp\left(\dfrac{-x^2}{4 \kappa t} \right)$

provided $\kappa = \dfrac{1}{2} \sigma_w^2 \delta t$

If δt is not constant but jumps are of duration τ_i, the random process is over $\delta \boldsymbol{x}$

with variance σ_x. A necessary condition is than $\langle \tau \rangle$ is finite for which $\kappa = \dfrac{\sigma_x^2}{2 \langle \tau \rangle}$

By adding advection by $\boldsymbol{U}$ we obtain the Fokker-Planck equation

$$\frac{\partial}{\partial t} P_{\boldsymbol{X}} = \boldsymbol{U} . \nabla P_{\boldsymbol{X}} = \kappa \Delta P_{\boldsymbol{X}}$$

which is also the advection-diffusion equation for the passsive tracer

Diffusive regime in transport (Taylor)

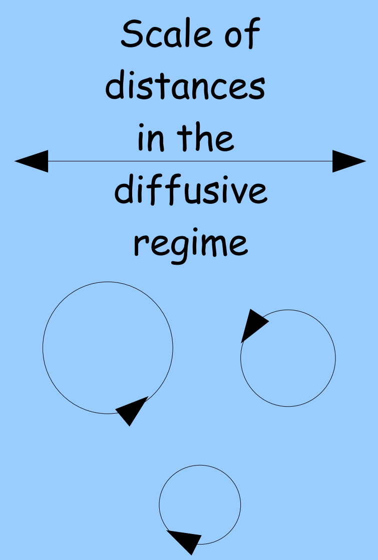

We neglect here molecular diffusion and show that at large scales where dispersion exceeds the size of most energetic eddies, transport is again diffusive.

In Lagrangian coordinates, motion of a parcel is

$$\boldsymbol{x}(\boldsymbol{a},t)=\boldsymbol{x}(\boldsymbol{a},0)+\int_0^t \boldsymbol{u}(\boldsymbol{x}(\boldsymbol{a},s),s)\,ds$$

where $x(\boldsymbol{a},t)$ is position at time t of parcel which was in $\boldsymbol{a}$ at time 0 (hence $\boldsymbol{x}(\boldsymbol{a},0)=\boldsymbol{a}$)

For each parcel with initial position $\boldsymbol{a_i}$, define

$$\boldsymbol{x_i}(t)=\boldsymbol{x}(a_i,t) \text{ and } \boldsymbol{v_i}(t)=\boldsymbol{u}(\boldsymbol{x}(\boldsymbol{a_i},t),t)$$

Hence, $\dfrac{d}{dt}(\boldsymbol{x_i}-\boldsymbol{a_i})^2=2(\boldsymbol{x_i}-\boldsymbol{a_i})\,\boldsymbol{v_i}=2\int_0^t \boldsymbol{v_i}(t)\,\boldsymbol{v_i}(s)\,ds$,

and after averaging over ensemble

$$\frac{d}{dt}\langle(\boldsymbol{x_i}-\boldsymbol{a_i})^2\rangle=2\int_0^t S(t-s)\,ds=2\int_0^t S(s)\,ds$$

where $S(t-s)=\langle\boldsymbol{v_i}(t)\,v-i(s)\rangle$ is the Lagrangian velocity correlation, assuming homogeneity and stationnarity.

This can be solved as

$$\langle(\boldsymbol{x_i}-\boldsymbol{a_i})^2\rangle=2\int_0^t (t-s)\,S(s)\,ds$$

If $S(s)$ decays fast enough, and for $t\gg I$

$$\langle(\boldsymbol{x_i}-\boldsymbol{a_i})^2\rangle\sim 2Dt \text{ with } D=\int_0^\infty S(s)\,ds$$

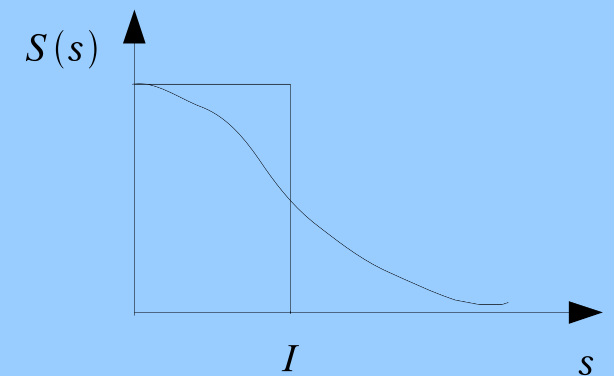

Integral scale I

$$\int_0^\infty S(s)\,ds=\langle v^2\rangle I$$

Cautions

The limit does not mean the process is Gaussian since higer order moments $\langle x^p \rangle$ with $p > 2$ can be far from Gaussian values long after the regime $\langle x^2 \rangle \sim 2Dt$ is reached. Nethertheless, this regime is known as the diffusive regime.

If the integral $\int_0^\infty S(s)\,ds$ diverges, the diffusive regime does not exist. For instance if $S(s) \sim s^{-\eta}$ with $0 < \eta < 1$, the regime is super-diffusive

$$\langle \boldsymbol{x}^2 \rangle \sim t^{2-\eta}$$

If now $\int_0^\infty S(s)\,ds = 0$, but if $\int_0^t (t-s) S(s)\,ds$ diverges with t, we have a sub-diffusive regime. For instance if $S(s) \sim s^{-\eta}$ with $1 < \eta < 2$ for large enough times, we have again $\langle \boldsymbol{x}^2 \rangle \sim t^{2-\eta}$ but with an exponent less than 1

Stretching and generation of tracer gradient

General equation : $\frac{\partial}{\partial t} c + \mathbf{u} \cdot \nabla c = \kappa \nabla^2 c + \text{source}$

For a pure deformation $u = \alpha x$ and $v = -\alpha y$:

In the absence of diffusion and source:
c and area conserved + stretching

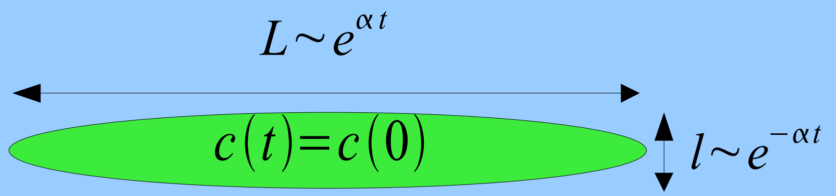

With diffusion:

$$\frac{\partial}{\partial t} c + \alpha x \frac{\partial}{\partial x} c - \alpha y \frac{\partial}{\partial y} c = \kappa \nabla^2 c$$

Diffusion and advection balance at scale $l_d = \sqrt{2 \kappa / \alpha}$

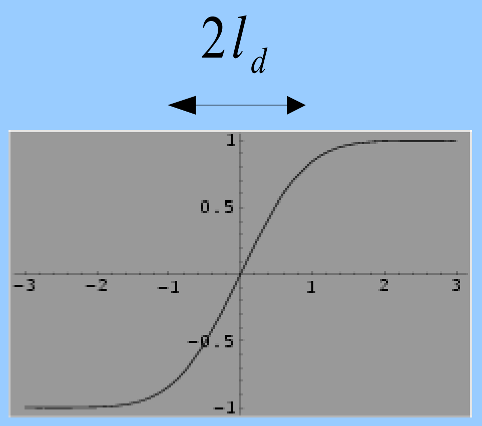

Stationary solution for a density front depending on y only: $c = A \,\mathrm{Erf}(y / l_d)$
reached in $t \approx \alpha^{-1}$ from steep initial condition and in $t \approx \alpha^{-1} \ln(L_0 / l_d)$ from smooth initial condition at scale L_0

Impulsive solution

$$c(x, y, t) = \frac{1}{\pi f g} \exp\left(-\frac{x^2}{f^2} - \frac{y^2}{g^2}\right)$$

with $f^2 = \frac{\kappa}{\alpha}(e^{2\alpha t} - 1)$ and $g^2 = \frac{\kappa}{\alpha}(1 - e^{-2\alpha t})$

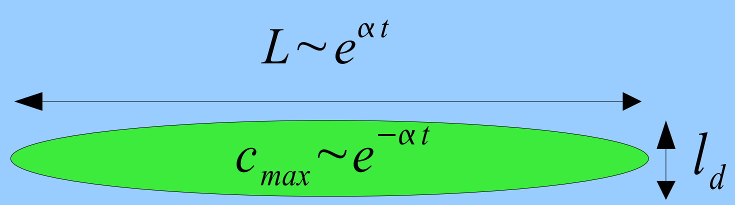

Another interesting separable solution, initially sinusoidal in both x and y

$$c(x,y,t)=A(t)\cos(k e^{-\alpha t}x)\cos(k e^{\alpha t}y)$$

with $A(t)=\exp(-l^2 k^2 \sinh 2\alpha t)$, $l=\sqrt{\frac{\kappa}{\alpha}}$ being a separation constant.

The gradient is

$$|\nabla c|^2=\frac{k^2}{2}\cosh(2\alpha t)\exp(-2 l^2 k^2 \sinh 2\alpha t).$$

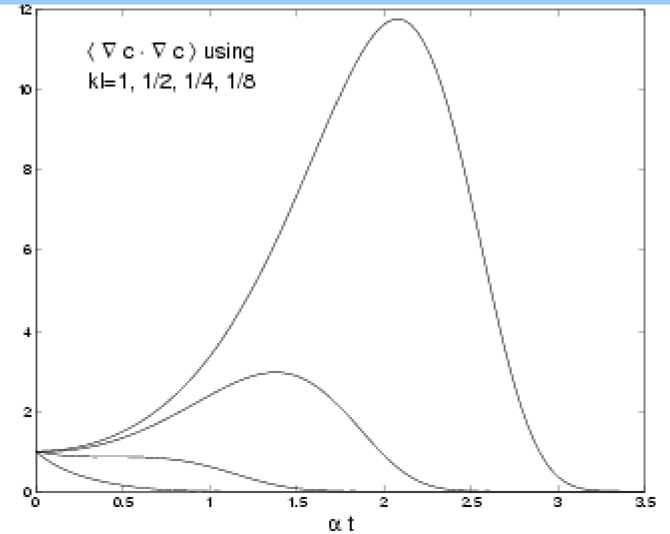

Figure 8: The mean square of the concentration gradient. If $k\ell \ll 1$ then the concentration gradient grows until $t = t_*$ in (54) and then decreases precipitiously. If $k\ell \geq 1/2$ then diffusion always overpowers strain and the mean square gradient decreases monotonically to zero.

Blob dynamics

Along the direction of stretching: exponential elongation of the blob

Along the direction orthogonal to the shear, two stages
- exponential narrowing until $t^{*} \sim \alpha^{-1} \ln(\alpha/\kappa)$
- saturation of the width of the blob at the diffusive scale $l_d=(2\ \kappa/\alpha)^{1/2}$
-> exponential growth of the blob, exponential decay of the concentration
This second stage shared for blob or δ-like initial conditions

In the case of a sinusoidal solution

- first stage until t* for which the wave stretches and shrinks exponentially, and the gradient grows exponentially
- second stage of super exponential decay
-> paradox ?

Diffusion is felt after a time t* which depends only logarithmically upon κ

A more general solution to the sinusoidal problem

Let the velocity be a linear function of $\boldsymbol{x}$

$\boldsymbol{v}=\boldsymbol{x}\cdot\boldsymbol{\sigma}(t)$ where $\boldsymbol{\sigma}(t)$ is a matrix with zero trace.

For a single Fourier mode: $c(\boldsymbol{x},t)=\hat{c}(\boldsymbol{k_0},t)\exp(i\,\boldsymbol{k}(t)\cdot\boldsymbol{x})$ with $\boldsymbol{k_0}=\boldsymbol{k}(0)$ and $\hat{c}(\boldsymbol{k_0},0)=\boldsymbol{c_0}(\boldsymbol{k_0})$

The advection-diffusion equation is

$$\partial_t\hat{c}+i\,\boldsymbol{x}\cdot\partial_t\boldsymbol{k}\,\hat{c}+i(\boldsymbol{x}\cdot\boldsymbol{\sigma}\cdot\boldsymbol{k})\hat{c}=-\kappa\,k^2\hat{c}$$

Since this holds far all $\boldsymbol{x}$

$$\partial_t\boldsymbol{k}=-\boldsymbol{\sigma}\cdot\boldsymbol{k}$$

$$\partial_t\hat{c}=-\kappa\,k^2\hat{c}$$

Hence $\boldsymbol{k}(t)=\boldsymbol{T_t}\cdot\boldsymbol{k_0}$, with $\partial_t\boldsymbol{T_t}=-\boldsymbol{\sigma}(t)\cdot\boldsymbol{T_t}$, and $\boldsymbol{T_0}=Id$, $det\,\boldsymbol{T_t}=1.$

If $\boldsymbol{\sigma}$ is fixed then $\boldsymbol{T_t}=\exp(-\boldsymbol{\sigma}\,t)$

$$\hat{c}(\boldsymbol{x},t)=\int\hat{c}(\boldsymbol{k_0},t)\exp(i\,\boldsymbol{x}\cdot\boldsymbol{k}(t))\,d^d k_0$$

$$\hat{c}(\boldsymbol{x},t)=\int\hat{c}_0(\boldsymbol{k_0})\exp\left(i\,\boldsymbol{x}\cdot\boldsymbol{T_t}\cdot\boldsymbol{k_0}-\kappa\int_0^t(\boldsymbol{T_t}\cdot\boldsymbol{k_0})^2ds\right)d^d\boldsymbol{k_0}$$

Recalling

$$\hat{c}(\boldsymbol{x},t)=\int \hat{c}_0(\boldsymbol{k_0})\exp\left(i\,\boldsymbol{x}\cdot\boldsymbol{T_t}\cdot\boldsymbol{k_0}-\kappa\int_0^t(\boldsymbol{T_t}\cdot\boldsymbol{k_0})^2\,ds\right)d^d\boldsymbol{k_0}$$

If $\boldsymbol{\sigma}=\begin{pmatrix}\alpha & 0\\ 0 & -\alpha\end{pmatrix}$, $\quad \boldsymbol{k_0}=(k,l)$, $\quad \boldsymbol{x}=(x,y)$

then $\boldsymbol{T_t}=\begin{pmatrix}e^{-\alpha t} & 0\\ 0 & e^{\alpha t}\end{pmatrix}$ and $\boldsymbol{k}(t)=(k\,e^{-\alpha t},l\,e^{\alpha t})$

$$\int_0^t ds\,(\boldsymbol{T_s}\cdot\boldsymbol{k_0})^2=\frac{1}{2\alpha}\left(l^2\left(e^{2\alpha t}-1\right)+k^2\left(1-e^{-2\alpha t}\right)\right)$$

Introducing $\tilde{l}=l\,e^{\alpha t}$, the solution is

$$c(x,y,t)=e^{-\alpha t}\int_{-\infty}^{\infty}dk\int_{-\infty}^{\infty}d\tilde{l}\,\hat{c}_0(k,\tilde{l}\,e^{-\alpha t})\exp\left(i\,\boldsymbol{k}(t)\cdot\boldsymbol{x}-\frac{\kappa}{2\alpha}(\tilde{l}^2+k^2)\right)$$

Replacing $\hat{c}_0(k,\tilde{l}\,e^{-\alpha t})$ by the inverse Fourier transform

$$\hat{c}_0\left(k,\tilde{l}\,e^{-\alpha t}\right)=\frac{1}{(2\pi)^2}\int c_0(x',y')\exp(-i\,k\,x'-i\,\tilde{l}\,e^{-\alpha t}\,y')\,dx'\,dy'$$

We obtain

$$c(x,y,t)=\frac{e^{-\alpha t}}{(2\pi)^2}\iint dk\,d\tilde{l}\iint dx'\,dy'\,c_0(x',y')\exp\left(-i\,k\,x'-i\,\tilde{l}\,e^{-\alpha t}\,y'+i\,k\,e^{-\alpha t}\,x+i\,\tilde{l}\,y-\frac{\kappa}{2\alpha}\tilde{l}^2\right)$$

and after integration

$$c(x,y,t)=e^{-\alpha t}\int_{-\infty}^{\infty}dy'\,c_0(e^{-\alpha t}x,y')\,G\left(y-e^{-\alpha t}y';\sqrt{\kappa/\alpha}\right)$$

where $G(x;h)=\dfrac{1}{\sqrt{2\pi h^2}}\exp\dfrac{-x^2}{2h^2}$

$$c(x,y,t)=e^{-\alpha t}\int_{-\infty}^{\infty} dy'\, c_0(e^{-\alpha t}x, y')\, G\left(y-e^{-\alpha t}y'; \sqrt{\kappa/\alpha}\right)$$

where $G(x;h)=\frac{1}{\sqrt{2\pi h^2}}\exp\frac{-x^2}{2h^2}$

This formula shows

- the decay is exponential, no more super exponential

- the strip of width y results from the narrowing and smoothing of a strip of width y $e^{\alpha t}$

- the Fourier modes that contribute for large t are those for which l $e^{\alpha t}$ is still of order 1 or less. These "zero-modes" are those which decay less rapidly in time. They live in a cone of aperture $e^{-\alpha t}$ which shrinks exponentially with time.

- the decay rate is independent of the diffusivity

Lyapunov exponent

Evolution equations for a line element and the passive scalar gradient in the absence of diffusion and source are very similar since $\nabla\theta\cdot\mathbf{x}=\delta\theta$ is preserved

$$\frac{D}{Dt}\delta x_i=\frac{\partial u_i}{\partial x_j}\delta x_j \qquad \frac{D}{Dt}\frac{\partial\theta}{\partial x_i}=\frac{-\partial u_j}{\partial x_i}\frac{\partial\theta}{\partial x_j}$$

$$\left(\frac{D}{Dt}\ \text{time derivation along a given trajectory}\ \mathbf{x}(t)\right)$$

Over a time interval $[t_{0,}t_0+\tau]$:

$$\delta\mathbf{x}(t_0+\tau)=\mathbf{M}(t_{0,}t_0+\tau)\delta\mathbf{x}(t_0) \qquad \nabla\theta(t_0+\tau)=-\mathbf{M}^T(t_{0,}t_0+\tau)\nabla\theta(t_0)$$

Finite-time Lyapunov exponent

$$\lambda(\tau,\mathbf{x}(t_0))=\frac{1}{\tau}\ln\frac{|\mathbf{M}\delta\mathbf{x}|}{|\delta\mathbf{x}|}=\frac{1}{\tau}\ln\frac{|\mathbf{M}^T\nabla\theta|}{|\nabla\theta|}$$

At large τ, if the flow is ergodic, $\lambda(\tau,\mathbf{x}(t_0))$ tends to a unique $\bar{\lambda}$.
At intermediate τ, λ exhibits large spatial and temporal variations.

Finite time Lyapunov exponent in two-dimensional turbulence

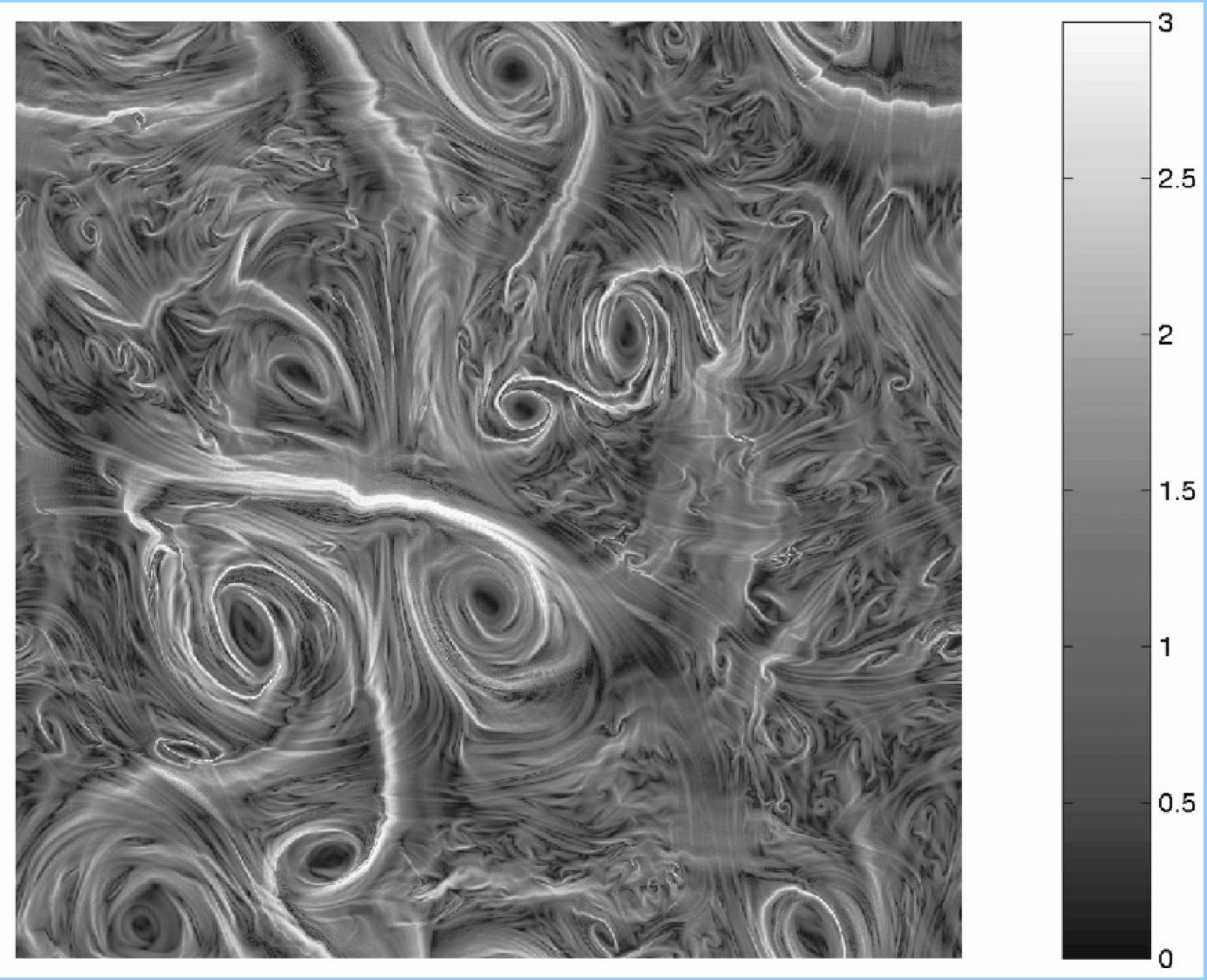

Lapeyre, 2002, Chaos, 12, 688-698

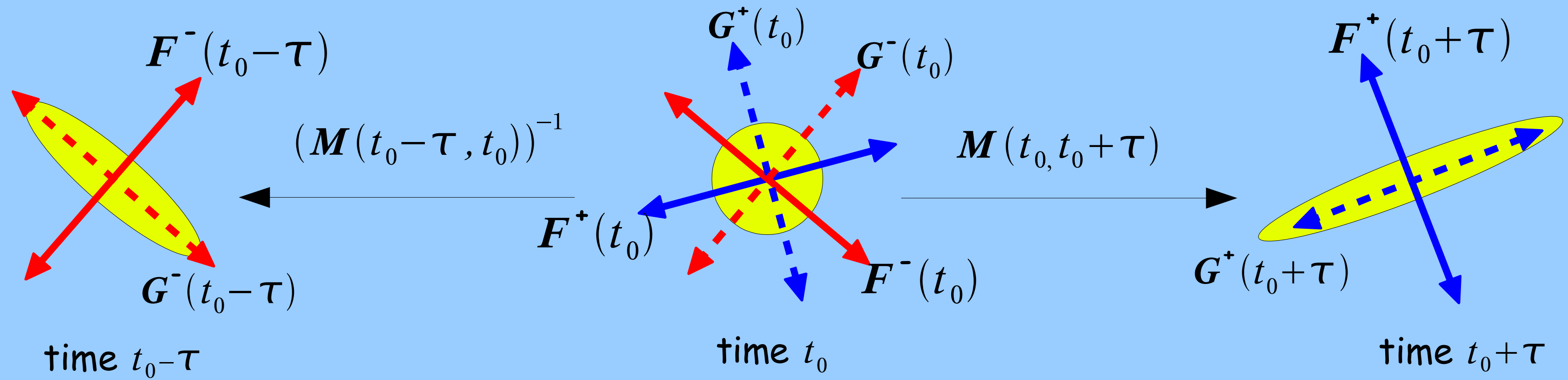

Stable eigendirection (future time)

$$M^T(t_0,t_0+\tau)\,M(t_0,t_0+\tau)\,F^+(t_0)=e^{-2\lambda(t_0,t_0+\tau)\tau}\,F^+(t_0)$$

$$M(t_0,t_0+\tau)\,F^+(t_0)=e^{\lambda(t_0,t_0+\tau)\tau}\,F^+(t_0+\tau)$$

Unstable eigendirection (past time)

$$\left(M(t_0-\tau,t_0)\,M^T(t_0-\tau,t_0)\right)^{-1}F^-(t_0)=e^{-2\lambda(t_0-\tau,t_0)\tau}\,F^-(t_0)$$

$$(M(t_0-\tau,t_0))^{-1}F^-(t_0)=e^{\lambda(t_0-\tau,t_0)\tau}\,F^-(t_0-\tau)$$

As τ gets large

all directions at t_0 but $F^+(t_0)$ get aligned with $G^+(t_0+\tau)$ in forward time

all directions at $t_0-\tau$ but $G^-(t_0,\tau)$ get aligned with $F^-(t_0)$ at t_0

Role of F and G is swapped as one considers gradient instead of separation

Gradient tends to align with $G^-(t_0)$ at t_0

The Lyapunov exponent as built from repeated uncorrelated stretching events

For each individual stretching event experienced by a parcel

$$\lambda_i = \frac{1}{\tau} \ln \frac{|\delta \boldsymbol{x}_i|}{|\delta \boldsymbol{x}_{i-1}|}$$

After n events

$$\lambda = \frac{1}{n\tau} \ln \frac{|\delta \boldsymbol{x}_i|}{|\delta \boldsymbol{x}_0|} = \frac{1}{n\tau} \ln \prod_{i=1}^{n} \frac{|\delta \boldsymbol{x}_i|}{|\delta \boldsymbol{x}_{i-1}|} = \frac{1}{n} \sum_{i=1}^{n} \lambda_i$$

Hence λ is a sum of n independent variables with $n \sim t$.

The pdf of λ is then $\left(\frac{t\, G''(\lambda)}{2\pi}\right)^{1/2} \exp\left(-t\, G(\lambda)\right)$

where G is the Cramèr function.

Here we use the large deviation theory which generalizes the central limit theorem for deviations exceeding the variance

$G(\lambda)$ is a convex function such that $G(\bar{\lambda}) = G'(\bar{\lambda}) = 0$

in the vicinity of $\bar{\lambda}$, $\quad G(\lambda) = G''\frac{(0)}{2}(\lambda - \bar{\lambda})^2$ recovers the Gaussian law.

References for the large deviation theory:
Ellis, Entropy, large deviation and statistical mechanics, Springer Verlag, NY, 1965
Frisch, Turbulence, CUP, 1995
Thiffeault, arXiv.nlin.CD/0502011, 2006

Let us consider now an initial distribution made with a number of wave packets with the same dominating wavenumber k_0 and with arbitrary orientation over N cells.

Each wave packet evolves according to the equations seen on p.36 with a stretching rate determined by the Lyapunov exponent experienced along its trajectory. Hence $k^{(i)}(t)=k_0\cos\phi^{(i)}\exp(\lambda^{(i)}t)$ where $\phi^{(i)}$ is the initial orientation of the main wavevector with respect to the compression axis $\boldsymbol{F}^-$.

For each wavepacket, the variance is

$$v^{(i)}(t)=\exp\left(-2\kappa\int_0^t k^{(i)2}\cos^2\phi^{(i)}\,ds\right)=\exp\left(-\kappa k_0^2\cos^2\phi^{(i)}\frac{\exp(2\lambda^{(i)}t)}{\lambda^{(i)}}\right)$$

The total variance is a superposition of all wave packets (which may overlap

$$v(t)=\sum_i v^{(i)}(t)$$

This sum can be made over all the values of $\lambda^{(i)}$ and $\phi^{(i)}$, assuming that $\phi^{(i)}$ is uniformly distributed

$$v(t)=\int_0^\infty P(\lambda,t)\,d\lambda\,\frac{\int_0^{2\pi}d\phi}{2\pi}\exp\left(\frac{-\kappa k_0^2}{\lambda}\cos^2\phi\exp(2\lambda t)\right)$$

Since $\int_0^{2\pi}\frac{d\phi}{2\pi}\exp(-a\cos^2\phi)\equiv e^{-a/2}I_0\left(\frac{a}{2}\right)\approx\frac{1}{\sqrt{\pi a}}$ for large a,

the variance is

$$v(t)=\int_\infty^0 d\lambda\,P(\lambda,t)\left(\frac{\lambda}{\pi k_0^2\kappa}\right)^2\exp(-\lambda t)$$

Using this variance

$$v(t)=\int_{\infty}^{0} d\lambda\, P(\lambda,t)\left(\frac{\lambda}{\pi k_0^2\kappa}\right)^{1/2}\exp(-\lambda t)$$

and the probability distribution of λ, that is $P(\lambda,t)=\left(\frac{t\,G''(\lambda)}{2\pi}\right)^{1/2}\exp(-t\,G(\lambda))$

we get

$$v(t)=\int_{0}^{\infty} d\lambda\left(\frac{t\,\lambda\,G''(\lambda)}{2\pi\kappa k_0^2}\right)^{1/2}\exp(-t(\lambda+G(\lambda)))$$

By Laplace approximation, the main contribution to this integral arises from the vicinity of λ_c such that $\lambda_c+G(\lambda_c)$ is minimum.

Hence

$$v(t)\sim\exp(-\gamma t)$$

with

$\gamma=\lambda_c+G(\lambda_c)\,G'(\lambda_c)=-1\ if\ G'(0)\leqslant-1$

$\gamma=G(0)$ if $G'(0)\geqslant-1$

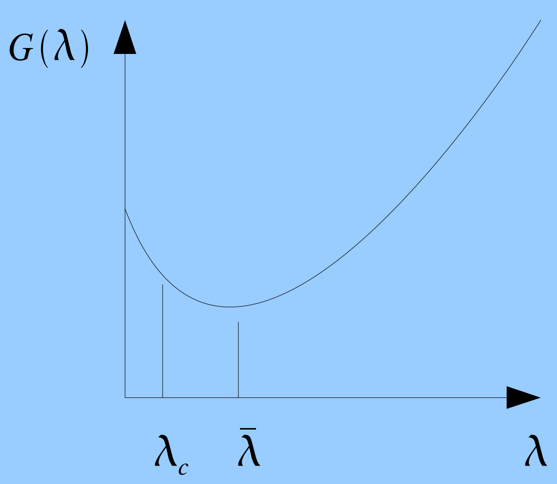

Evolution of a tracer blob under the combined action of stretching and diffusion

$l_d \approx \sqrt{\frac{\kappa}{\lambda}}$

Length $L \sim l_0 e^{\gamma_c \tau}$

$\theta_{max} \approx \theta_0 e^{-\gamma_c \tau}$

l_0 θ_0 $\mathbf{x}_0$

Advection
diffusion

over duration τ

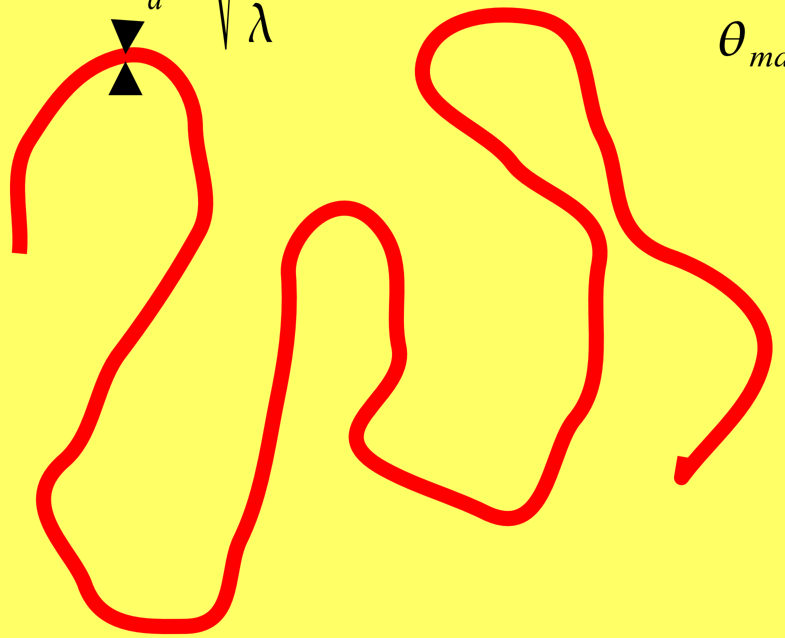

L_s *Characteristic size of synoptic (energetic) advecting structures*

Size of the dispersed blob

$R \sim \sqrt{\tau}$ *for* $\tau \gg \tau_0 = \bar{\lambda}^{-1} \ln(L_s / l_0)$

WHAT next?

In some recent works the local stretching leading to γ_c is challenged by another, global, theory where the decay is governed by solving an eigenvalue problem within the whole domain. This regime applies when the tracer over a domain which is much larger than the size of the main eddies.
Both regimes have been observed and tested in numerical experiments.

Referencess:
Pierrehumbert, 2000, Chaos, 10(1), 61-74
Sukhatme & Pierrehumbert, 2002, Phys. Rev. E, (66), 056302
Tsang et al., 2005, Phys. Rev. E, (71), 066301
Haynes & Vanneste, 2005, Phys. Fluids, (17), 097103

Predictions for the PDF of the tracer

For the forced case

$P(\theta)$ has a Gaussian core and exponential tails

$P(\nabla\theta)$ is a stretched exponential (decays faster than an exponential but slower than a Gaussian

$P(\Delta\theta,r)$ is like $P(\nabla\theta)$ for small r

$P(\Delta\theta,r) = \int P(\theta)P(\Delta\theta-\theta)d\theta$ for large r, with enhanced Gaussian core

For the decaying case

variance and other moments decay exponentially

$<\theta^n> \sim \exp(-\gamma_n T)$

$P(\theta)$ is non-Gaussian with fat tails

local theory predicts that all moments decay at the same rate $\gamma_n = \gamma$

global theory predicts a self-similar decay $\gamma_n = n\gamma$

Chertkov et al., 1995, Phys. Rev. E, 51(6), 5609-5627

Antonsen et al., 1996, Phys. Fluids 8(11), 3094-3104

Balkovsky & Fouxon, 1999, Phys. Rev. E, 60(4), 4164-4174

Falkovich, Gawedzki & Vergassola, 2001, Rev. Mod. Phys, 73, 913-975

* Pierrehumbert, 2000, Chaos, 10(1), 61-74

Sukhatme & Pierrehumbert, 2002, Phys. Rev. E, (66), 056302

1) By central limit theorem, the Lyapunov exponent has a Gaussian distribution for time $T \gg \tau_L$, Lagrangian correlation time of the flow

$$P(\lambda, T) = \sqrt{\frac{aT}{\pi}} \exp(-aT(\lambda - \bar{\lambda})^2)$$

2) In the forced case and without diffusion, $\frac{d\theta}{dt} = f$ where f is a random force at scale L_s

Over a time T, large with respect to the correlation time of the force, the PDF for θ is Gaussian with variance $\langle f^2 \rangle T$ (like for a random walk).

3) With diffusion, the variance builds up until $T \approx \tau_d = \lambda^{-1} \ln(L_s / l_d)$.

Therefore $P(\theta \| \lambda) \sim \exp(\frac{-\theta^2}{2\langle f^2 \rangle \tau_d})$, and

$$P(\theta) = \int_0^\infty P(\lambda, \tau_d) P(\theta \| \lambda) d\lambda \sim \int_0^\infty \exp -[\frac{\theta^2}{2\langle f^2 \rangle \tau_d} + \frac{a}{\tau_d}(\ln(\frac{L_s}{l_d}) - \bar{\lambda}\tau_d)^2] d\tau_d$$

Major contribution arises from the vicinity of $\tau_d = \frac{1}{\bar{\lambda}} \sqrt{\left(\ln \frac{L_s}{l_d}\right)^2 + \frac{\theta^2}{2a\langle f^2 \rangle}}$

4) For $\theta \ll 2a\langle f^2 \rangle (\ln L_s / l_d)^2$, that is for a range of θ growing like the logarithm of the Peclet number, the resulting distribution is Gaussian.
For much larger θ, major contribution arises from $\tau_d \sim |\theta|$ leading to an exponential tail of the PDF.

5) In the decay case, we assume an initial distribution of the tracer at scale L_s.
After a time $T \gg \tau_d$, *a well-mixed parcel of size* l_d *combines approximately*
$N = (l_d / L_s) \exp(\lambda T)$ *independant contributions. Therefore* $P(\theta \| \lambda)$ *is Gaussian with variance proportional to* N

$$P(\theta \| \lambda) \sim \exp(-b \frac{l_d}{L_s} e^{\lambda T} \theta^2), \text{ and}$$

$$P(\theta) = \int_0^\infty P(\lambda, \tau_s) P(\theta \| \lambda) d\lambda \sim \int_0^\infty \exp - [\frac{l_d}{L_s} e^{\lambda T} \theta^2 + a T (\lambda - \bar{\lambda})^2] d\lambda$$

The exponent is minimized when $2a(\lambda - \bar{\lambda}) + b(l_d / L_s) e^{\lambda T} \theta^2 = 0$.
For a range θ *shrinking as* $Pe\, e^{-\lambda T}$, *the tracer PDF is dominated by* $\lambda = \bar{\lambda}$
For fixed θ *it is dominated by the scaling of the PDF of* λ *for small* λ *and should have fat tails.*

adapted from Pierrhumbert, Chaos, 2000

The main point to recall is that PDF for tracers or tracer gradients always exhibit fat tails. Large deviations from the mean are much more frequent than for a Gaussian distribution. These large deviations are mostly governed by the less stretched regions of the flow.

Tracer PDF for a lattice model of advection-diffusion

Pierrehumbert, 2000

alternate shift

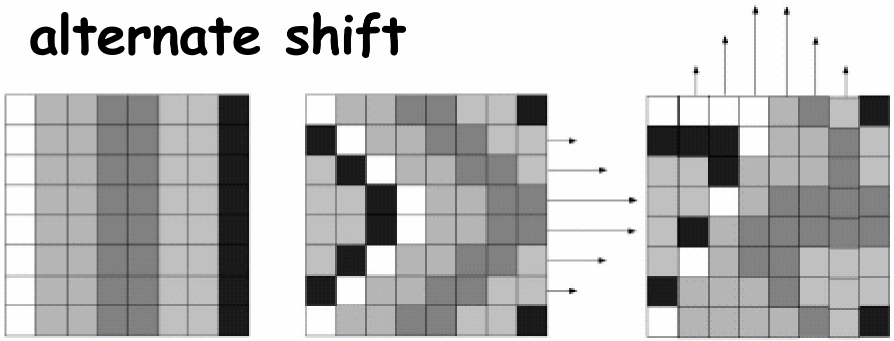

forced case

Gaussian core + exponential tails

decaying case

stretched exponential

self-similar PDF

$P(q,t)=P_1(\theta/\sigma(t))/\sigma(t)$

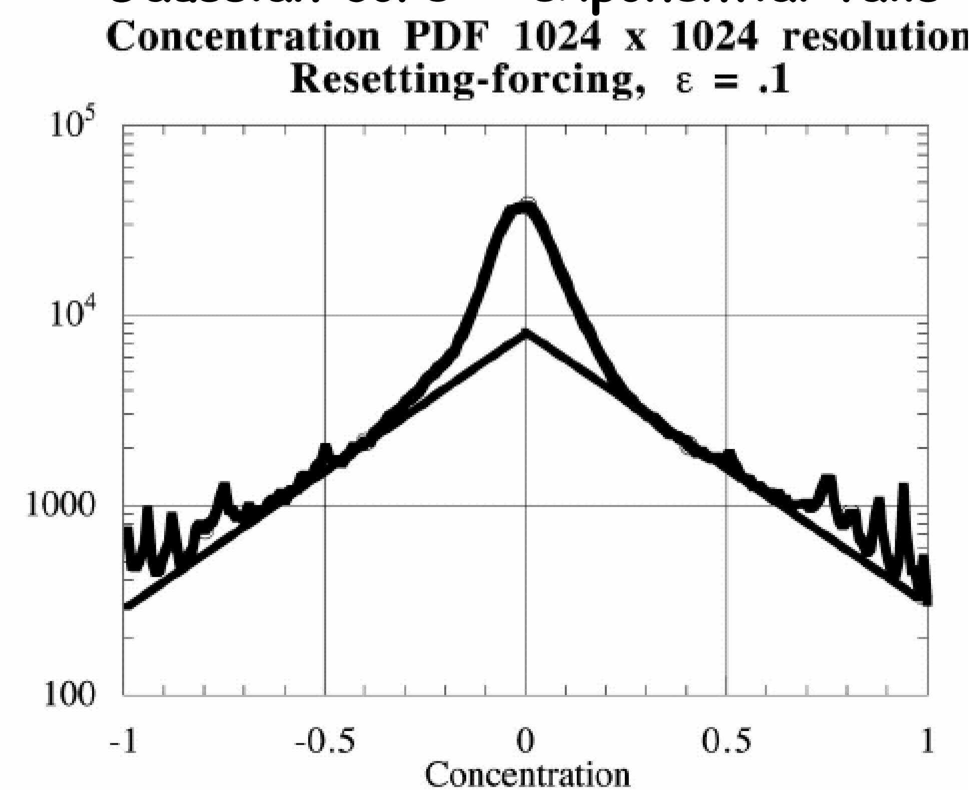

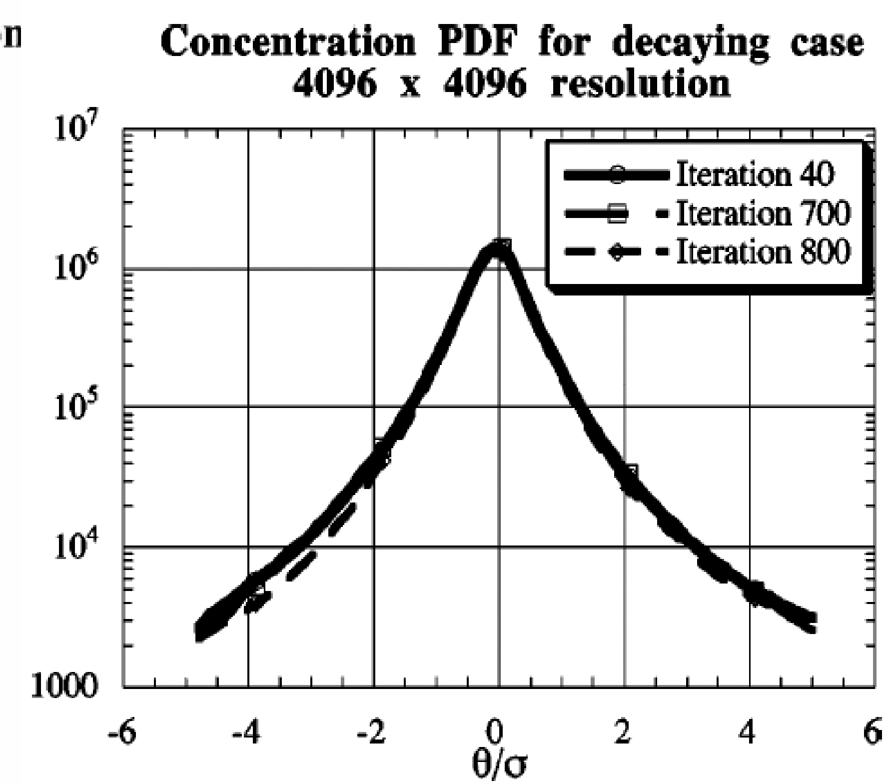

PDF of ∇[O3] calculated from retro-trajectories starting along a vertical profile using 3D ECMWF winds

(Legras, 2002)

PDF

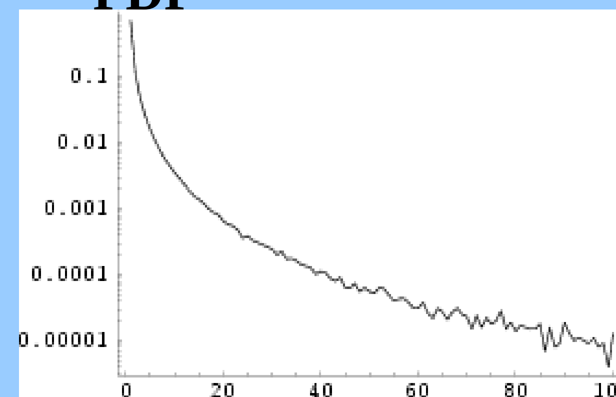

∇[O3]

PDF of tracer differences from ER2 flights

(Hu & Pierrehumbert, GRL, 2002)

r=200 m

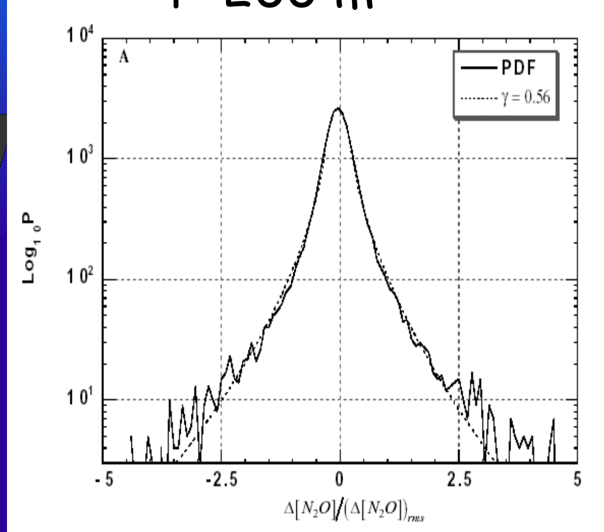

r=90 km

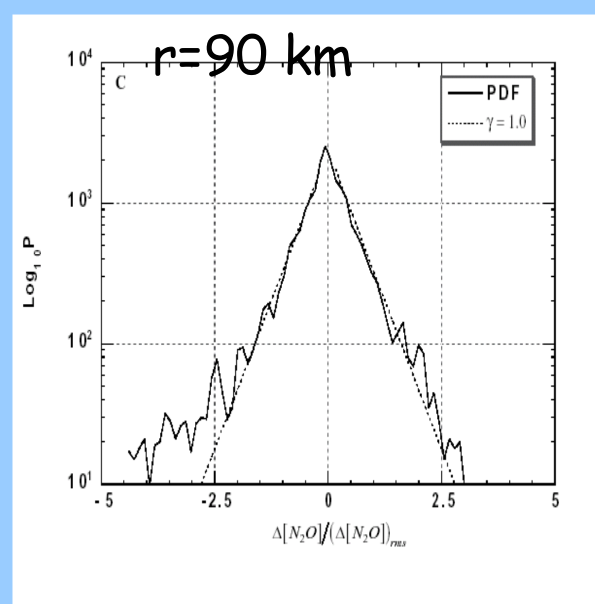

r=160 km

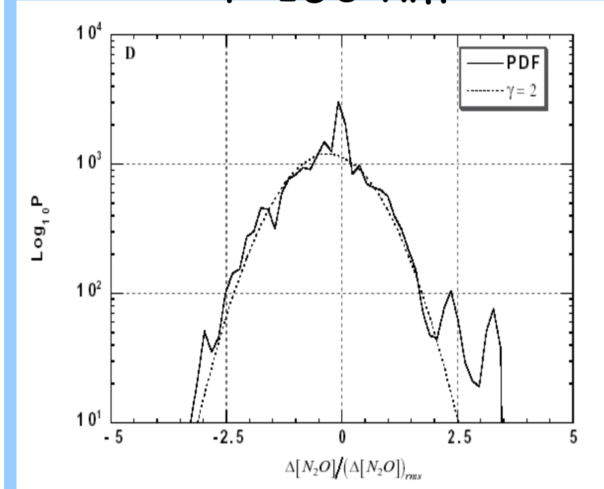

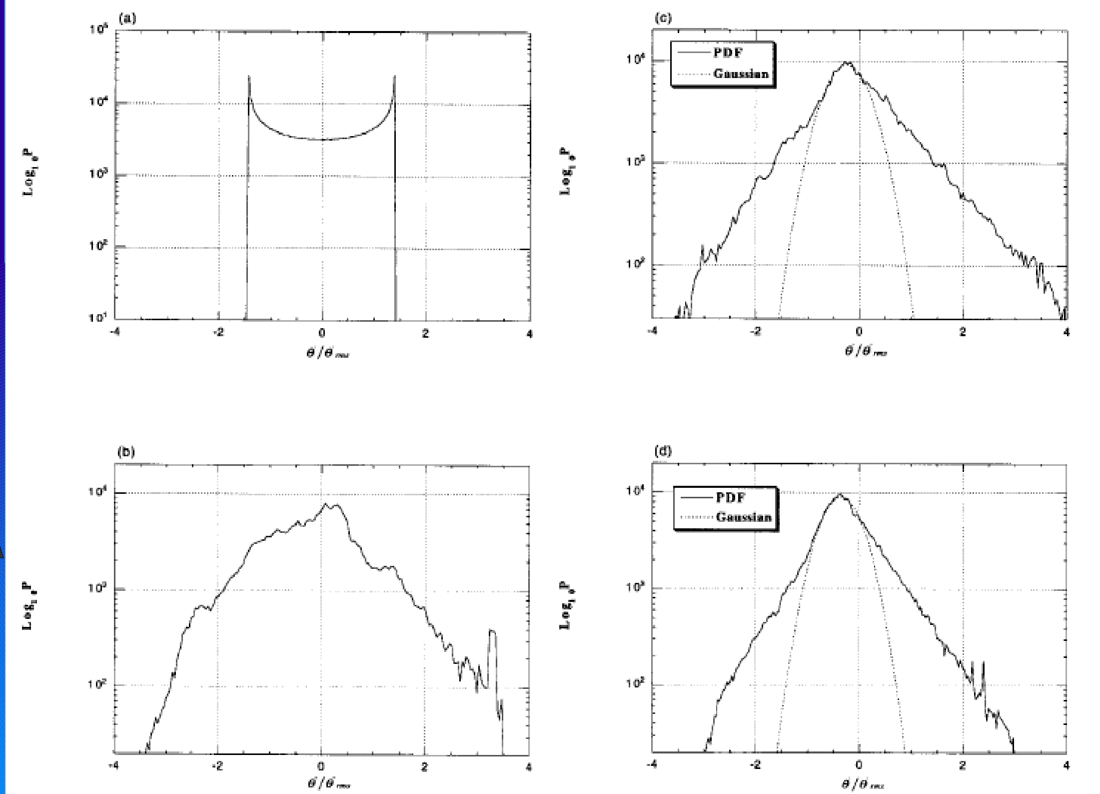

Distributions of decaying tracers advected by stratospheric flow with diffusion

Hu & Pierrehumbert, JAS, 2001

With initial inhomogeneities in the zonal direction

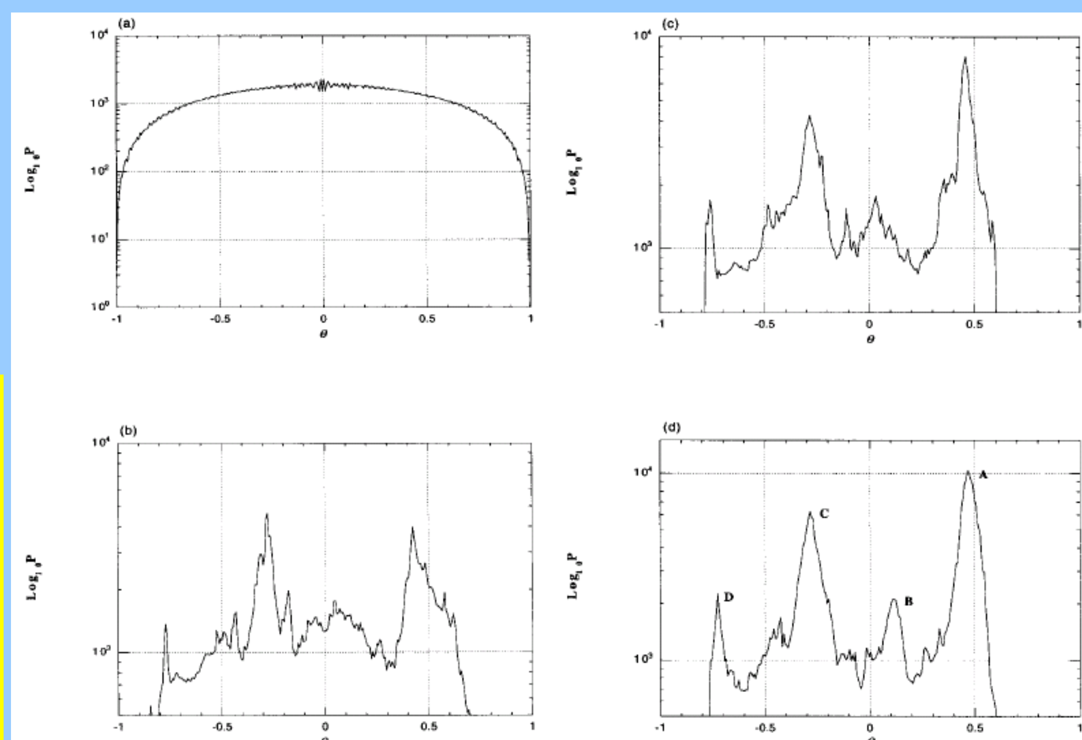

With initial inhomogeneities in the meridional direction

What about the spectrum of tracer variance?

Using observed winds, it is possible to show, using the stretching theory and the combined effect of horizontal strain and vertical shear, that the variance spectrum is influenced by dissipation at much larger scale than the naïve estimate $(\kappa/\lambda)^{1/2}$ and can be steeper than k^{-1}.
Ref: Haynes and Vanneste, J. Atmos. Sci., 2004, 61, pp. 161-178

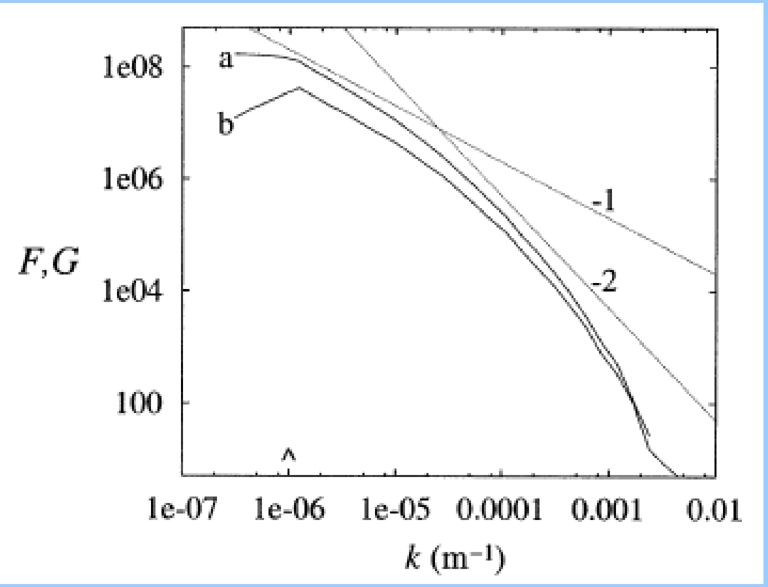

Summary of part II.C Blob and wave-packet dynamics in 2D flows

1. Under the action of fixed strain (α) + diffusion (κ)

- A blob elongates exponentially as exp (αt) in the direction of extension while keeping a fixed limit size $\sim(\kappa/\alpha)^{1/2}$ in the direction of compression.
- The concentration of tracer in the blob decays as exp(- αt).
- Diffusion is slaved to the strain which governs the decay rate

- A single Fourier mode or wave packet exhibit temporary growth of the gradient in the direction of compression followed by super exponential decay of the variance (and gradient) as exp ($-\kappa^2$ k_0 exp(2 αt))

As a blob can be considered as a linear combination of wave packets, the paradox is resolved by the fact that decay is governed by the initial wavenumbers with slowest decay mode. The modes which have not yet decayed after time t are located in a cone (in Fourier space) of angle ~exp(- αt).

Summary of part II.C Blob and wave-packet dynamics

2. Under the more general condition of a smooth time varying flow

The Lyapunov exponent describes the growth of both infinitesimal separation and tracer gradient along the path of a parcel carried by the flow.

At given time t_0 and location x_0, stable direction is the single direction of separations that will not grow but decay under future evolution. Initial gradients orthogonal to this direction are also the only one that do not decay.

Unstable direction is the direction of separation that do not grow for reverse temporal evolution. It is also the direction along which tend to align almost all separations initiated at earlier times, the gradient tend to align perpendicularly with the unstable direction. Hence, the observed tracer contours are expected to align with the unstable direction in the vicinity of x0 at time t_0, for any passive tracer.

Summary of part II.C Blob and wave-packet dynamics

2. Under the general condition of a smooth time varying flow and after statistical averaging taking into account the evolution of wave packets and the distribution of Lyapunov exponent

An exponential decay rate γc is predicted

The distribtion of the tracer, its gradient and differences over short distances exhibit are non Gaussian with fat tails indicating that large fluctuations are realtively frequent.

It also predicts a scalar spectrum which is steeper (in wavenumber) than the prediction of the standard spectral theory.

These predictions can be checked experimentally on real flows.

Part III: Deterministic non diffusive stirring within the Hamiltonian framework

- 1 Hamiltonian form of the 2D advection equation
- 2 Canonical change of variables
- 3 Integrable Hamiltonian, action-angle variables.
- 4 Poincaré maps
- 5 Perturbation of an integrable Hamiltonian, Hamilton-Jacobi equation.
- 6 Preserved tori, formulation of the KAM theorem.
- 7 Breaking of resonant tori
- 8 Invariant stable and unstable hyperbolic manifolds
- 9 Hyperbolic tangle, and chaos
- 10 Lobe dynamics

III.1 Hamiltonian form of the 2D-advection equation

$$\psi(x,y) \qquad u=\frac{-\partial\psi}{\partial y} \qquad v=\partial\frac{\psi}{\partial x} \qquad \longleftrightarrow \qquad H(\boldsymbol{p},\boldsymbol{q}) \qquad \dot{\boldsymbol{p}}=\frac{-\partial H}{\partial \boldsymbol{q}} \qquad \dot{\boldsymbol{q}}=\frac{\partial\psi}{\partial \boldsymbol{p}}$$

1 degree of freedom
two-dimensional phase space

N degrees of freedom
2N dimensional phase space

Time dependence in $\psi(x,y,t)$ can be treated as an extra degree of freedom in the Hamiltonian. [new Hamiltonian is $\psi(x,y,q_2)+p_2$]

3D stationary flows can be treated essentially as 2D time dependent flows
no Hamiltonian structure for the advection by 3D non stationary flows.

Hamiltonian dynamics preserves the symplectic area $\oint \boldsymbol{p}\cdot d\,\boldsymbol{q}$

Useful references: Ott, Chaos in dynamical systems, CUP, 1993
Ottino, The Kinematics of Mixing: Stretching, Chaos and Transport, CUP, 1989

III.2 Canonical change of variables

Canonical variable transform for Hamiltonian from $(\boldsymbol{p},\boldsymbol{q})$ to $(\boldsymbol{p}',\boldsymbol{q}')$

Conveniently performed using the generating function $S(\boldsymbol{p}',\boldsymbol{q},t)$

such that
$$\boldsymbol{p}=\frac{\partial S(\boldsymbol{p}',\boldsymbol{q},t)}{\partial \boldsymbol{q}}$$
$$\boldsymbol{q}'=\frac{\partial S(\boldsymbol{p}',\boldsymbol{q},t)}{\partial \boldsymbol{p}'}$$

and $H(\boldsymbol{p}',\boldsymbol{q}',t)=H(\boldsymbol{p},\boldsymbol{q})+\dfrac{\partial S}{\partial t}$

Example

$(x,y)\rightarrow(\rho^2,?)$ $\quad\rho^2=x^2+y^2$ $\quad x=\sqrt{\rho^2-y^2}=\dfrac{\partial S(\rho^2,y)}{\partial y}$

hence $S=\dfrac{1}{2}\left\{y\sqrt{\rho^2-y^2}+\rho^2\arctan\left(\dfrac{y}{\rho^2-y^2}\right)\right\}$

and $\dfrac{\partial S(\rho^2,y)}{\partial \rho^2}=\dfrac{1}{2}\arctan\dfrac{y}{x}=\dfrac{\theta}{2}$

The couple of new conjugate polar coordinates is $(\rho^2,\dfrac{\theta}{2})$

III.3 Integrable Hamiltonian

An Hamiltonian is integrable if there are N invariants of motion including the Hamiltonian itself if it does not depend on time.

Trajectories are then restrained to a torus of dimension N in the phase space of dimension $2N$

Stationary 2D flows are integrable

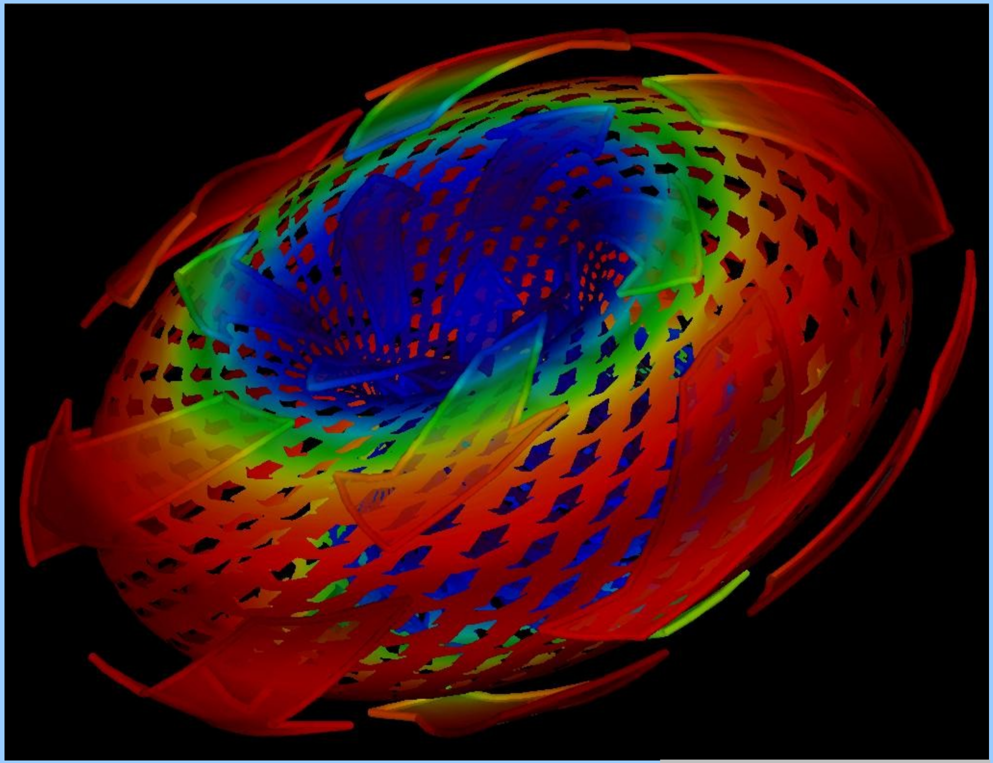

H. Löffelmann

When an Hamiltonian system is integrable it is possible to find a set of coordinates $\boldsymbol{p}=\{p_i\}$ and $\boldsymbol{q}=\{q_i\}$ such that $\frac{\partial H}{\partial q_i}\equiv 0.$

Such a set of (action-angle) coordinates $(\boldsymbol{I},\boldsymbol{\theta})$ can be obtained choosing $I_i=\frac{1}{2\pi}\oint_{\gamma_i}\boldsymbol{p}.d\boldsymbol{q}$ for each irreducible contour on the torus.

[In 2D, I is just a relabelling of ψ by the area of each ψ-contour.]

In this case, $\frac{dI_i}{dt}=0$ and $\frac{d\theta_i}{dt}=\frac{\partial H}{\partial I_i}=\omega_i(\boldsymbol{I})$

and θ_i increases by 2π for each loop along γ_i

A system is quasi-periodic with N frequencies if there is no integer vector $\boldsymbol{m}=\{m_i\}$ such that $\sum_i m_i\omega_i=0$

Example: $\psi=x^2+\frac{y^2}{\lambda^2}$, thus $I=\frac{1}{2}\lambda\psi$

$$x=\frac{X}{\lambda}=\frac{\partial S}{\partial y} \text{ with } X=\sqrt{\psi\lambda^2-y^2}$$

and $S=\frac{1}{2\lambda}\left(yX+\lambda^2\psi\arctan\left(\frac{y}{X}\right)\right)$

Hence : $\theta=\frac{\partial S}{\partial I}=\arctan\left(\frac{y}{\lambda x}\right)$

and $\frac{d\theta}{dt}=\frac{2}{\lambda}$

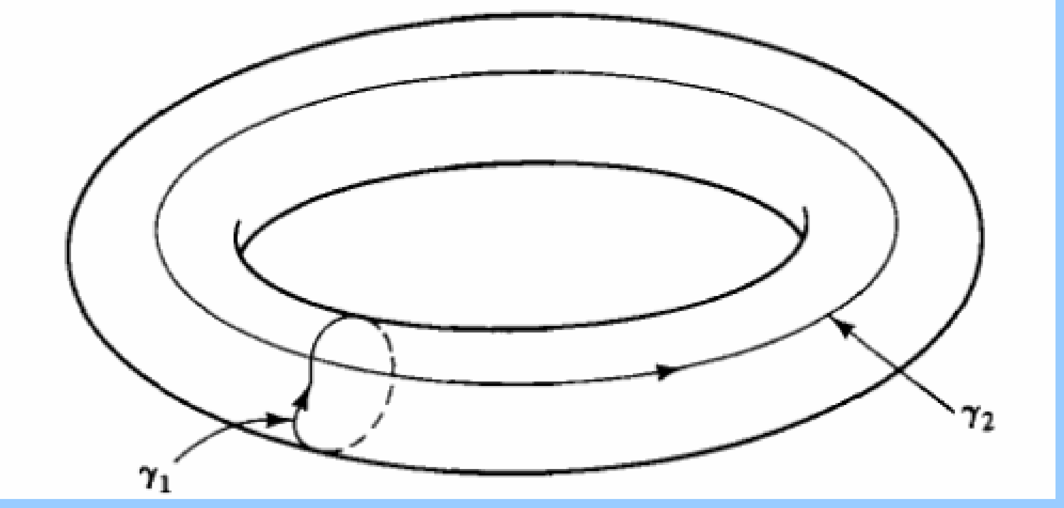

III.3 (contd) Action-angle variables

Let us make a pause to introduce the Poincaré map

III.4 Poincaré map

If $\psi(x,y,t)$ is periodic of period T, time t can be transformed into an angle $\theta = \dfrac{2\pi t}{T}$

The Poincaré map is defined from time sections at $\ldots, -2T+\tau, -T+\tau, \tau, T+\tau, 2T+\tau, \ldots$

Map: $R(\boldsymbol{x}(t),t) = \boldsymbol{x}(t+T)$

The Poincaré map is area preserving or sympletic in dimensions larger than 2

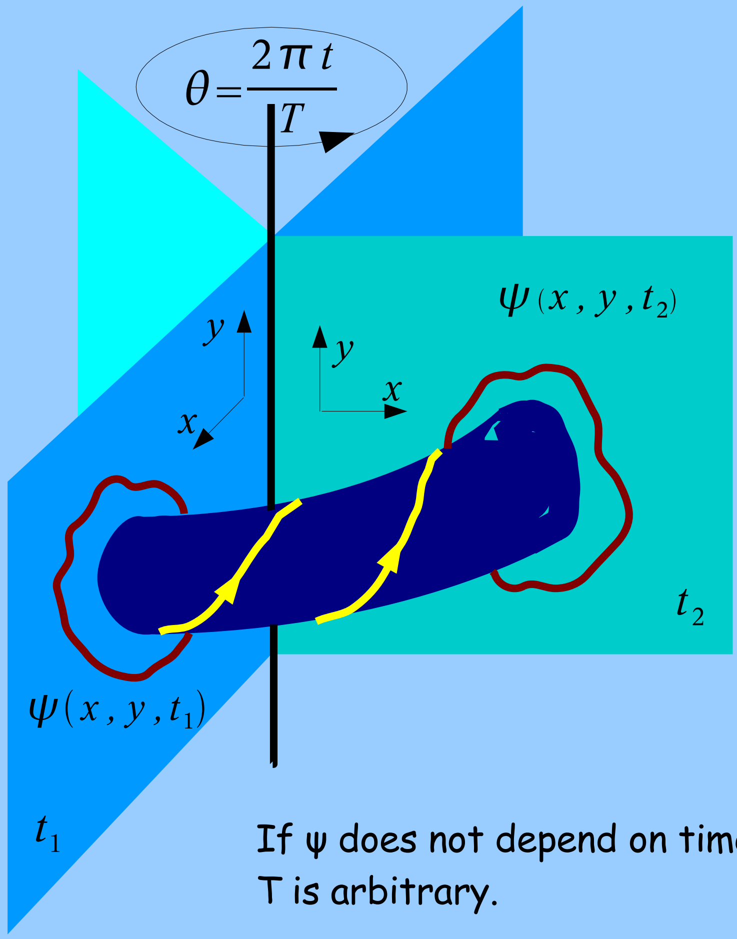

If ψ does not depend on time, T is arbitrary.

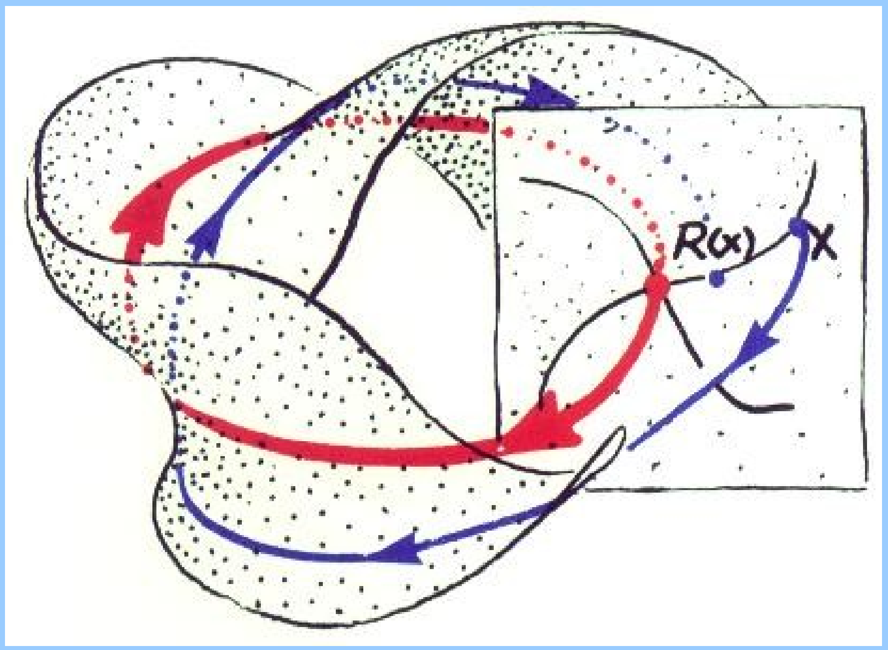

Ottino

Let us return now to our integrable Hamiltonian, consider that it is time-independent and apply some small perturbation, also time-independent assuming, for the moment, that it remains integrable

Using the non-perturbed action-angle coordinates, the perturbed Hamiltonian is

$$H(\boldsymbol{I},\boldsymbol{\theta})=H_0(I)+\epsilon H_1(\boldsymbol{I},\boldsymbol{\theta})$$

If it is integrable, there are new action coordinates $\boldsymbol{I}'$ such that

$$H(\boldsymbol{I},\boldsymbol{\theta})=H'(\boldsymbol{I}')$$

Here we use again the trick of the generating function $S(\boldsymbol{I}',\boldsymbol{\theta})$ such that

$$\boldsymbol{I}=\frac{\partial S(\boldsymbol{I}',\boldsymbol{\theta})}{\partial\boldsymbol{\theta}}\qquad\qquad \boldsymbol{\theta}'=\frac{\partial S(\boldsymbol{I}',\boldsymbol{\theta})}{\partial\boldsymbol{I}'}$$

and we try to solve pertubatively the Hamilton-Jacobi equation

$$H\left(\frac{\partial S}{\partial\boldsymbol{\theta}},\boldsymbol{\theta}\right)=H'(\boldsymbol{I}')$$

with $S=\boldsymbol{\theta}\cdot\boldsymbol{I}'+\epsilon S_1+\epsilon^2 S_2+\dots$

At order 0 : $\boldsymbol{I}'=\boldsymbol{I}$ and $\boldsymbol{\theta}=\boldsymbol{\theta}'$

The perturbed problem writes

$$H_0\left(\boldsymbol{I}'+\epsilon\frac{\partial S_1}{\partial\boldsymbol{\theta}}+\epsilon^2\frac{\partial S_2}{\partial\boldsymbol{\theta}}+\dots\right)+\epsilon H_1\left(\boldsymbol{I}'+\epsilon\frac{\partial S_1}{\partial\boldsymbol{\theta}}+\dots,\boldsymbol{\theta}\right)=H'(\boldsymbol{I}')$$

At order 0: $H_0(\boldsymbol{I})=H'(\boldsymbol{I}')$

At order 1: $\dfrac{\boldsymbol{\omega_0}\cdot\partial S_1}{\partial\boldsymbol{\theta}}+H_1(\boldsymbol{I}',\boldsymbol{\theta})=0$ with $\boldsymbol{\omega_0}(\boldsymbol{I}')=\dfrac{\partial H_0}{\boldsymbol{I}}(\boldsymbol{I}')$

III.5 Perturbed Hamiltonian

III.6 KAM theorem

At order 1: $\frac{\boldsymbol{\omega}_0 \cdot \partial S_1}{\partial \boldsymbol{\theta}} + H_1(\boldsymbol{I}', \boldsymbol{\theta}) = 0$ with $\boldsymbol{\omega}_0(\boldsymbol{I}') = \frac{\partial H_0}{\boldsymbol{I}}(\boldsymbol{I}')$

Let us know expand $H_1(\boldsymbol{I}', \boldsymbol{\theta})$ and $S_1(\boldsymbol{I}', \boldsymbol{\theta})$ as a Fourier series in θ

$$H_1 = \sum_{\boldsymbol{m}} \hat{H}_{1,\boldsymbol{m}}(\boldsymbol{I}') \exp(i\, \boldsymbol{m} \cdot \boldsymbol{\theta})$$
$$S_1 = \sum_{\boldsymbol{m}} \hat{S}_{1,\boldsymbol{m}}(\boldsymbol{I}') \exp(i\, \boldsymbol{m} \cdot \boldsymbol{\theta})$$

Hence

$$\hat{S}_{1,\boldsymbol{m}}(\boldsymbol{I}') = \frac{i}{\boldsymbol{m} \cdot \boldsymbol{\omega}_0(\boldsymbol{I}')} \hat{H}_{1,\boldsymbol{m}}(\boldsymbol{I}') \exp(i\, \boldsymbol{m} \cdot \boldsymbol{\theta})$$

Clearly, the convergence of the pertubative series requires that there is no integer vector $\boldsymbol{m}$ such that $\boldsymbol{m} \cdot \boldsymbol{\omega}_0(\boldsymbol{I}') = 0$

The Kolmogorov-Arnold-Moser theorem says that there are plenty of surviving tori such that $|\boldsymbol{m} \cdot \boldsymbol{\omega}_0| > K(\omega_0) |\boldsymbol{m}|^{-(N+1)}, \forall\, \boldsymbol{m}$
Unbroken tori are transport barriers (in 2D)
There are, however, a large number or resonant tori.
Their ensemble is dense but of Lebesgue measure 0

III.7 Breaking of resonant tori

What happens to resonant tori (Poincaré-Birchoff theorem) ?

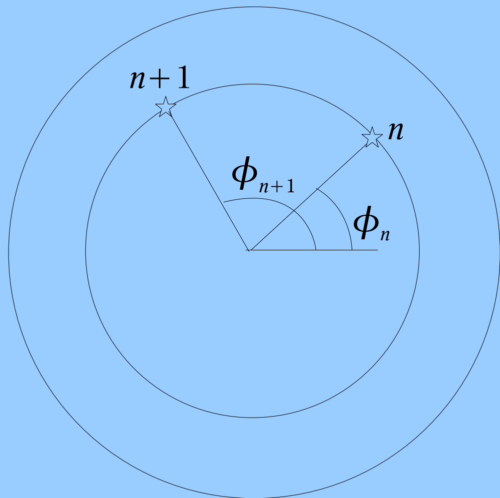

The only case we will consider is that of the Poincaré section of a 1 degree time-independent system $\psi(x, y)$ with an added perturbation of period T

The non perturbed map R is such that

$$r_{n+1} = r_n$$

$$\phi_{n+1} = \phi_n + 2\pi \frac{\omega(r_n)}{\omega_T} \qquad [2\pi]$$

with $\omega_T = \dfrac{2\pi}{T}$

Notice that the period of the Poincaré section is chosen according to the period of the applied perturbation. This is equivalent to increase the dimension of the problem to accommodate the time-dependent perturbation.

If the torus $\tilde{r}$ is resonant, then $\omega(\tilde{r})/\omega_T = p/q$ rational and R^q is identity over the cercle $\tilde{r} : \phi_{n+q}(\tilde{r}) = \phi_n(\tilde{r})$

Now the perturbed map R' is

$$r_{n+1} = r_n + \epsilon\, g(r_n, \phi_n)$$

$$\phi_{n+1} = \phi_n + 2\pi \frac{\omega(r_n)}{\omega_T} + \epsilon\, h(r_n, \phi_n) \qquad [2\pi]$$

which means $\phi_{n+q}(\tilde{r}) = \phi_n(\tilde{r}) + \epsilon\, k(\tilde{r}, \phi_n)$

If in addition $\dfrac{\partial \omega}{\partial r} \neq 0$, q elliptic points and q hyperbolic points are generated along the tori $\tilde{r}$

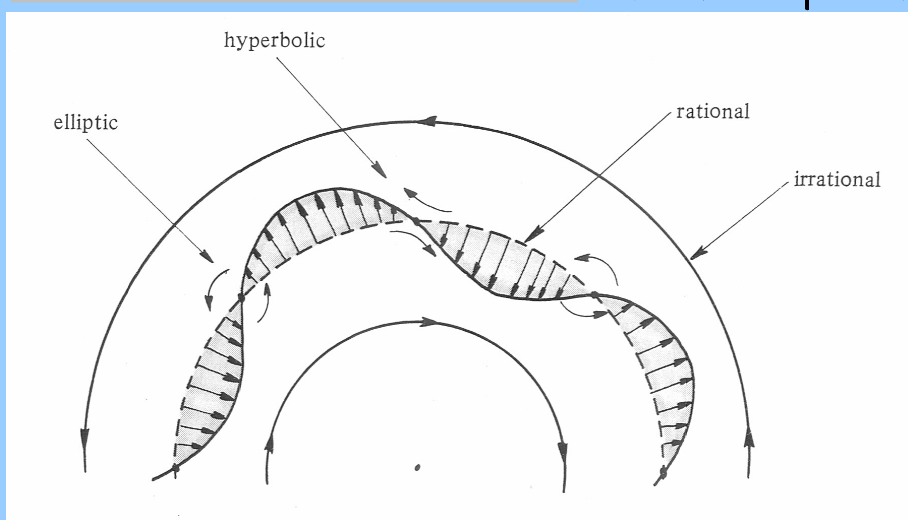

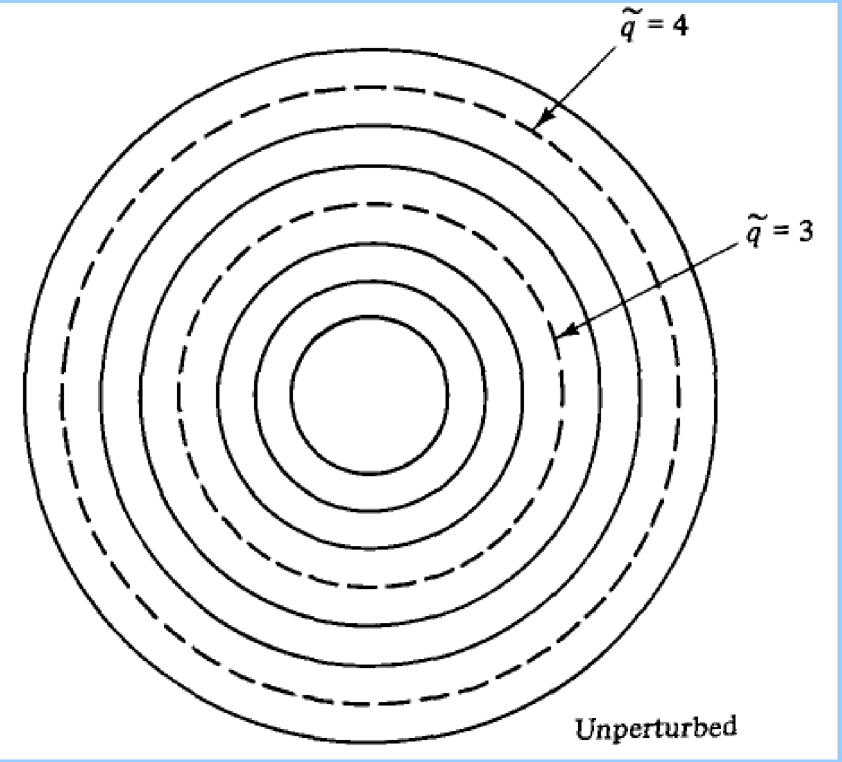

Generation of elliptic and hyperbolic points by breaking tori

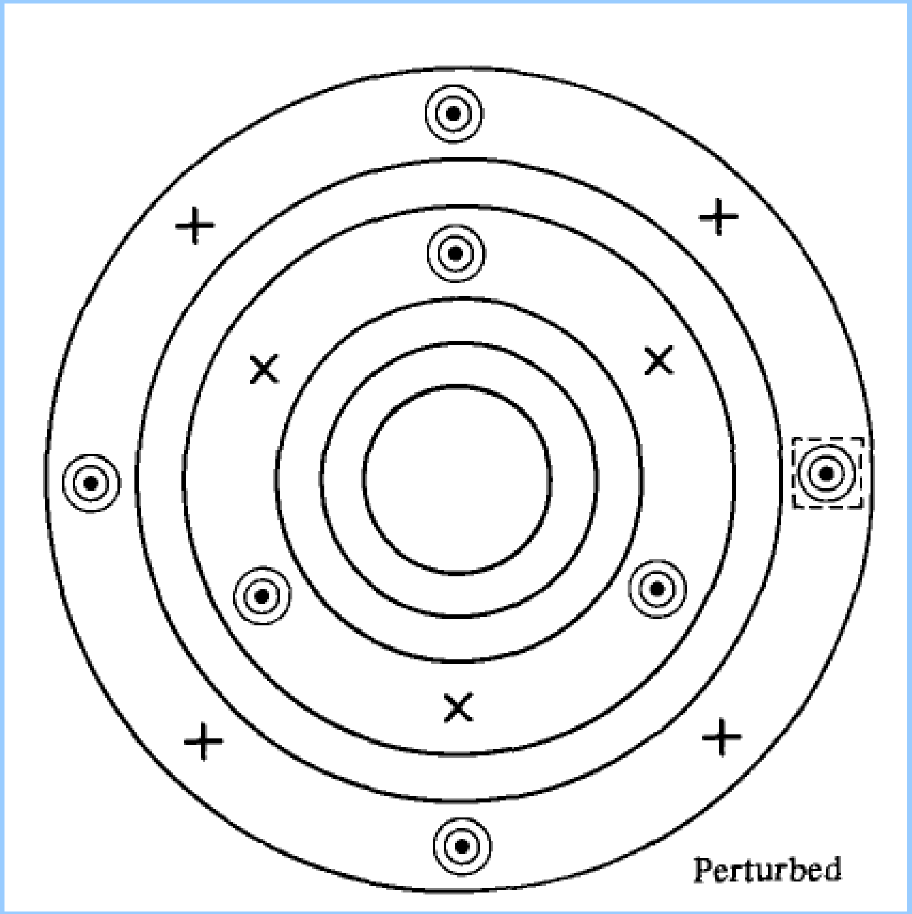

Width of the broken zone

In I is $\sim \left| \dfrac{\partial \omega}{\partial I} \right|^{1/2}$

In ω is $\sim \left| \dfrac{\partial \omega}{\partial I} \right|^{-1/2}$

Two important degenerate cases

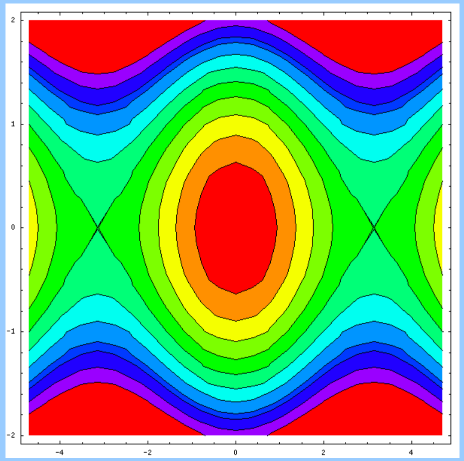

Hyperbolic points already in the unperturbed map

Example $\psi(x,y)=y^2-\cos(x)$

This corresponds to a case where $\omega(\text{separatrix})=0$

Those tori break very easily.

Leads to mixed layer.

(critical layers in the fluid mechnaics literatrure)

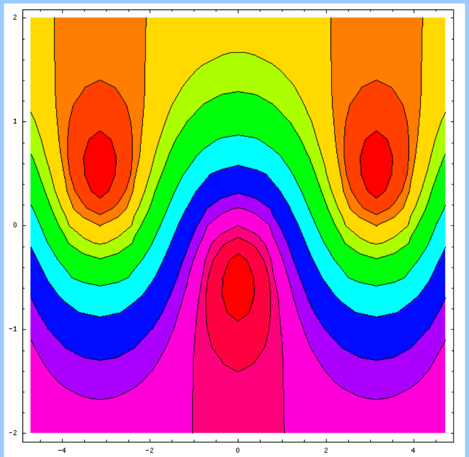

The non-twist condition $\dfrac{\partial \omega}{\partial I}=0$

is met on some tori.

Such tori, if non resonant, are very robust

because resonant tori in the vicinity break over

width $\left|\dfrac{\partial \omega}{\partial I}\right|^{1/2}$

This case is relevant for jets and meandering currents.

Leads to transport barriers

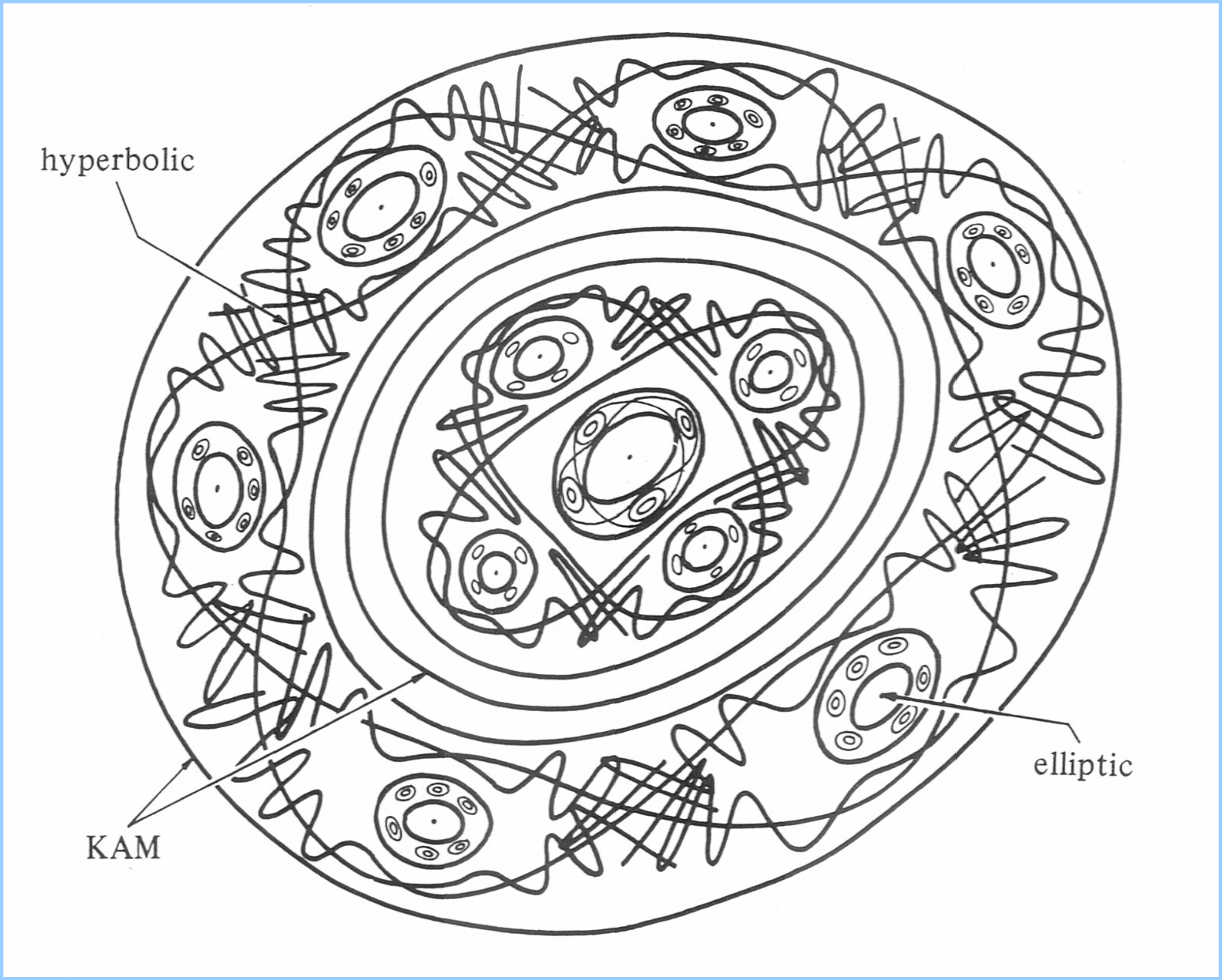

Ottino

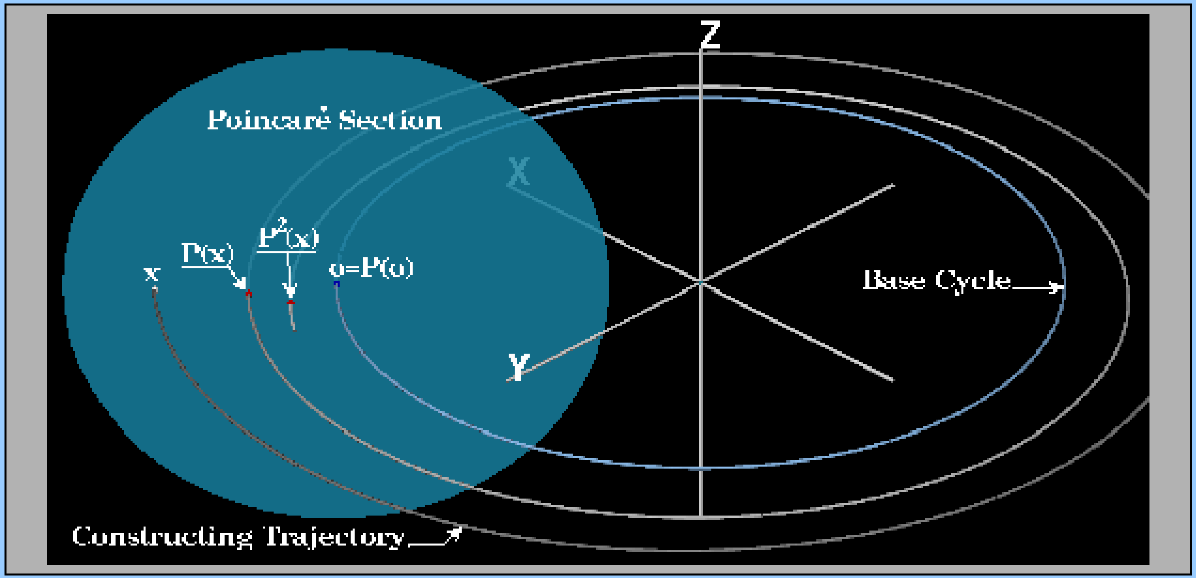

III.7 Invariant stable and unstable hyperbolic manifolds

H. Löffelmann

Generation of
an invariant curve from
a fixed hyperbolic point

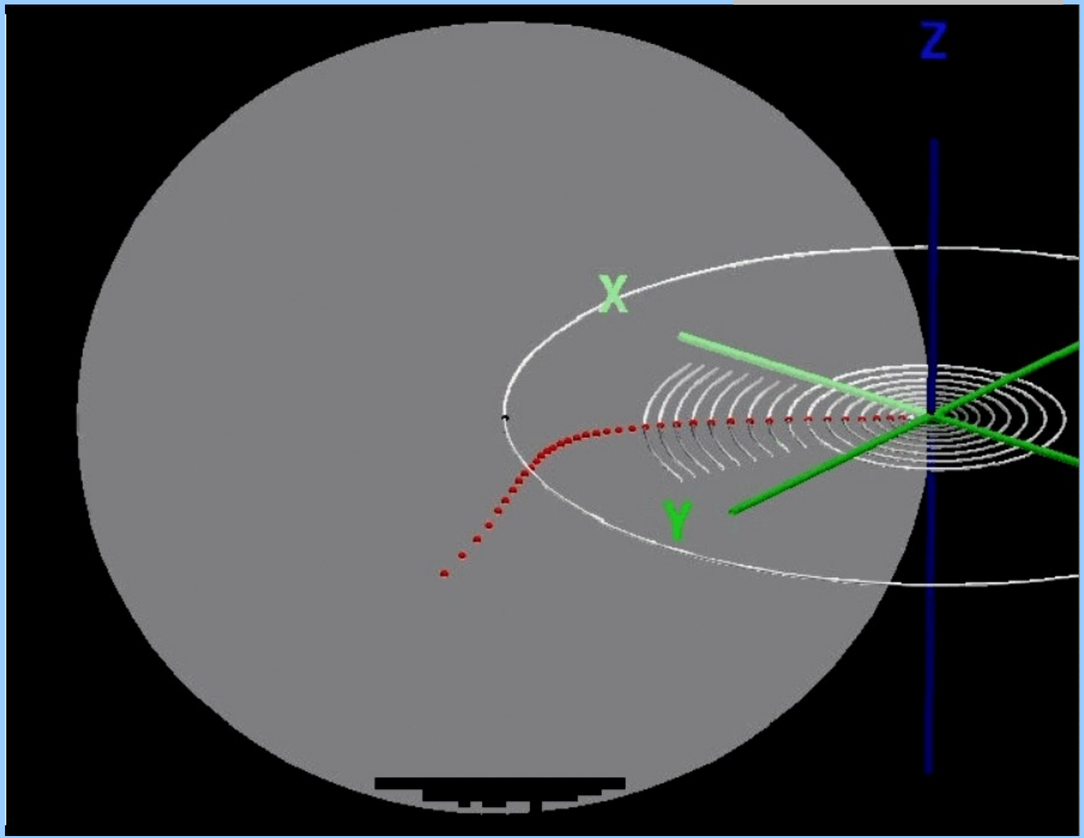

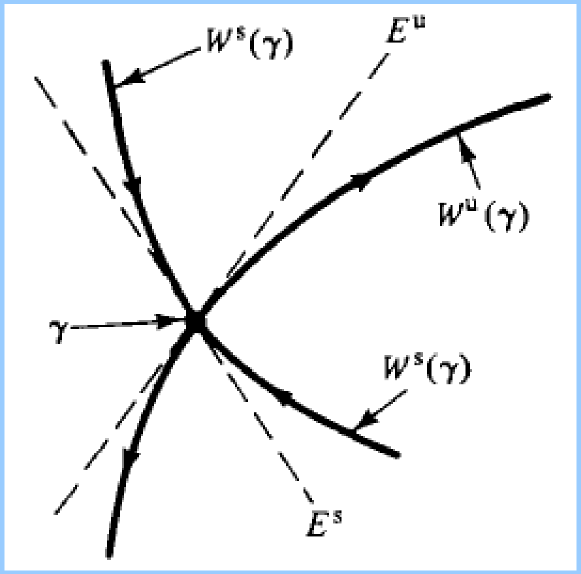

Trajectories contained in the stable manifold W_s converge to the hyperbolic point as time -> ∞ and trajectories contained in the unstable manifold W_u converge to the hyperbolic point as time -> -∞.

They are tangent to linear stable and unstable directions of the hyperbolic point

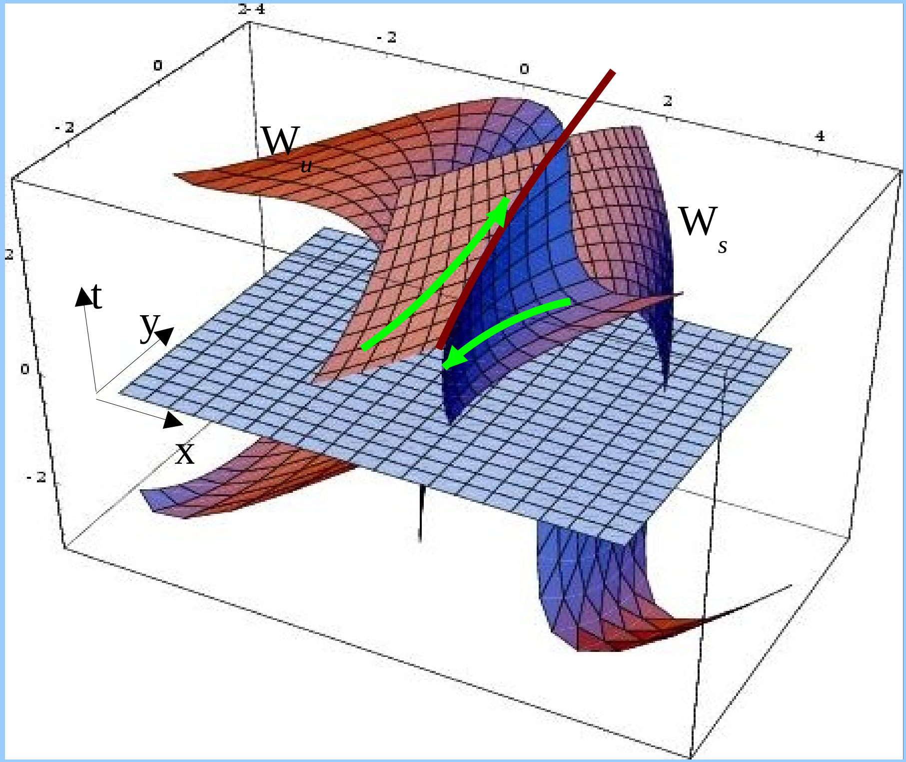

Stable or unstable manifolds can fold but cannot cross themselves (due to symplectic properties).

The stable and unstable manifold of an hyperbolic point, or of two adjacent hyperbolic points, can cross and, worse, if they cross once, they must cross infinitely many times.

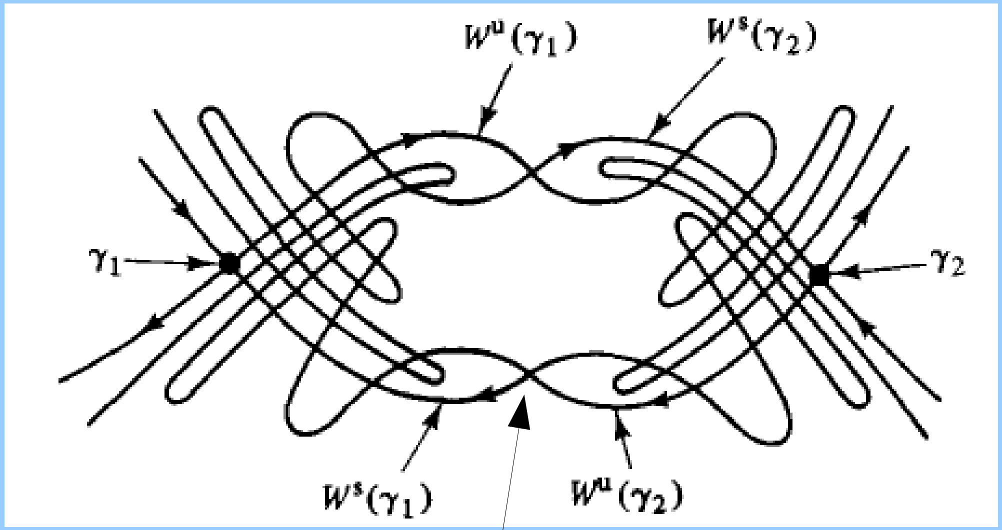

Heteroclinic point

III.9 Hyperbolic tangle and chaos

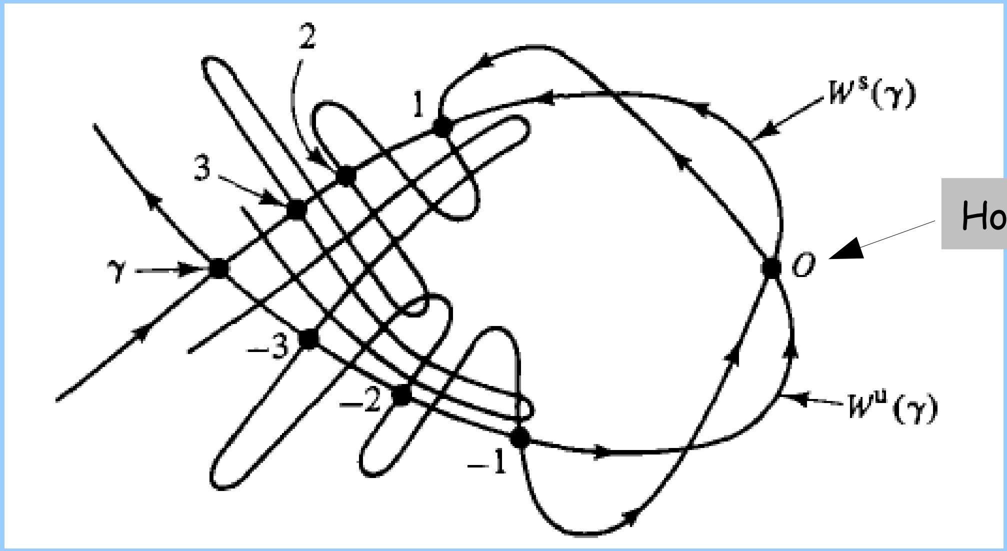

Homoclinic point

Dots are images and pre-images of the homoclinic point by the Hamiltonian mapping.

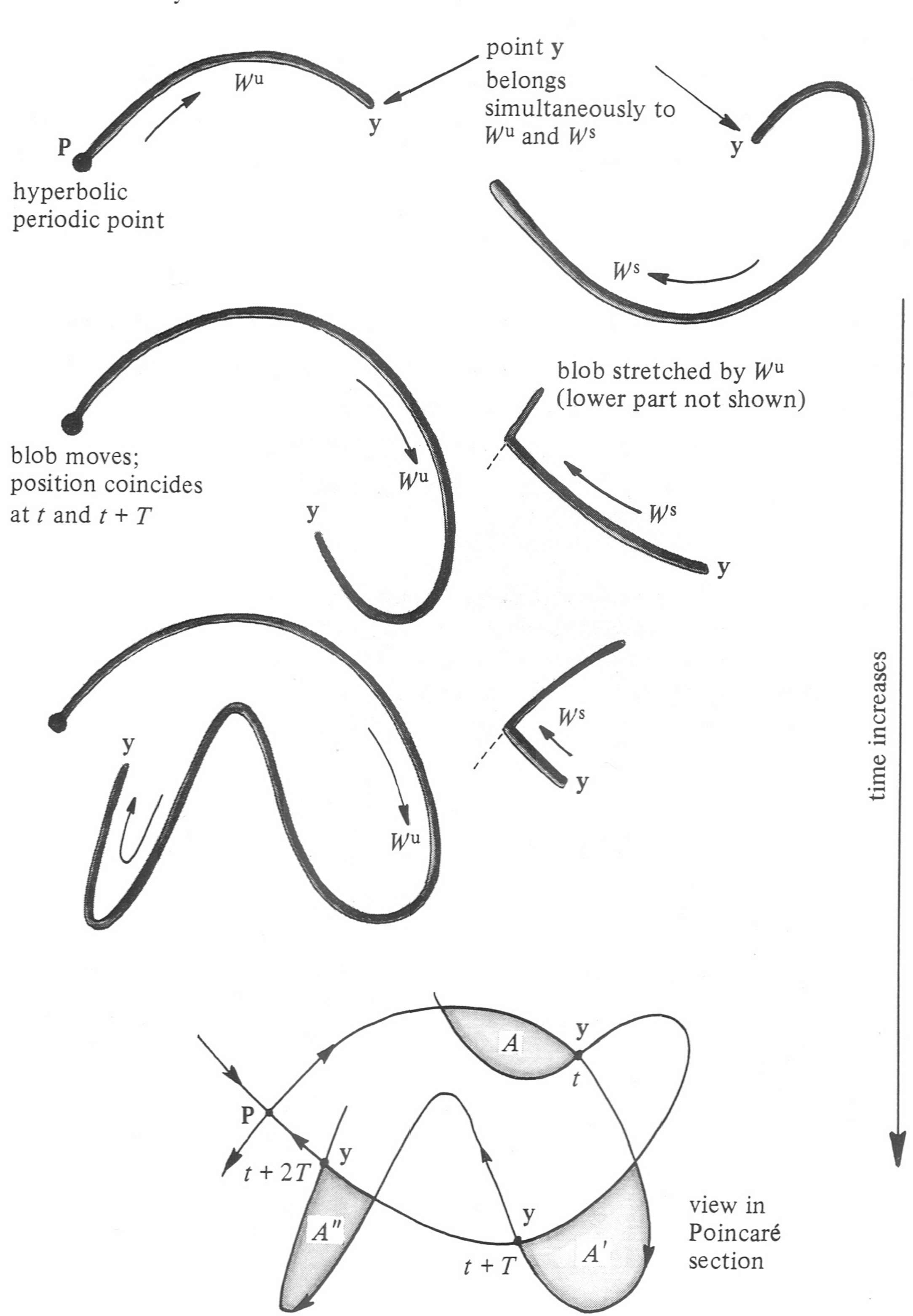
point y
belongs
simultaneously to
W^u and W^s
P
hyperbolic
periodic point
W^u
y
y
W^s
blob stretched by W^u
(lower part not shown)
blob moves;
position coincides
at t and $t + T$
W^u
y
W^s
y
y
W^s
y
W^u
time increases
A
y
t
P
$t + 2T$
y
A''
y
$t + T$
A'
view in
Poincaré
section

Ottino

Hence, chaos

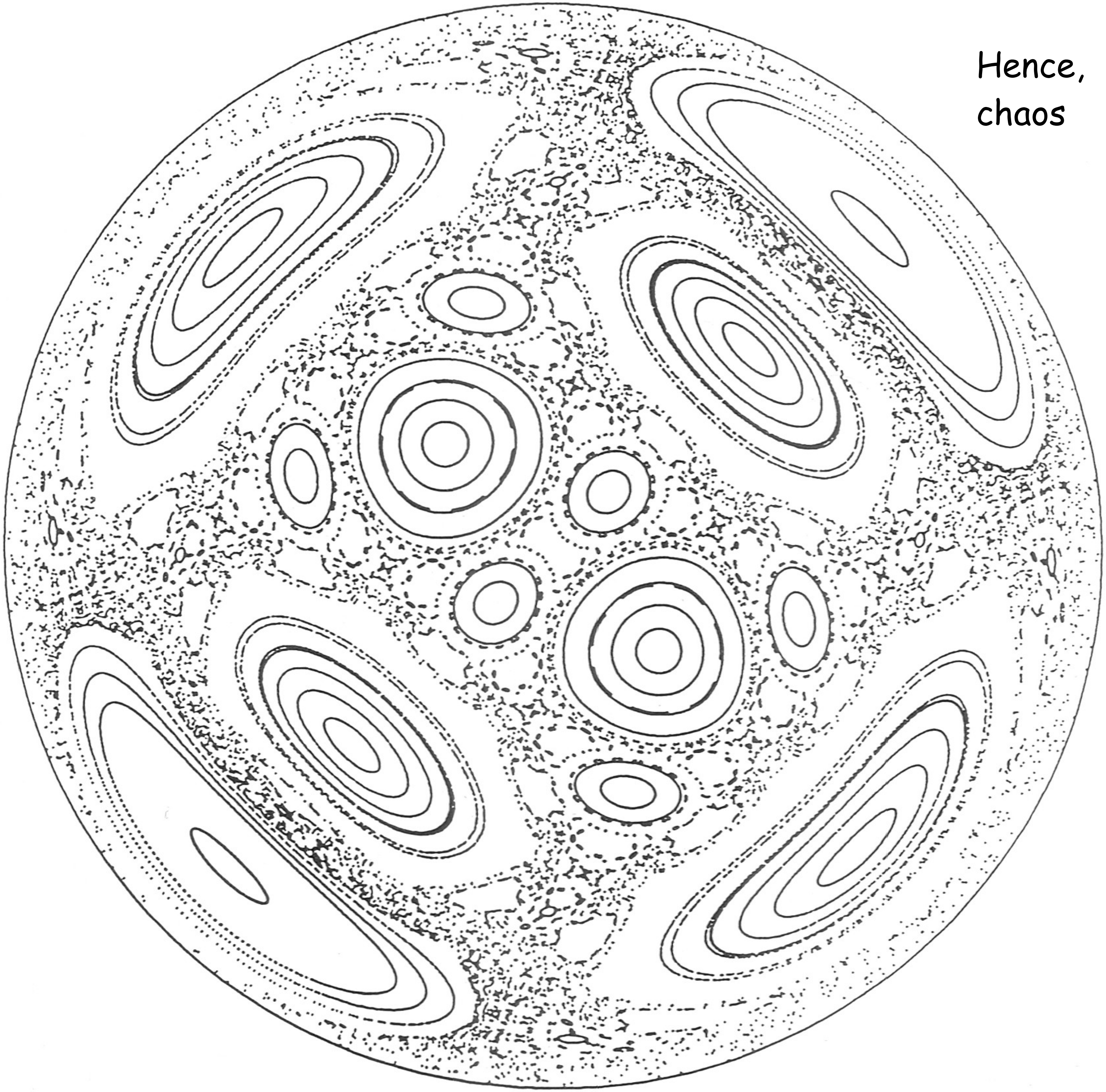

Relation with Lyapunov exponents:

The Lyapunov exponent (calculated in the $t \to \infty$ limit) is zero for integrable orbits of an Hamiltonian system.

Non zero (positive) Lyapunov exponents characterizes chaos.

Ergodic theorem (Oseledec) says that the Lyapunov exponent is unique within a chaotic domain except for a set of (Lebegue) measure 0.
This leaves the possibility of lines of high or low Lyapunov embedded within the chaotic domain.

III.10 Lobe dynamics

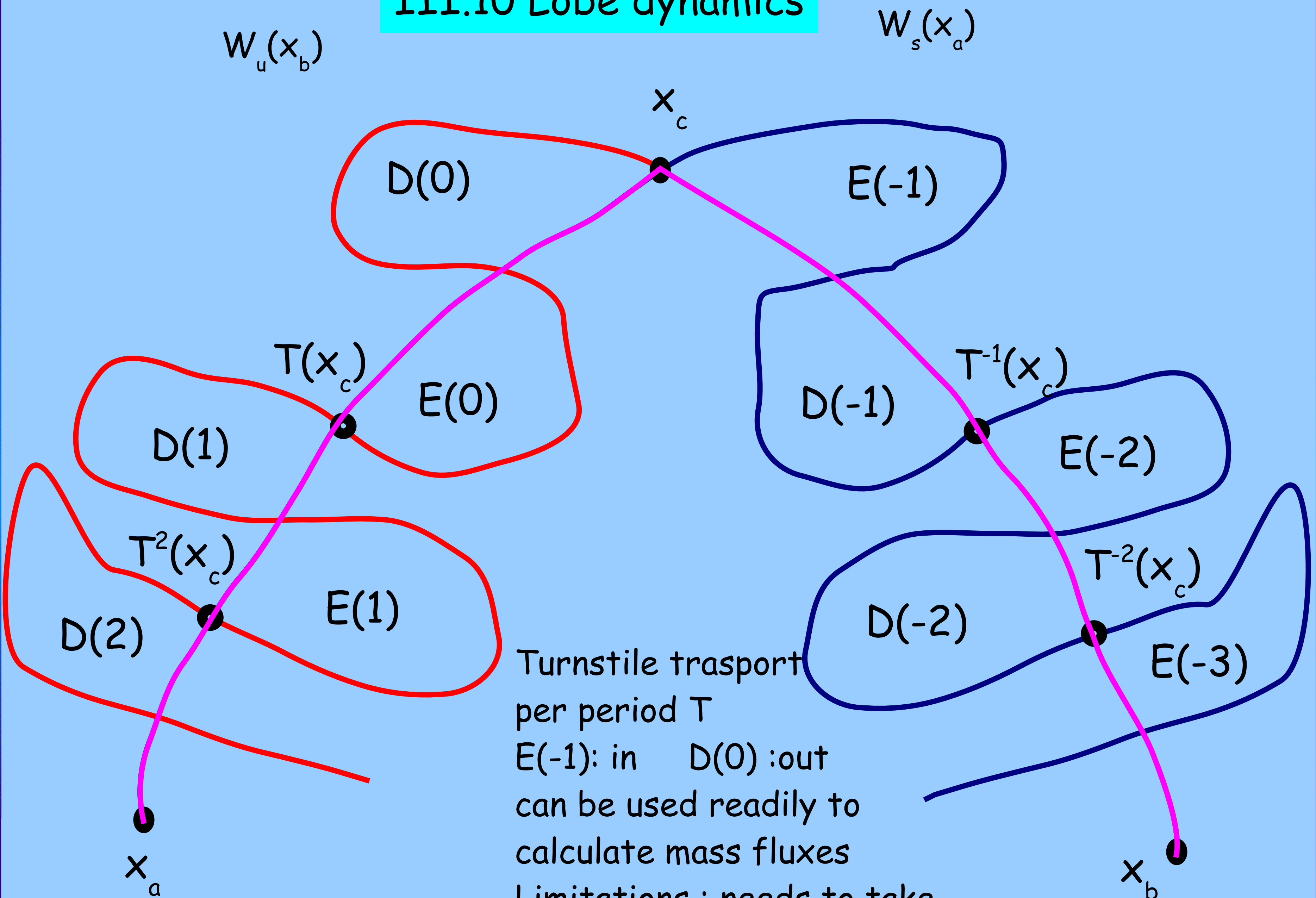

Turnstile trasport per period T

E(-1): in D(0) :out

can be used readily to calculate mass fluxes

Limitations : needs to take into account islands and lobe intersections

Part III Summary

- Advection by 2D incompressible flow is readily put under Hamiltonian form
- Stationary 2D flows are integrable
- In a general integrable system of degree N, motion is restricted to tori of dimension N in the 2N phase space
- Tori are characterized by a set of N frequencies with are said non resonant when they are incommensurate
- A generic perturbation breaks resonant tori but many non resonant tori remain unbroken (KAM)
- In 2D stationary flows, resonance is possible with a periodic perturbation.
- Unbroken tori in 2D are barriers to transport.
- Most easily broken tori are separatrices if the streamfunction
- Most robust tori lie near the core of jets satisfying non-twist condition.
- Chaos is generated by intersecting hyperbolic stable and unstable manifolds.
- Lyapunov exponent is positive only in chaotic regions.
- Lobe dynamics can be used to calculate transport whenevr it is relevant to consider hyperbolic manifolds as frontier boundaries.

Part IV Stirring and transport barriers real flows

IV.A Hyperbolic skeleton of non periodic flows

- 1 Stable and unstable invariant lines and surfaces
- 2 Local criteria
- 3 Finite size Lyapunov exponents
- 4 Distinguished hyperbolic trajectories
- 5 Numerical and laboratory example
- 6 Transport in the Mediterranea – Lagrangian coherent structures
- 7 Hyperbolic skeleton of the polar vortex – lobe dynamics at work, mixing layer and transport barrier

IV.B A quantitative measure of exchange across barriers

Part IV Stirring and transport barriers real flows

IV.A Hyperbolic squeleton of non periodic flows

IV.B A quantitative measure of transport across barriers

- 1 Effective diffusivity
- 2 Effective diffusivity in the atmosphere
- 3 The failure in comparing effective diffusivity and Lyapunov exponents
- 4 The solution to the failure: the transverse Lyapunov exponent
- 5 Applications

IV.A.1 Stable and unstable hyperbolic invariant lines and surfaces

Hyperbolic trajectories are non stationary and frame independent extensions of stagnation points.

Trajectories contained in the stable manifold W_s converge to the hyperbolic trajectory as time -> ∞ and trajectories contained in the unstable manifold W_u converge to the hyperbolic trajectory as time -> -∞.

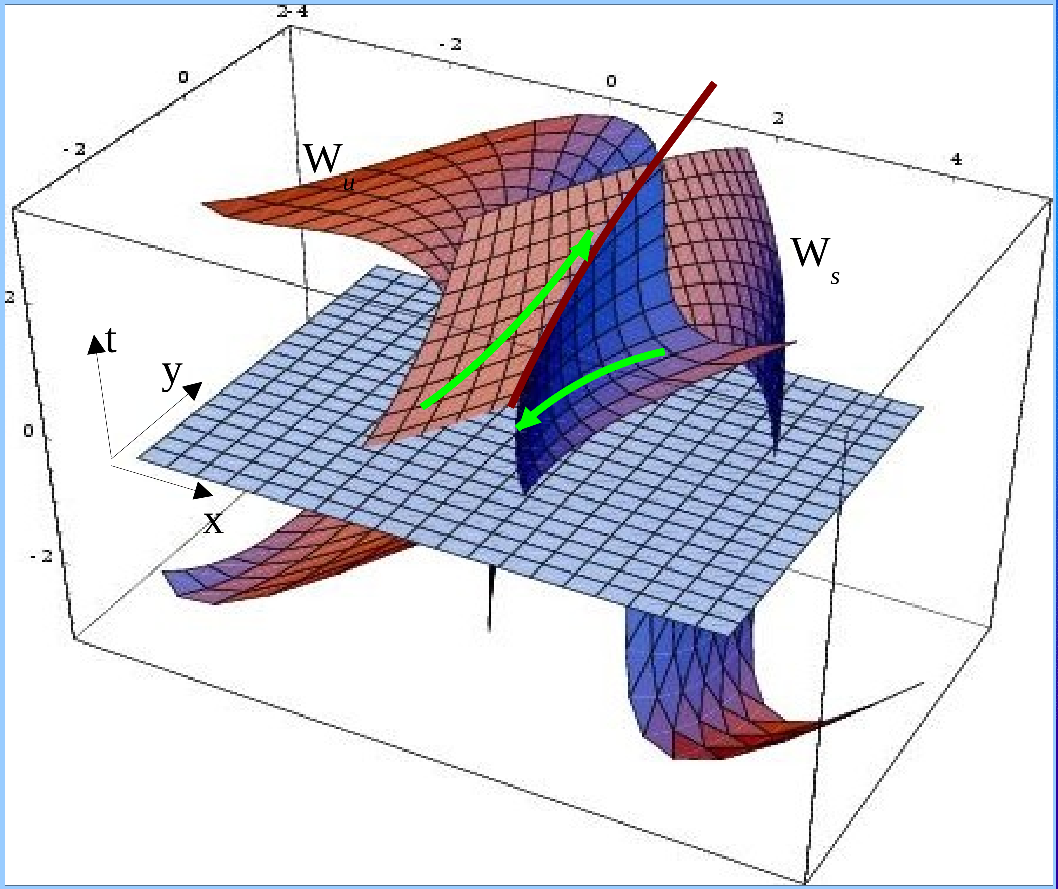

Definition of hyperbolic lines and surfaces

Haller and Yuan, 2000

Finite-time instability requires exponential separation on arbitrarily short time intervals

M is an unstable material surface, in (x, y, t), on the time interval I_u if there is a positive exponent λ_u such that for any close enough initial condition $\boldsymbol{p}(\tau)=(\boldsymbol{x}(\tau), \tau)$ and for any small time step $h>0$ we have, for τ and $\tau+h$ from I_u

$$\mathrm{dist}(\mathbf{p}(\tau+h), M) \geqslant \mathrm{dist}(\mathbf{p}(\tau), M) \exp(\lambda_\mathrm{u} h)$$

$$\text{or } |N(\mathbf{x}(\tau+h), \tau+h) \cdot DF^h(\mathbf{x_0}) N(\mathbf{x_0}, \tau)| \geqslant \exp(\lambda_\mathrm{u} h)$$

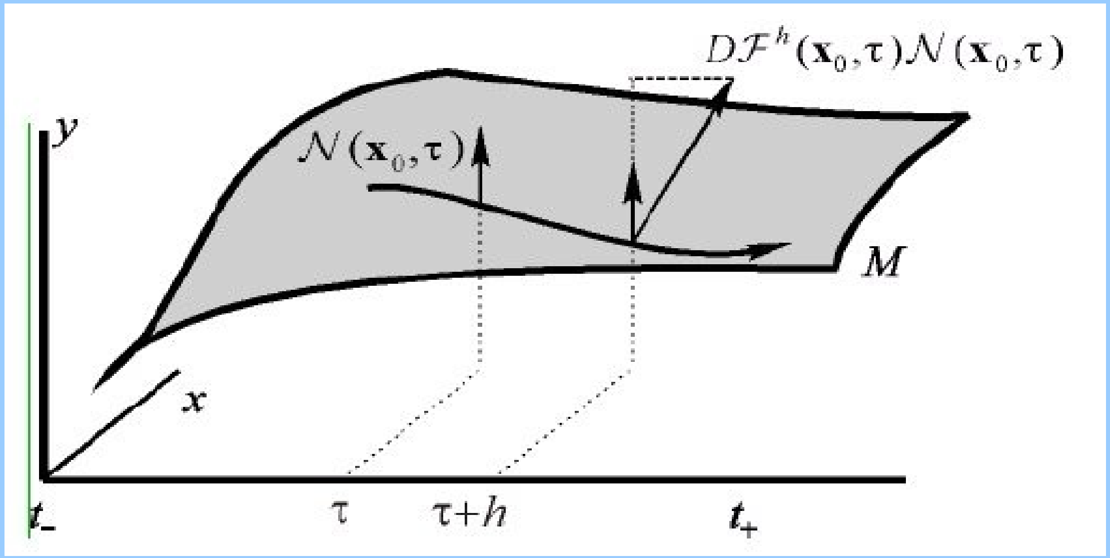

A stable material surface is a smooth material surface that is unstable backward in time.

An unstable (stable) material line is the t=constant section of an unstable (stable) material surface.

Both referred as hyperbolic material surfaces (lines)

If the flow is incompressible, trajectories

must converge to each other on M .

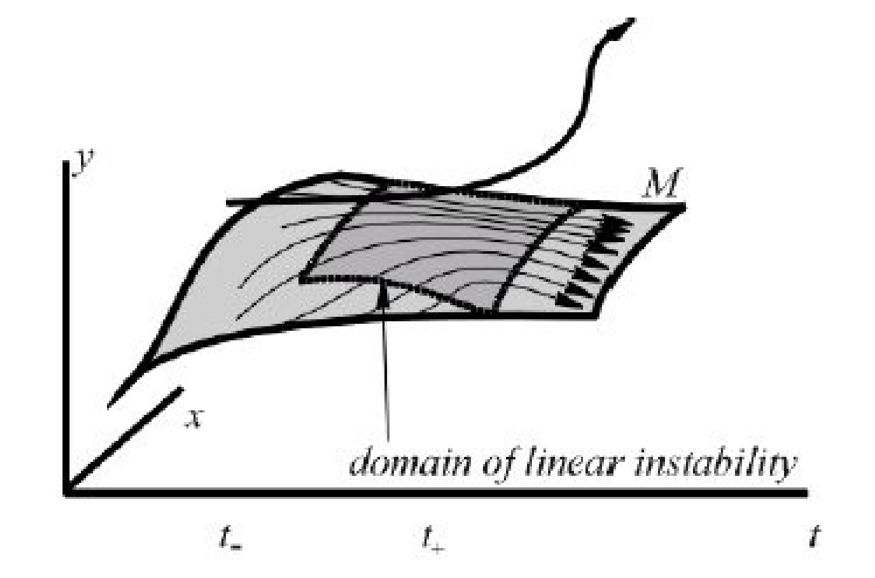

Okubo-Weiss criterion for Eulerian hyperbolicity

$\det\nabla u < 0$: hyperbolic region, particles separate exponentially
$\det \nabla u > 0$: elliptic region, particles circle around

This interpretation requires, however, the flow to be frozen along a material trajectory. Not true generally.

Using strain coordinates

Introduce Ω, the rotation rate of of the strain axes. The effective rotation is $\Omega_{eff} = \omega/2 - \Omega$ (ω vorticity). Then define $r=\Omega_{eff}/\sigma$ where σ is the strain rate, then:
$|r| < 1$: hyperbolic region
$|r| > 1$: elliptic region (Hua-Klein-Okubo-Weiss)

IV.A.2 Local criteria

Generalised criterion in the strain basis
(Lapeyre, Hua & Legras, 2001; Haller, 2001b)

Transform the dispersion equation from the fixed frame to the frame of the strain axis using the rotation matrix $\mathbf{R}$ defined by the orthonormal basisof the eigenvectors of the strain matrix $\nabla \mathbf{u} + {}^{T}\nabla \mathbf{u}$.

If the line element ξ satisfies $\dot{\xi} = \nabla \mathbf{u} \, \xi$ in the fixed frame, the rotated element $\xi' = \mathbf{R}^{-1} \xi$ satisfies

$$\dot{\xi}' = (\mathbf{R}^{-1} \nabla \mathbf{u} \, \mathbf{R} - \mathbf{R}^{-1} \dot{\mathbf{R}}) \, \xi' = [\nabla \mathbf{u}]_{\text{strain}} \, \xi',$$

where the matrix $[\nabla \mathbf{u}]_{\text{strain}}$ is a function of the strain rate σ and the effective rotation.

Defining $r = \dfrac{\text{effective rotation}}{\text{strain}} = \dfrac{\text{vorticity - strain axis rotation}}{\text{strain}}$, the relative orientation ζ of the line element with the strain axis satisfies

$$\dot{\zeta} = \sigma (r + \cos(\zeta))$$

while the length of the line element satisfies

$$\frac{1}{|\xi|^2} \frac{D}{Dt} |\xi|^2 = \sigma \sin(\zeta)$$

Lapeyre, Klein & Hua, 1999 ; *Klein, Lapeyre & Hua*, 2000

Generalised criterion in the strain basis
(Lapeyre, Hua & Legras, 2001; Haller, 2001b)

Transform the dispersion equation from the fixed frame to the frame of the strain axis using the rotation matrix $\mathbf{R}$ defined by the orthonormal basisof the eigenvectors of the strain matrix $\nabla\mathbf{u}+{}^{T}\nabla\mathbf{u}$.

If the line element ξ satisfies $\dot{\xi}=\nabla\mathbf{u}\,\xi$ in the fixed frame, the rotated element $\xi'=\mathbf{R}^{-1}\xi$ satisfies

$$\dot{\xi}'=(\mathbf{R}^{-1}\nabla\mathbf{u}\,\mathbf{R}-\mathbf{R}^{-1}\dot{\mathbf{R}})\,\xi'=[\nabla\mathbf{u}]_{\text{strain}}\,\xi',$$

where the matrix $[\nabla\mathbf{u}]_{\text{strain}}$ is a function of the strain rate σ and the effective rotation.

Defining $r=\dfrac{\text{effective rotation}}{\text{strain}}=\dfrac{\text{vorticity - strain axis rotation}}{\text{strain}}$, the relative orientation ζ of the line element with the strain axis satisfies

$$\dot{\zeta}=\sigma(r+\cos(\zeta))$$

while the length of the line element satisfies

$$\frac{1}{|\xi|^2}\frac{D}{Dt}|\xi|^2=\sigma\sin(\zeta)$$

Lapeyre, Klein & Hua, 1999 ; *Klein, Lapeyre & Hua*, 2000

Assuming that r *is slowing varying*

$|r|<1$ *defines the hyperbolic region H where the line element is growing exponentially* ¿

$|r|>1$ *defines the elliptic region E where the line element does not grow or grows weakly*

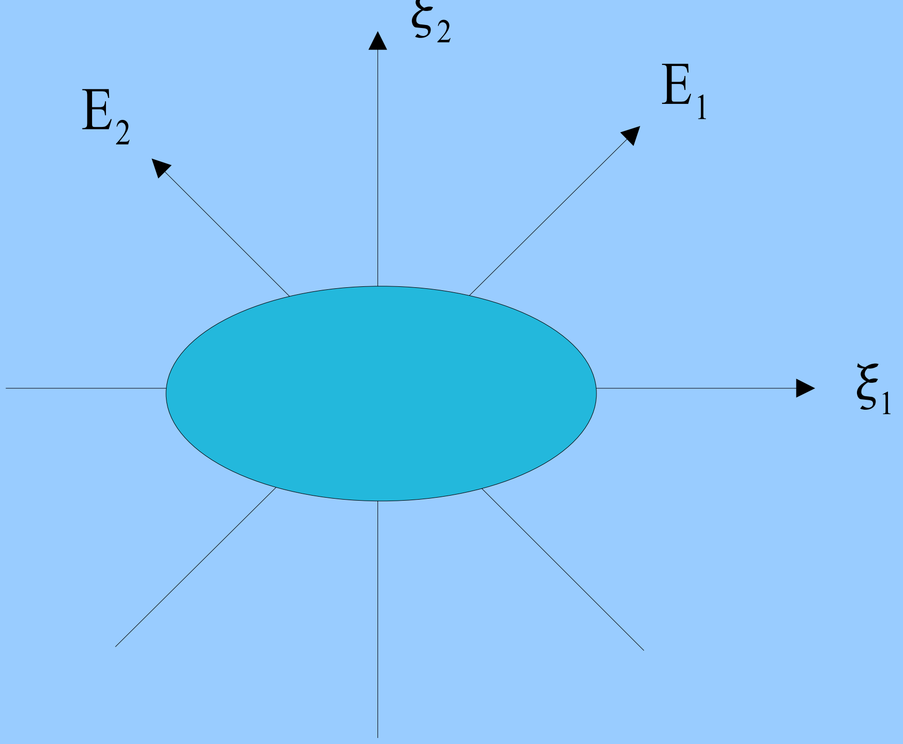

E_1 *and* E_2 *eigendirections of the strain operator* $\nabla u + \nabla^T u$

ξ_1 *and* ξ_2 *directions of zero extension ('zero strain set') (G. Haller, 2001)*

Detection of hyperbolic lines by finite-time statistics

Local extrema of patchiness (average displacement in one direction) [*Malhotra et al., 1998; Poje et al., 1999*]

Local extrema of Lyapunov exponents

Local extrema of relative dispersion or finite-size Lyapunov exponents [*Bowman, 2000; Joseph & Legras, 2001*]

Repelling material lines <--> stable manifolds of hyperbolic trajectories

Attracting material lines <--> unstable manifolds of hyperbolic trajectories

The definition of finite-time hyperbolic material lines implies non uniqueness. Two nearby unstable surfaces are such that $\mathrm{dist}_{t\in I}(M, M') < C\,\mathrm{e}^{-\lambda_u \tau_u}$ where τ_u is the length of I_u.

(Haller and Poje, 1998)

Material lines that are hyperbolic for long enough time intervals will appear to be locally unique up to exponentially small errors.

IV.A.3 Finite size Lyapunov exponents

Finite size Lyapounov exponents (FSLE)

Let $\delta(\mathbf{x},t,\tau)$ be the separation of a pair of particles at time $t+\tau$. The FSLE is

$$\mu(\mathbf{x},t,\delta_0,r) = \frac{1}{\tau}\ln r\,,$$

where τ is such that $\delta(\mathbf{x},t,\tau) = r\delta(\mathbf{x},t,0) = r\delta_0$. Hence τ is the required time to increase the separation by a factor r (Artale et al., 1997, Phys. Fluids).

For r of the order of a few units, μ describes the diffusion properties at scale δ_0. When $r \gg 1$, the stable and unstable manifolds are obtained by plotting the extrema of μ for forward and backward interation in time, respectively.

IV.A.4 Distinguished hyperbolic trajectories

Pair separation or FSLE do not distinguish any line for purely linear flows (e.g. $u = \gamma\, x$, $v = -g\, y$) for which all trajectories have the same stability properties.

Conjecture: Lines of maximum separation coincide with the repelling and attracting lines of the strongest hyperbolic trajectories. These lines form the hyperbolic skeleton of the flow.

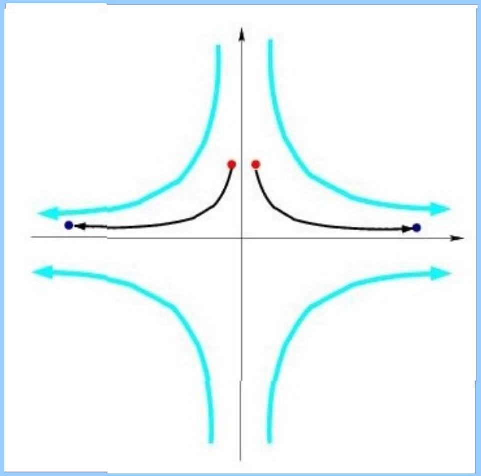

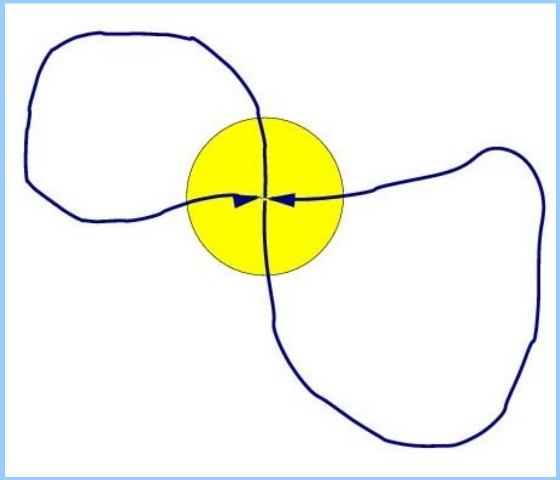

Example I: Locally hyperbolic flow $\psi(x,y)$ = -tanh(x) tanh(y)

Pair separation versus FSLE.
x0: absissa of the initial pair center. Initial separation: 0.1

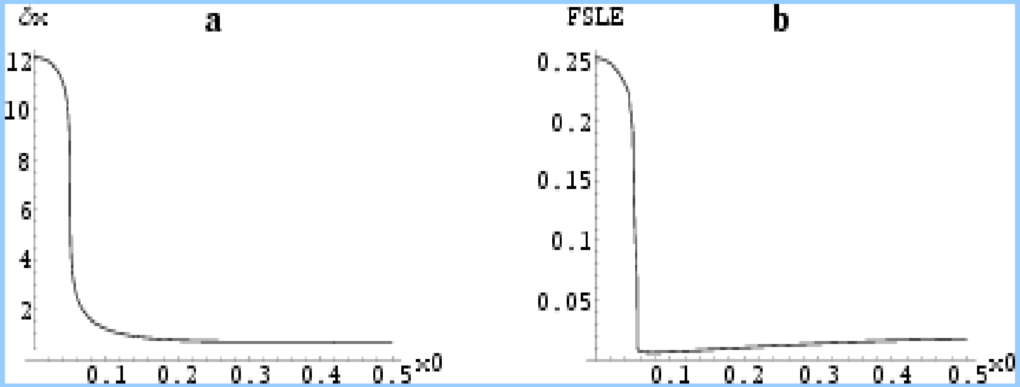

Example II: Pendulum flow $\psi(x,y) = 1/2\ y^2 - \cos(x)$

Pair separation versus FSLE.
ψ: streamfunction at the initial pair center.

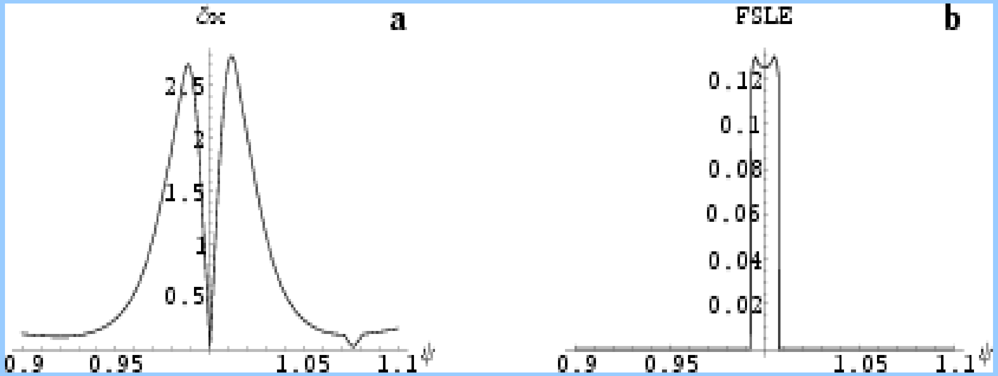

Example I

IV.A.5 numerical and laboratory experiments

A non integrable example: the forced Duffing equation

(Haller, 2000, Chaos)

$$\mathbf{x} = \mathbf{B}\mathbf{x} - \mathbf{N} + \begin{pmatrix} 0 \\ \sin \omega t \end{pmatrix} \qquad (1)$$

where

$$\mathbf{B} = \begin{pmatrix} \sin 2\omega t & \omega + \cos 2\omega t \\ -\omega + \cos 2\omega t & -\sin 2\omega t \end{pmatrix}$$

and

$$\mathbf{N} = (x \cos \omega t - y \sin \omega t)^3 \begin{pmatrix} \sin \omega t \\ \cos \omega t \end{pmatrix}.$$

Taking $\omega = 0.9$, the hyperbolic trajectory at $t = 0$ is on the y-axis in $y_c = 0.170042170231512...$ The unstable manifold is obtained numerically over five periods.

Unstable manifold of the forced Duffing equation

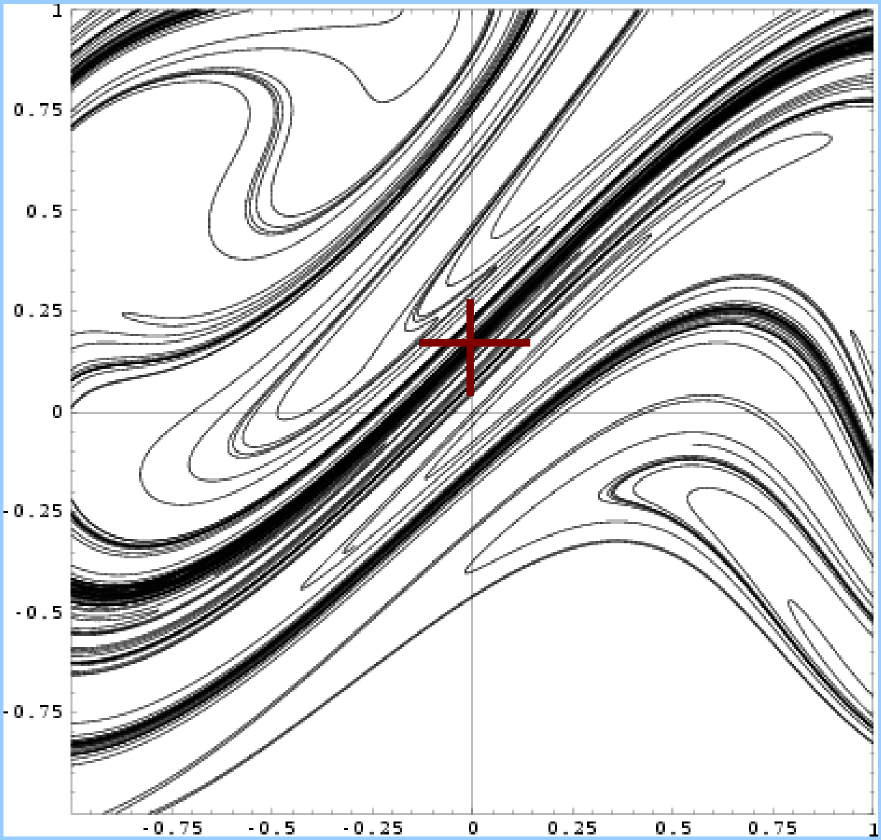

Detection of the hyperbolic lines for Duffing system (*Haller, 2000*)

(a) separation

(b) hyperbolic persistence T_u

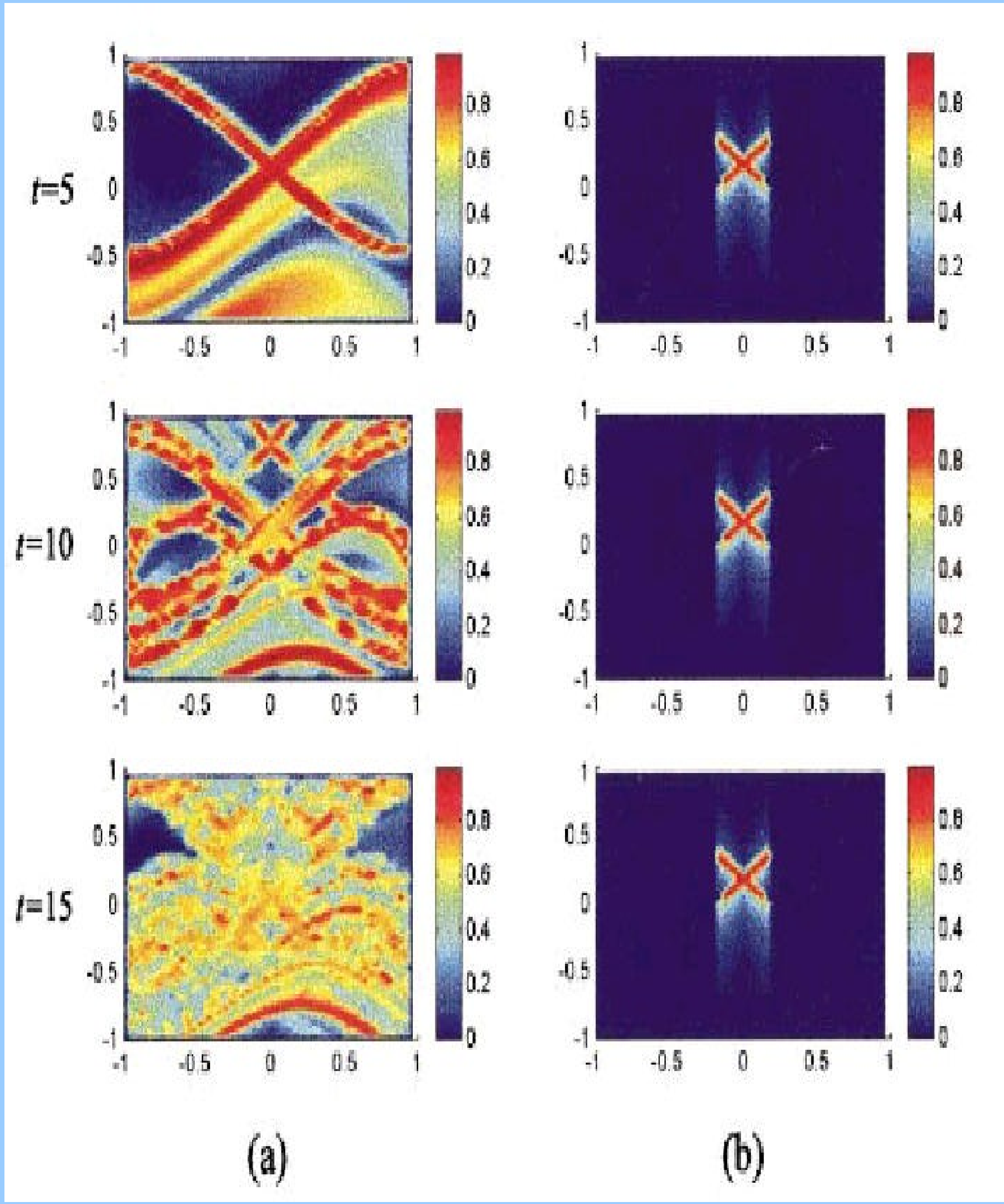

Unstable manifold

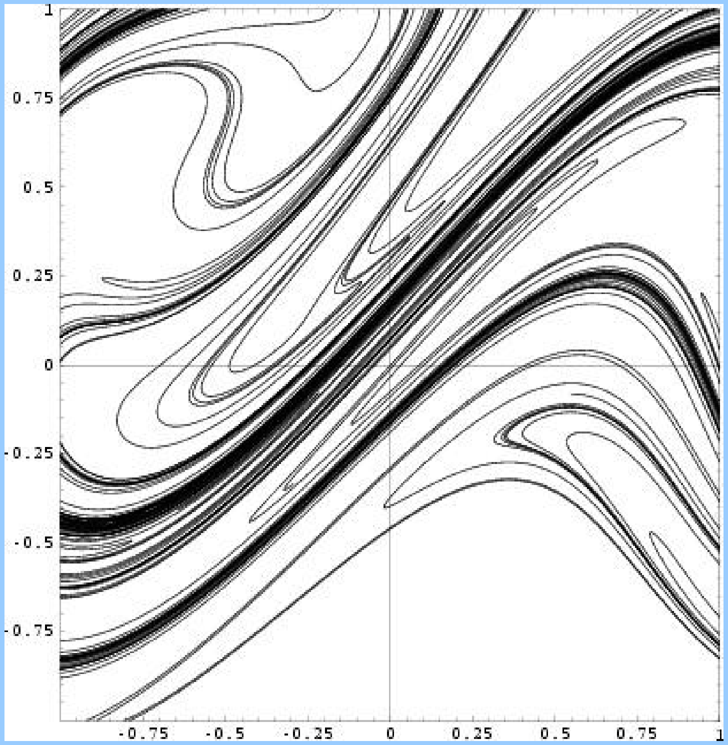

Finite-size Lyapunov exponents
(*Joseph and Legras, 2001*)

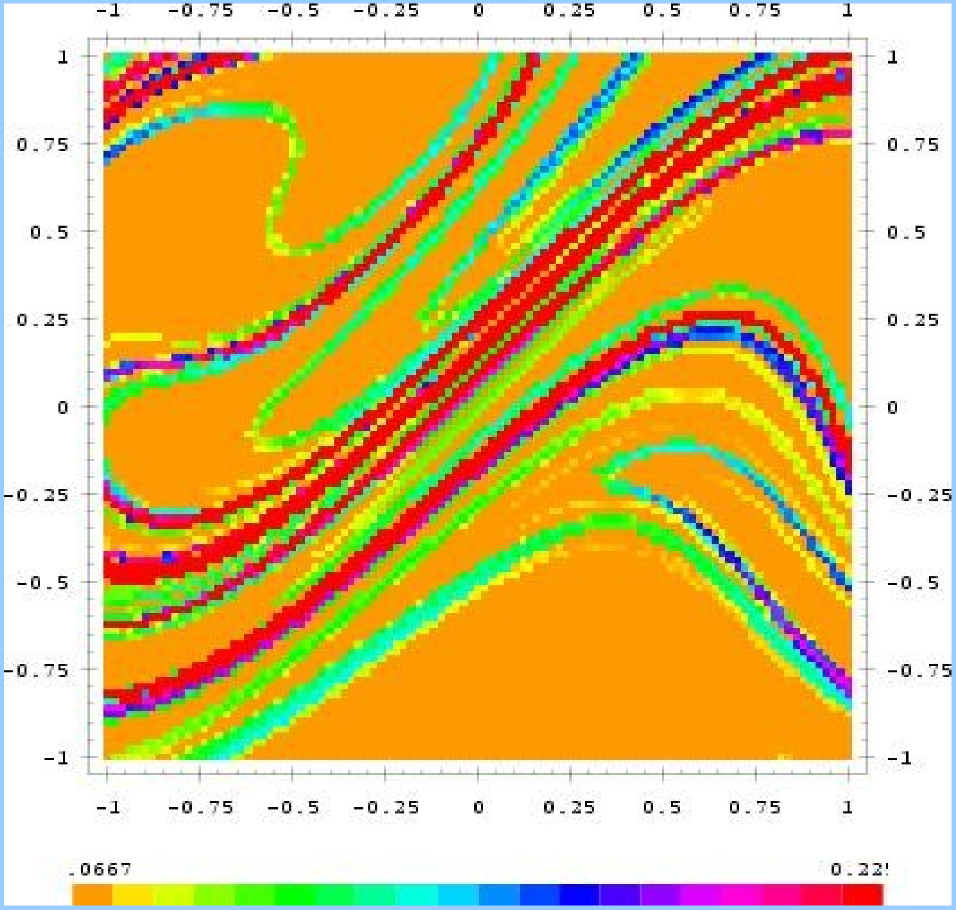

Example II:2-D experimental periodic flow (*Voth, Haller & Gollub, 2001*)

Experiment in a stratified electrolytic flow forced periodically. Parameters Re = UL/ν, $p = UT/L$ (mean path length)

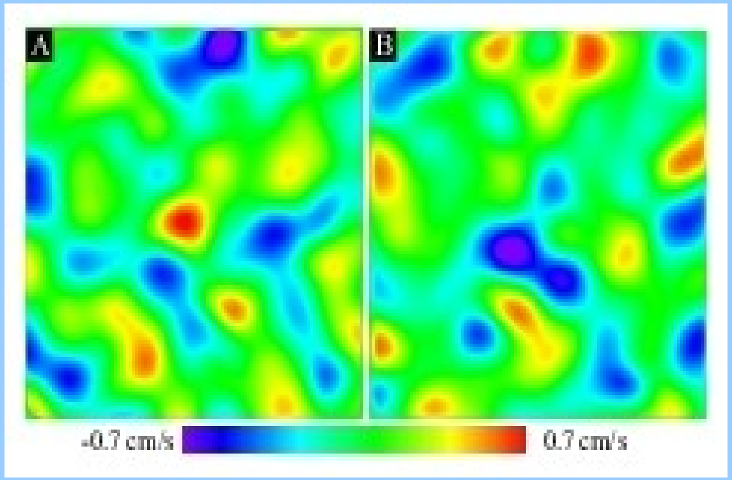

Map of one component of velocity at two different times (Re = 45, p=1)

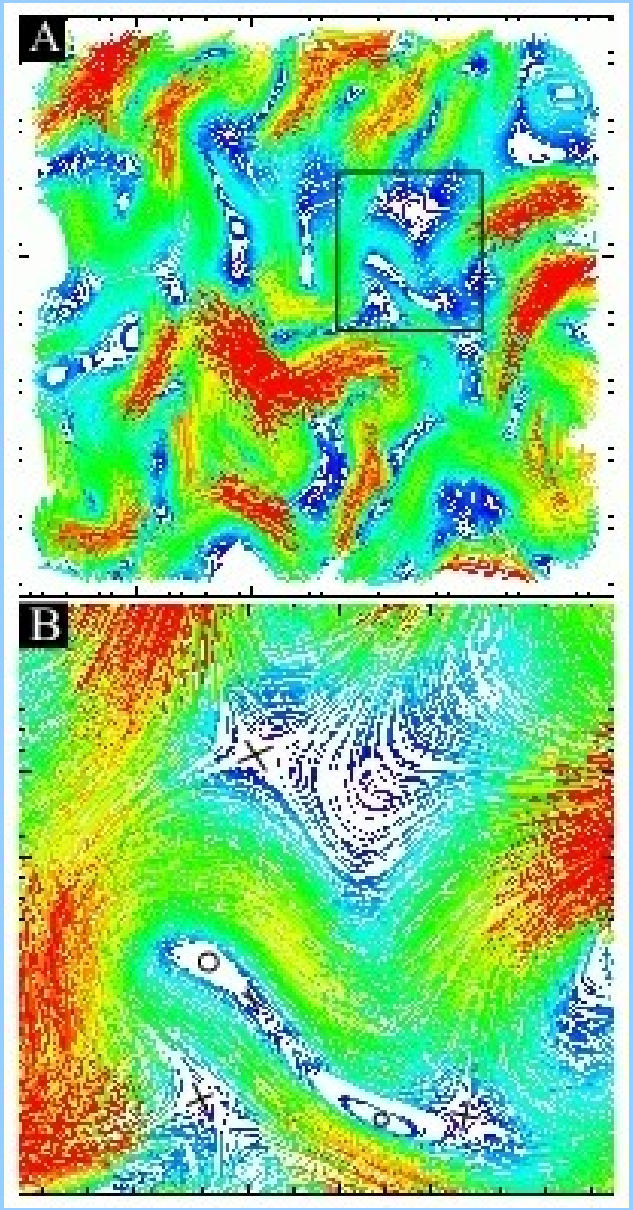

Poincaré map

A. Lines of maximum finite-time Lyapunov exponents for the backward map (compression or 'unstable manifold')

B. Concentration after 30 periods in the same phase as A

C. Superposition of the images A and B

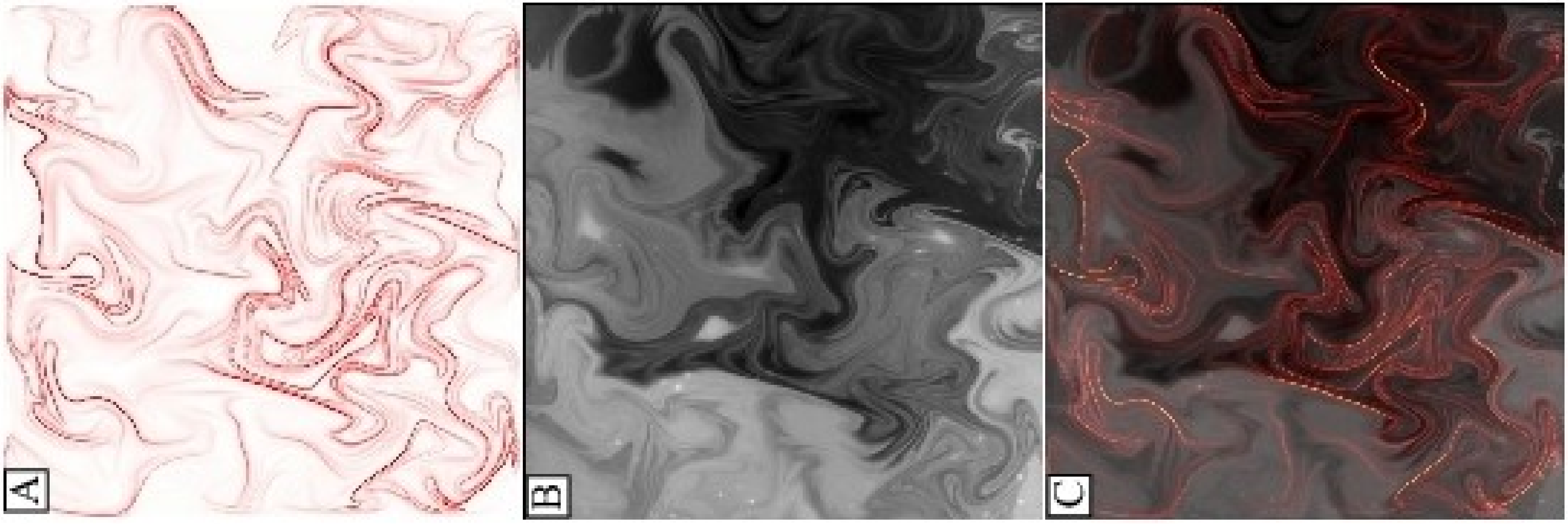

Intersection of stable and unstable material lines indicating the hyperbolic trajectories of the flow;

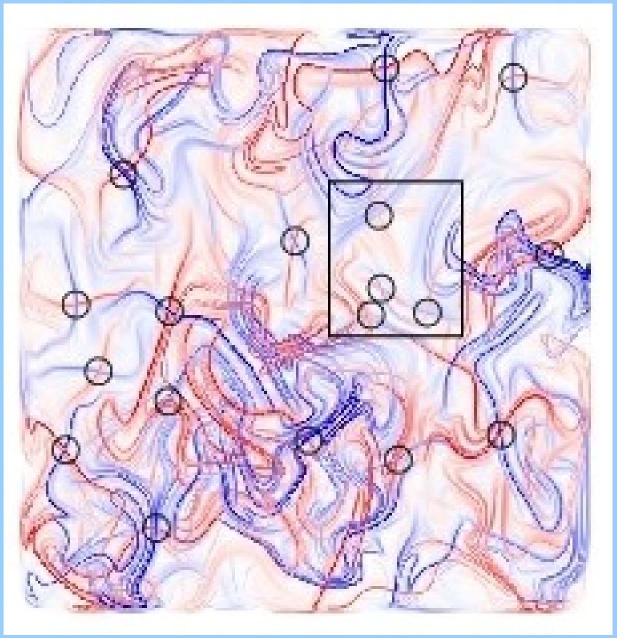

Superposition of the compression lines and the concentration, Re=115, p=5

Mesoscale Lagrangian structure of the Mediterranean surface

Example III

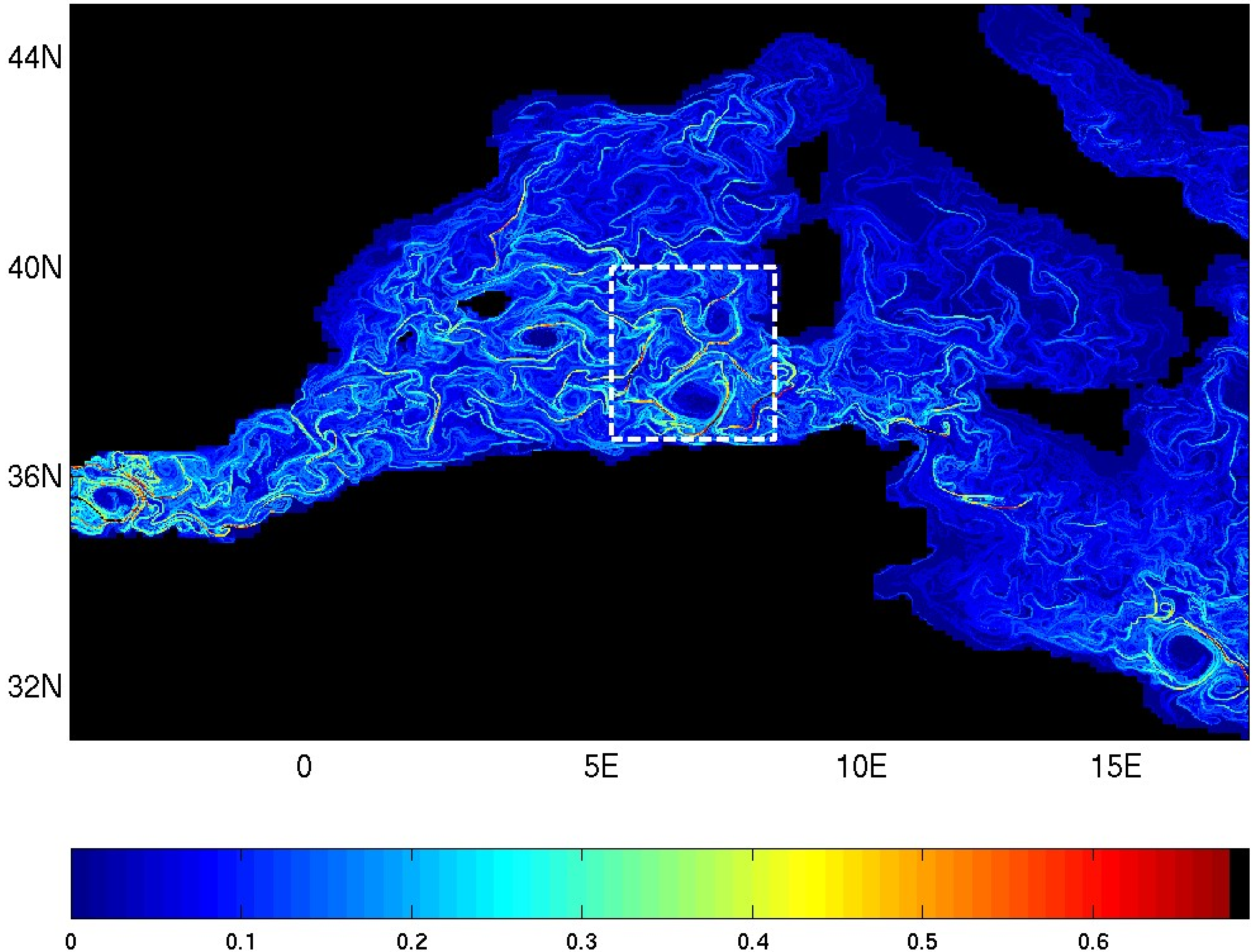

D'Ovidio et al., 2004, GRL, 31, LI7203, doi:10.029/2004GL020328.

1/day

Initial separation of 0.02 deg. (approx. 2.2 km),
final separation of 1 deg. (aprox 110 km)

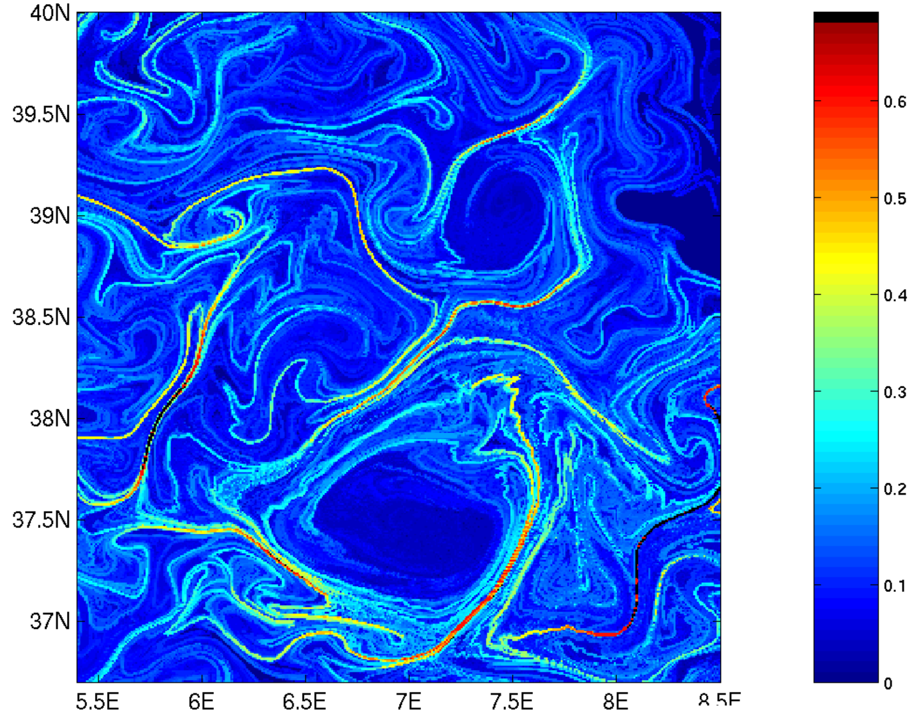

Forward and backward FSLEs (enlargement)

Incompressible field (statistically, backward and forward structures are similar)

The filaments in the backward-FSLE picture appears as the forward-in-time ones but rotated 90 deg.

Structure below the data grid spacing!

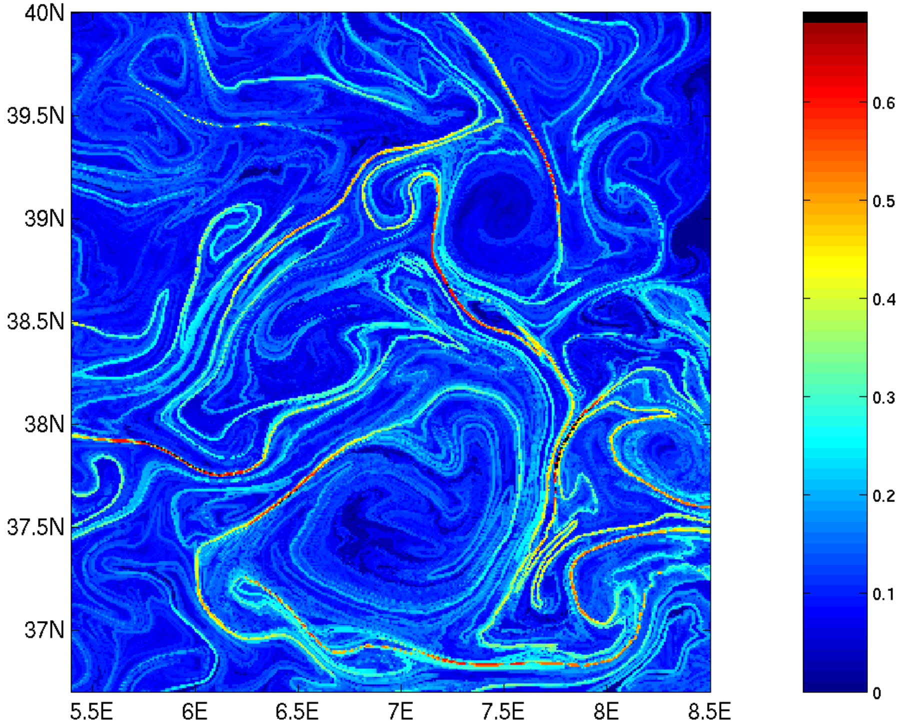

Intersection of stable and unstable material lines: hyperbolic trajectories

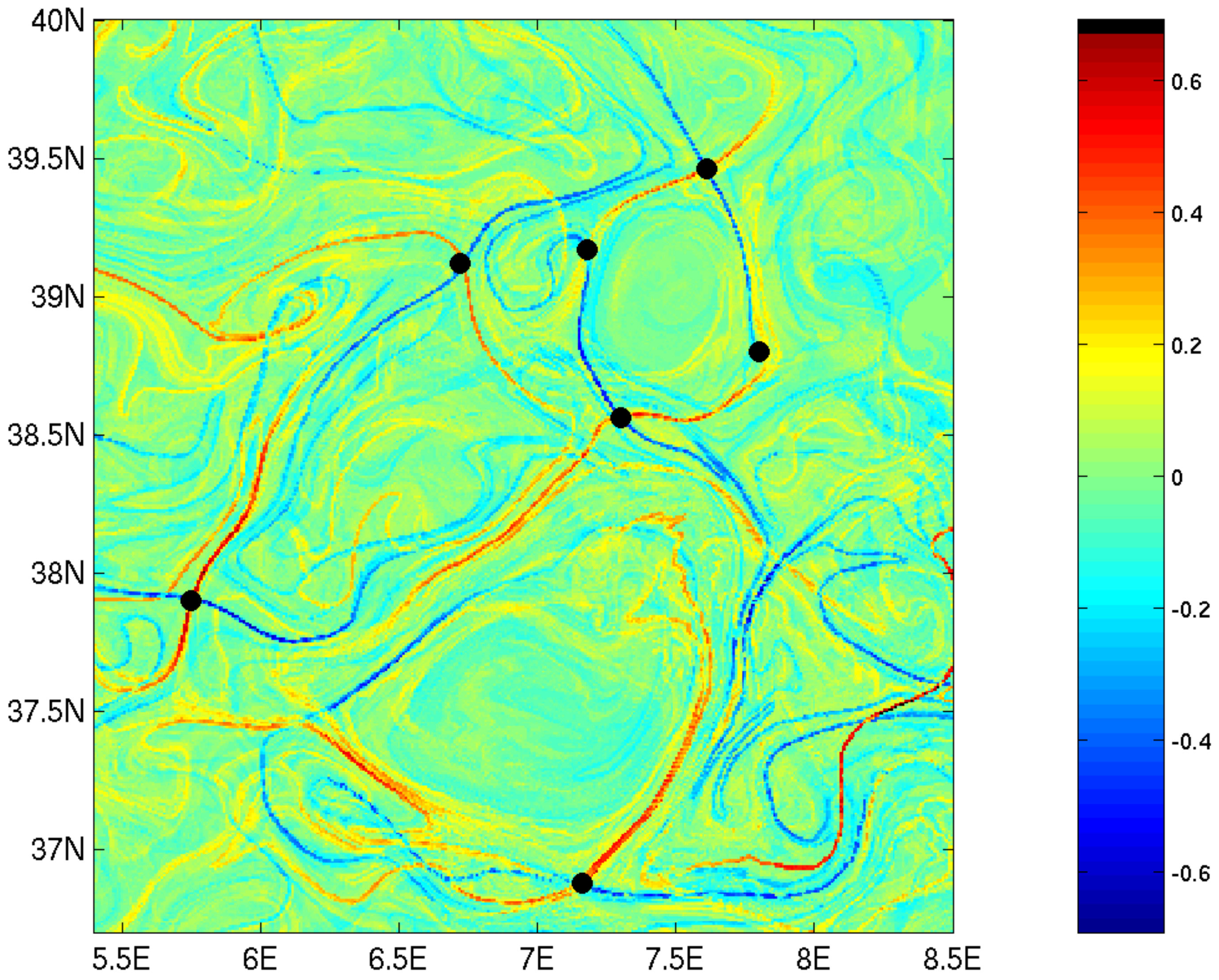

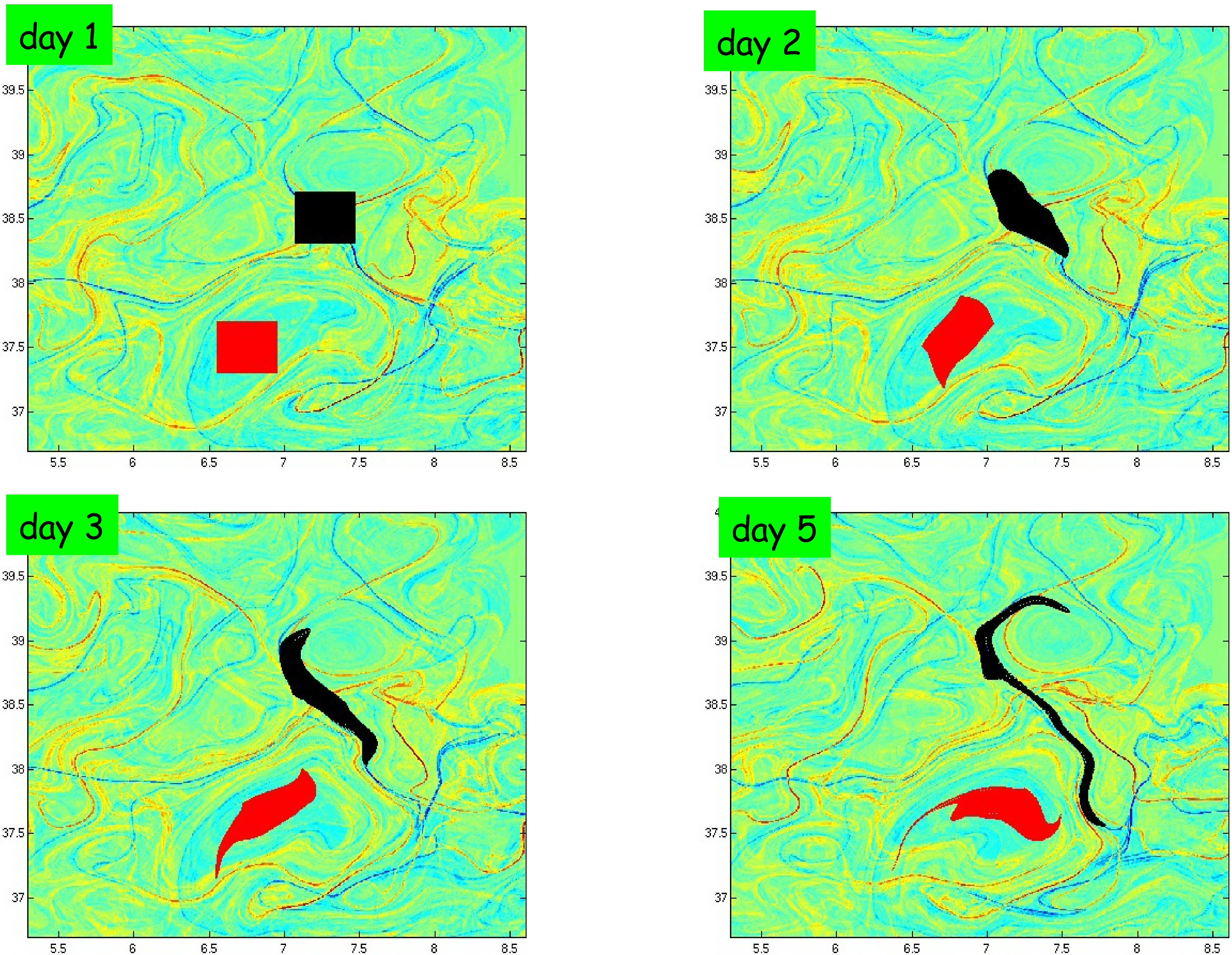
day 1
day 2
day 3
day 5
39.5
39
38.5
38
37.5
37
5.5
6
6.5
7
7.5
8
8.5

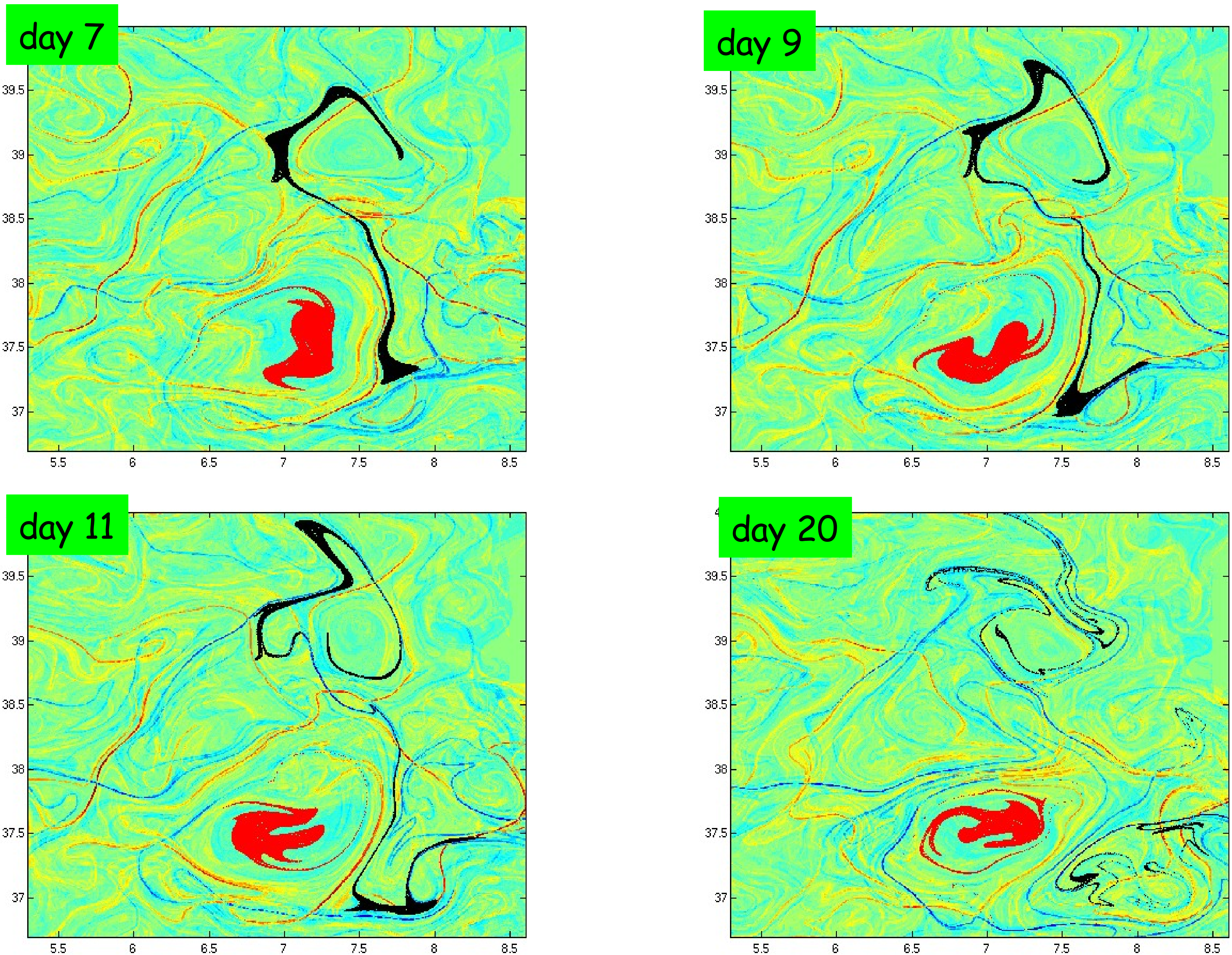
day 7
day 9
day 11
day 20
39.5
39
38.5
38
37.5
37
5.5
6
6.5
7
7.5
8
8.5

Mixing activity: time and space averages

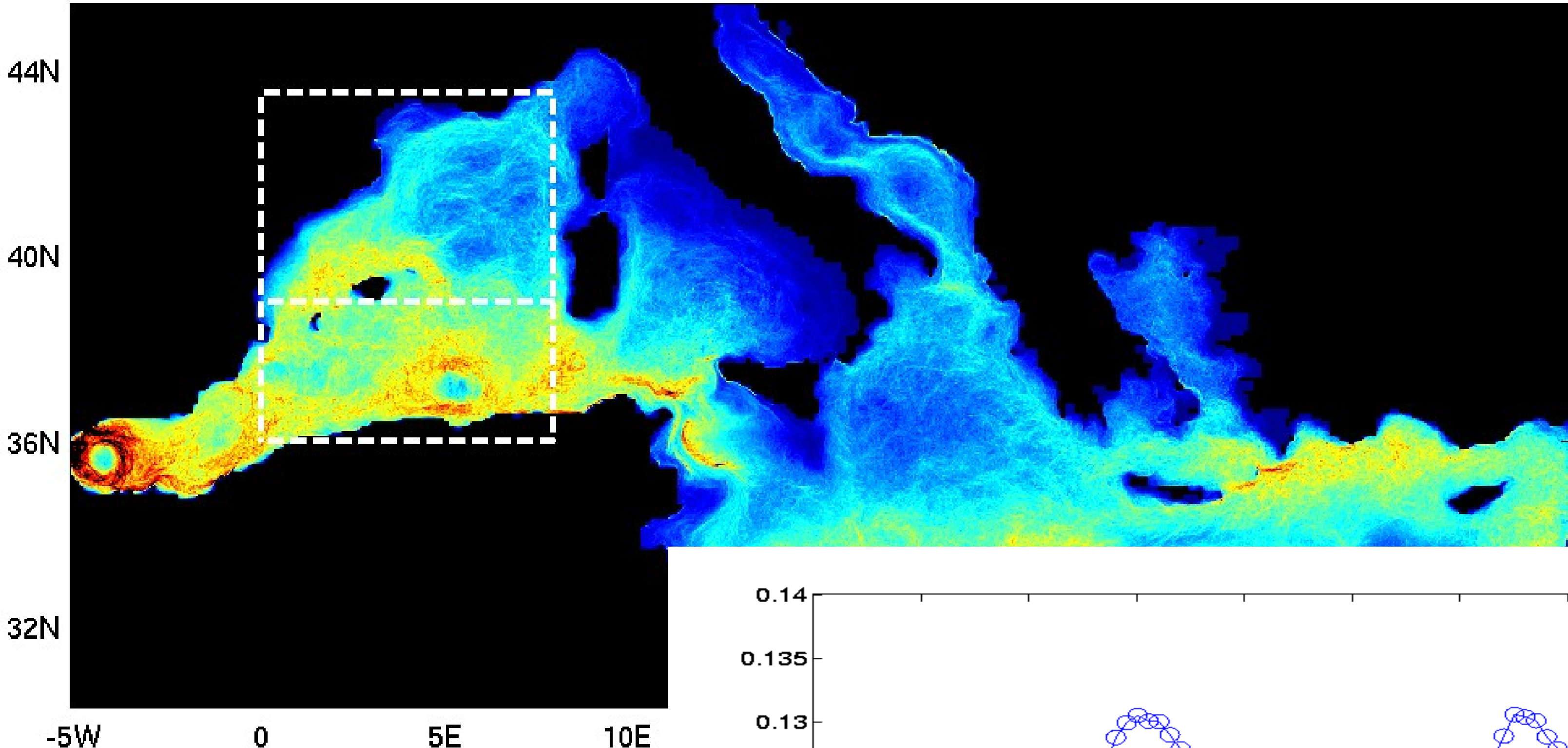

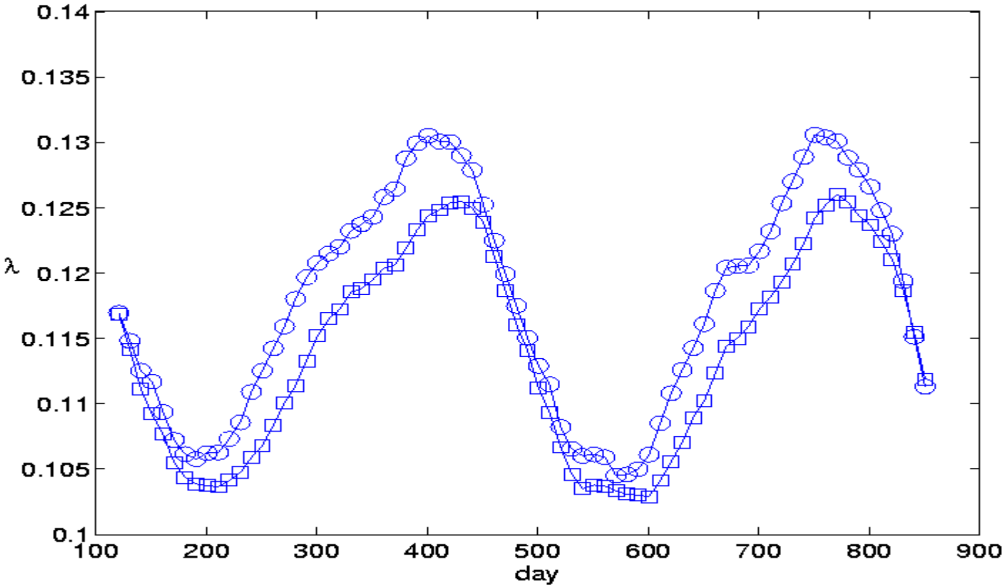

- The time average FSLE (1 year) divides the sea in regions of different mixing activity.
- The space average (whole basin) shows seasonal variations.

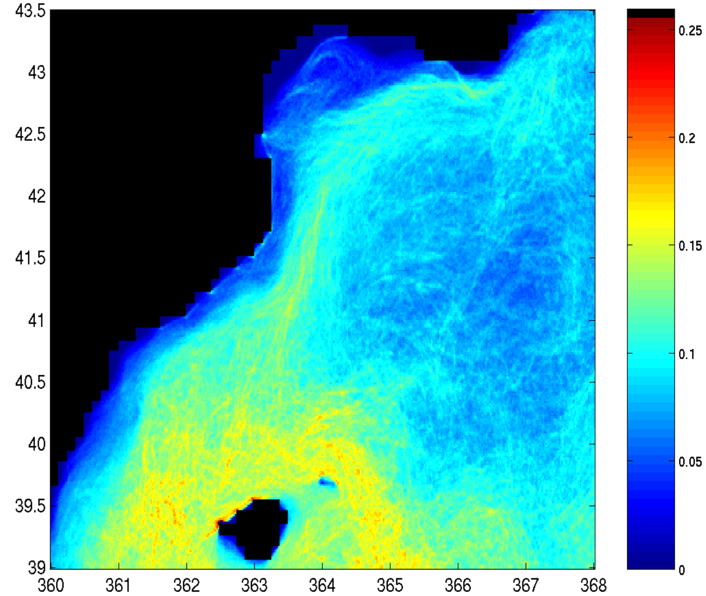

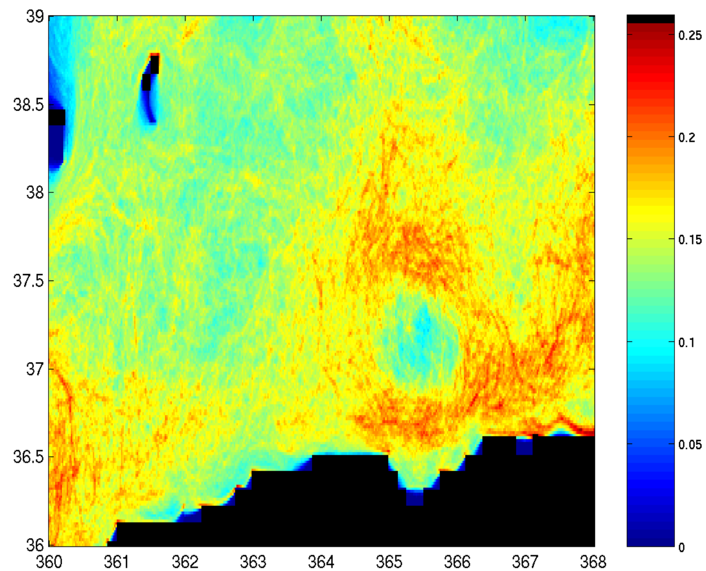

An example of two regions with different mixing behaviour: north and south of the Balearic Islands

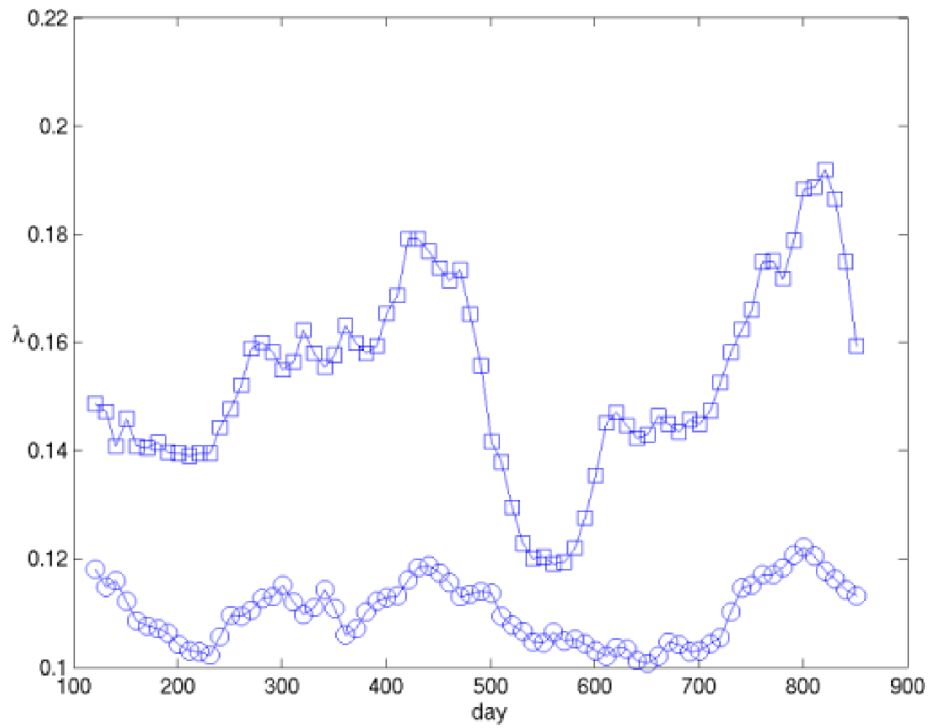

Comparison between chlorophyll distribution, the FSLE lines and Okubo-Weiss criterion (black lines)

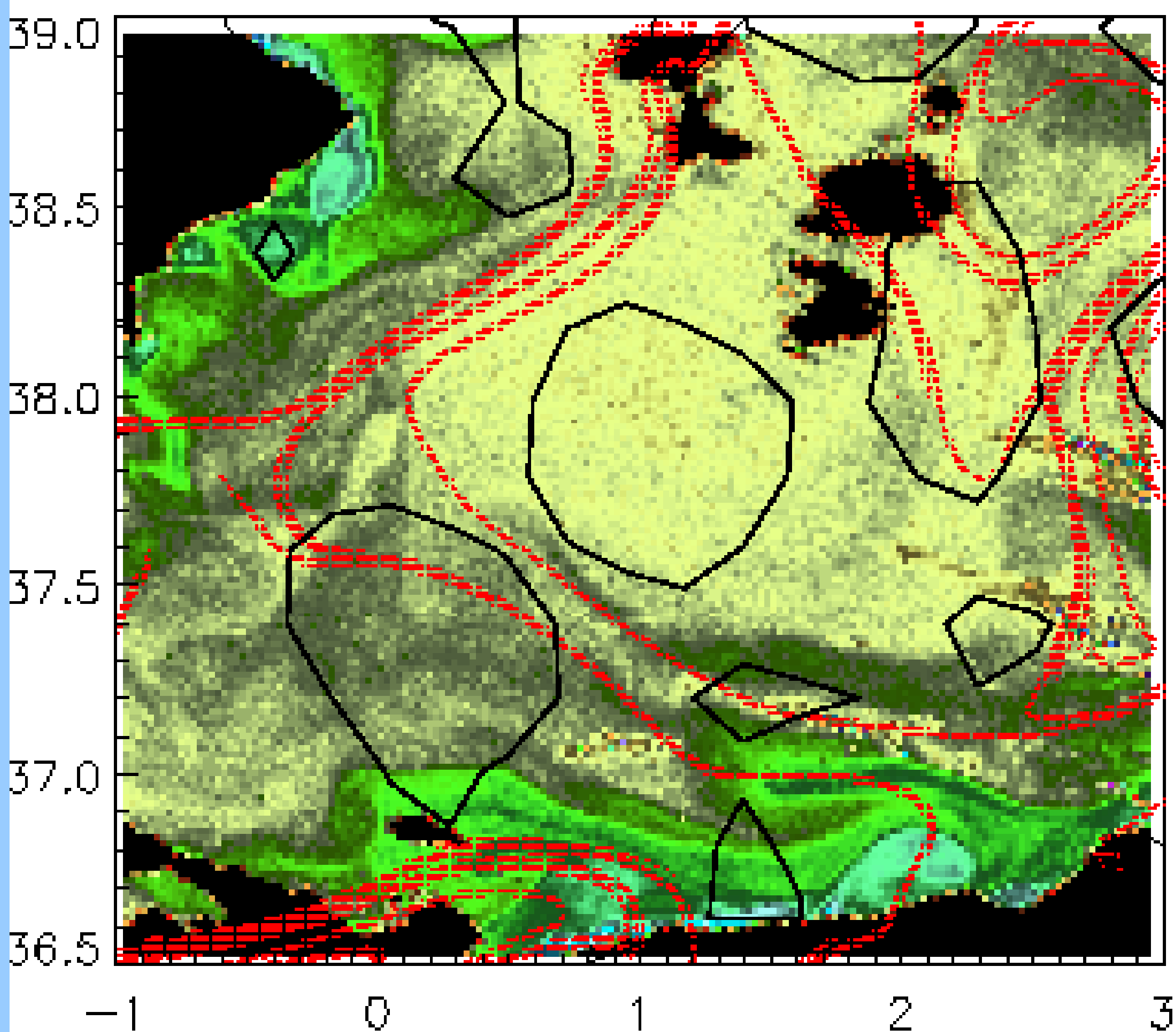

7 July 1996

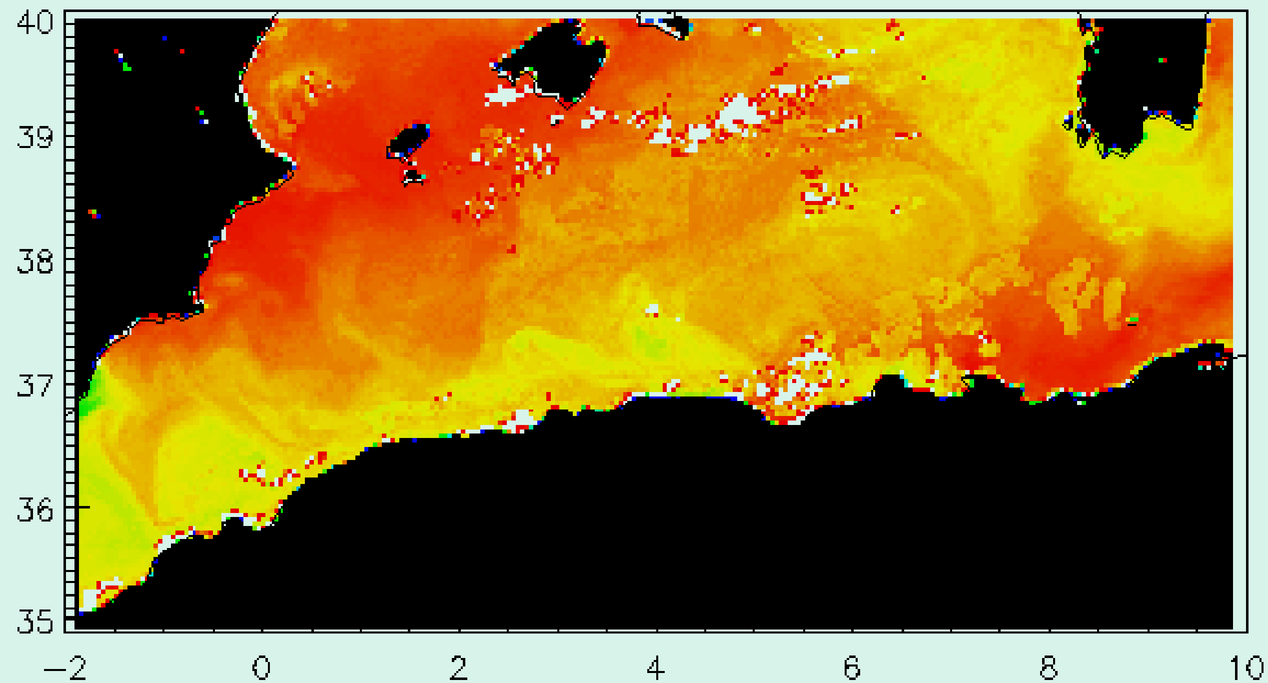

OW

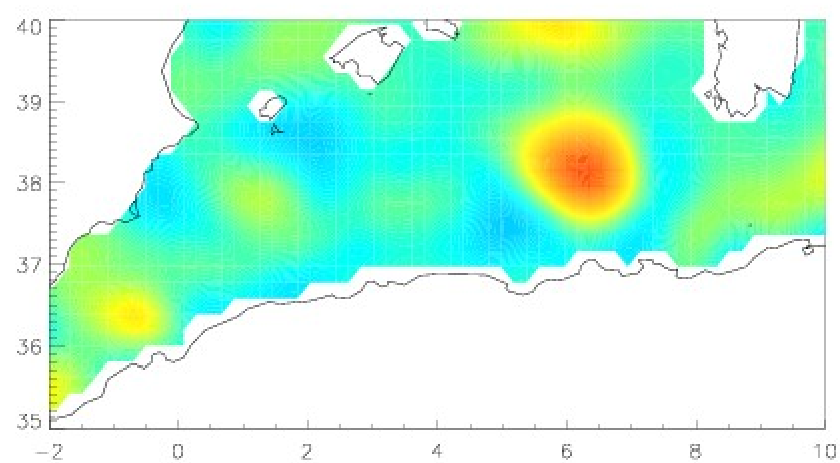

FSLE

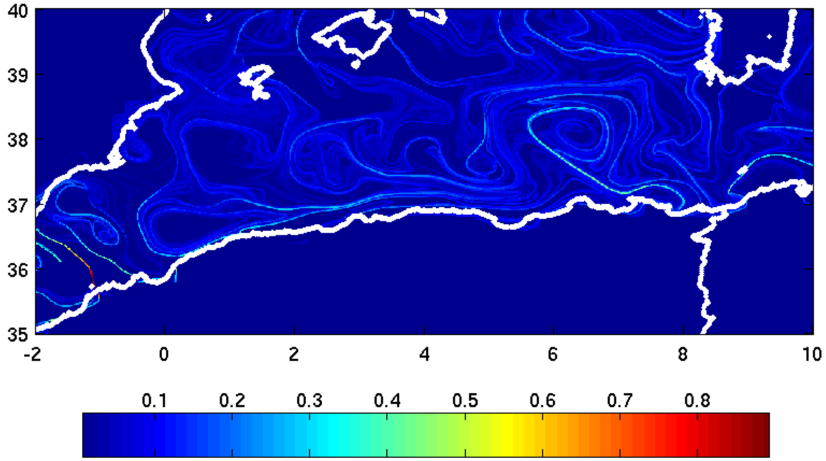

IV.A.7 Hyperbolic skeleton of the polar vortex

ExampleIV: The Antarctic polar vortex
(*Joseph & Legras, 2001)*

Attracting material lines (unstable manifold) and repelling material lines (stable manifold) shown as points with largest FSLE after backward and forward time integration over 9 days.
25 October 1996, 450K.

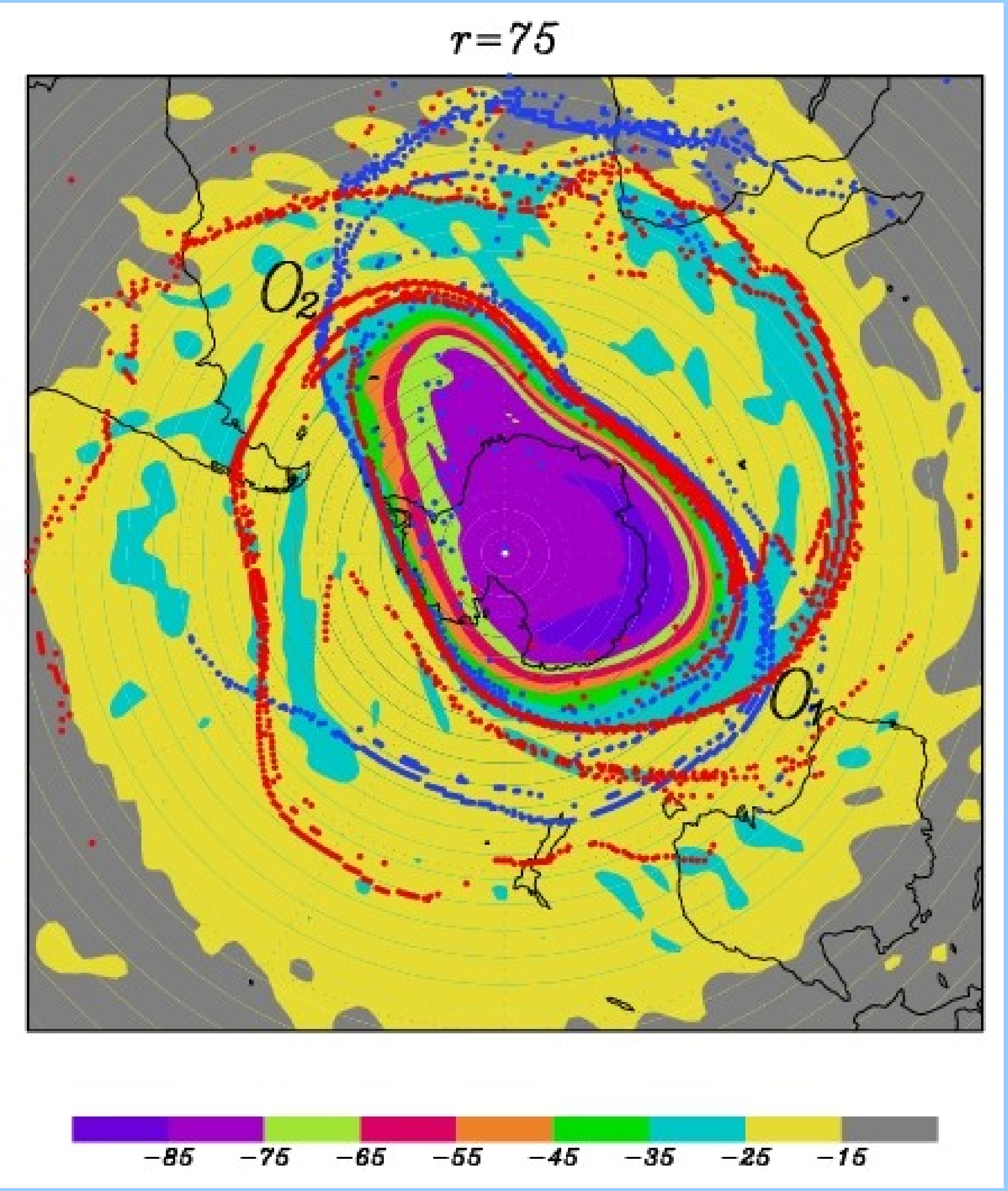

FSLE
large ratio
r=100
October 1996

attracting line (unstable manifold)
and
repelling line (stable manifold)

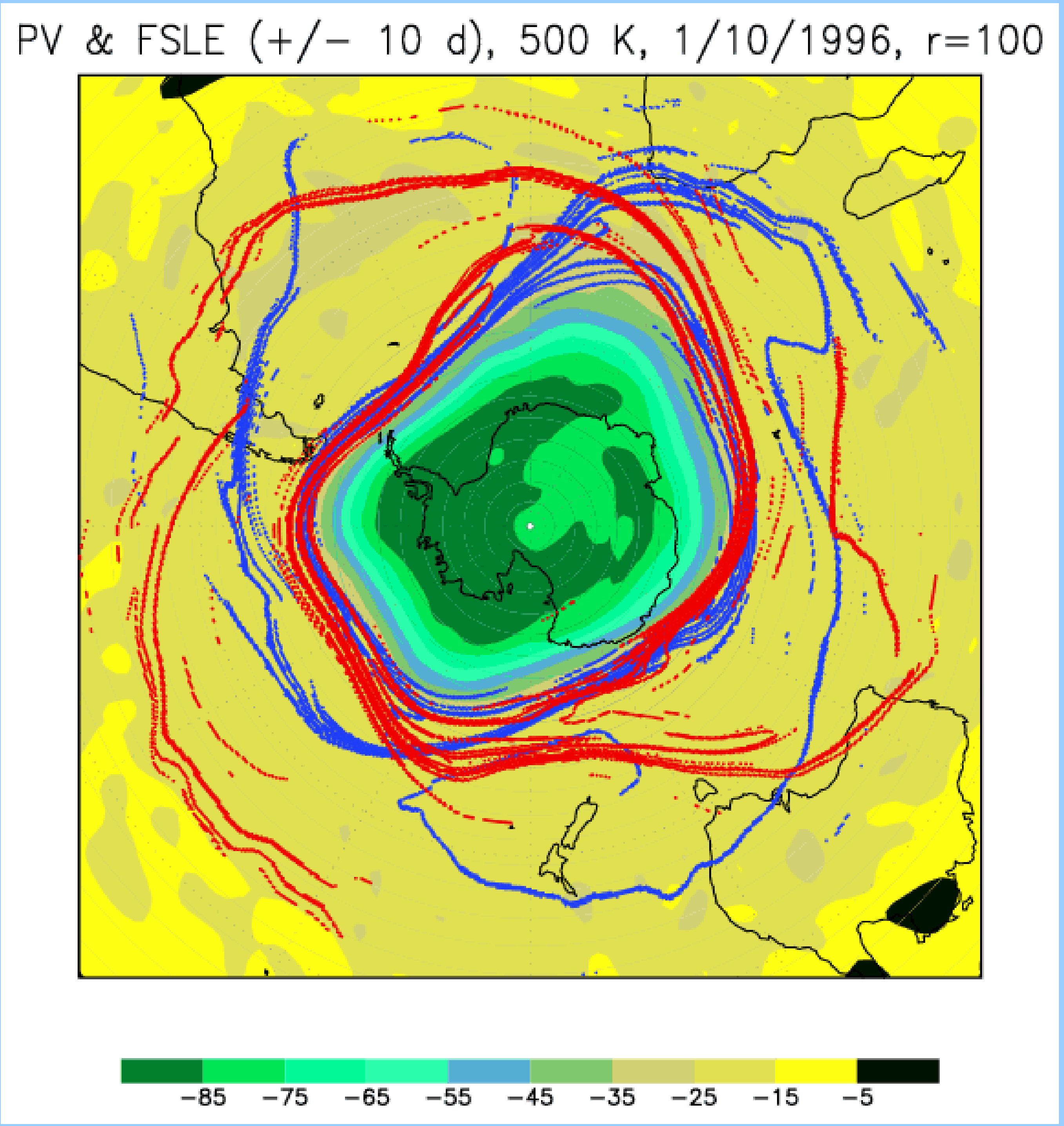

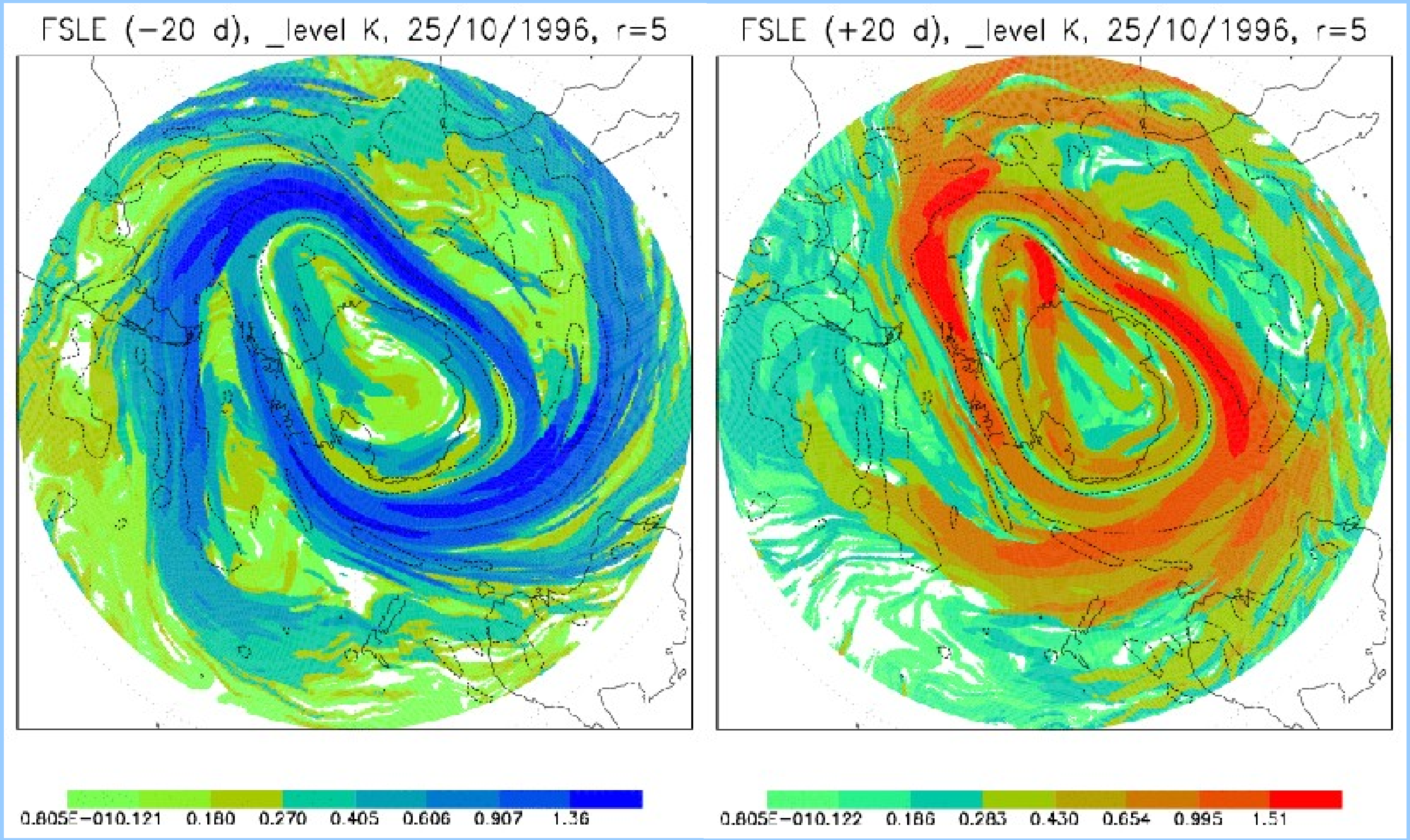

Backward FSLE

Forward FSLE

Local stirring time for FSLE with r=5

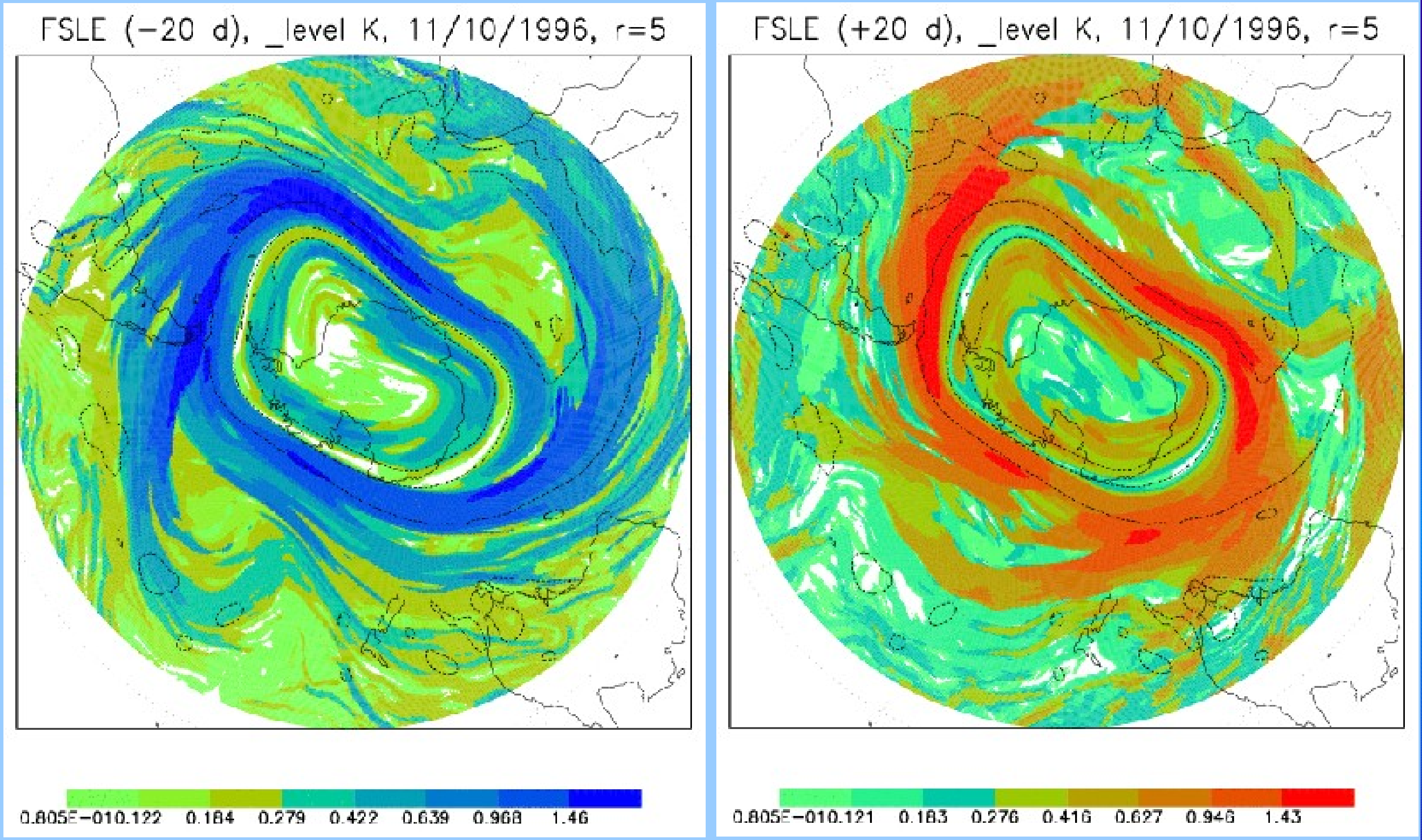

Backward FSLE **Forward FSLE**

Local stirring time for FSLE with r=5

IV.A.7 Lobe dynamics

The intersection of stable and unstable lines generate lobes.

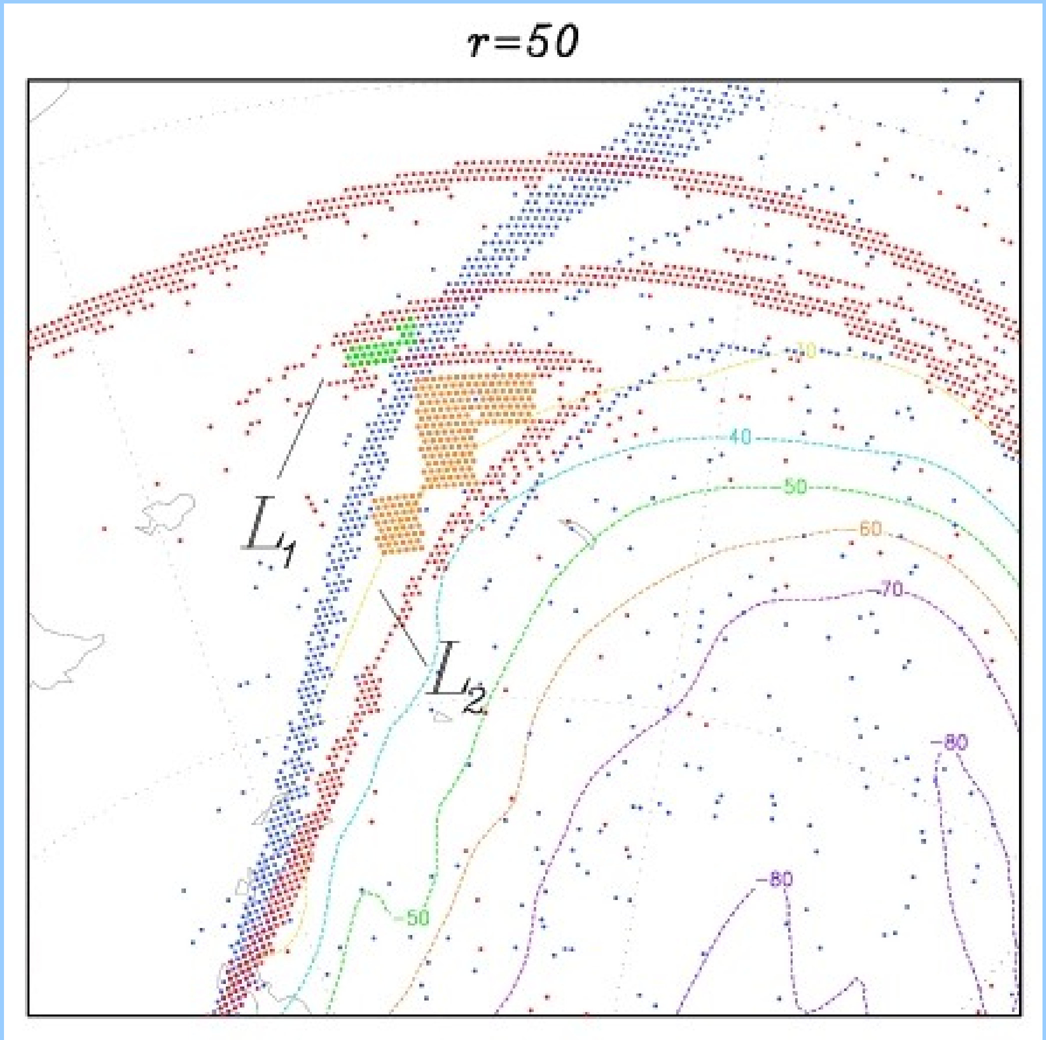

Turnstile process

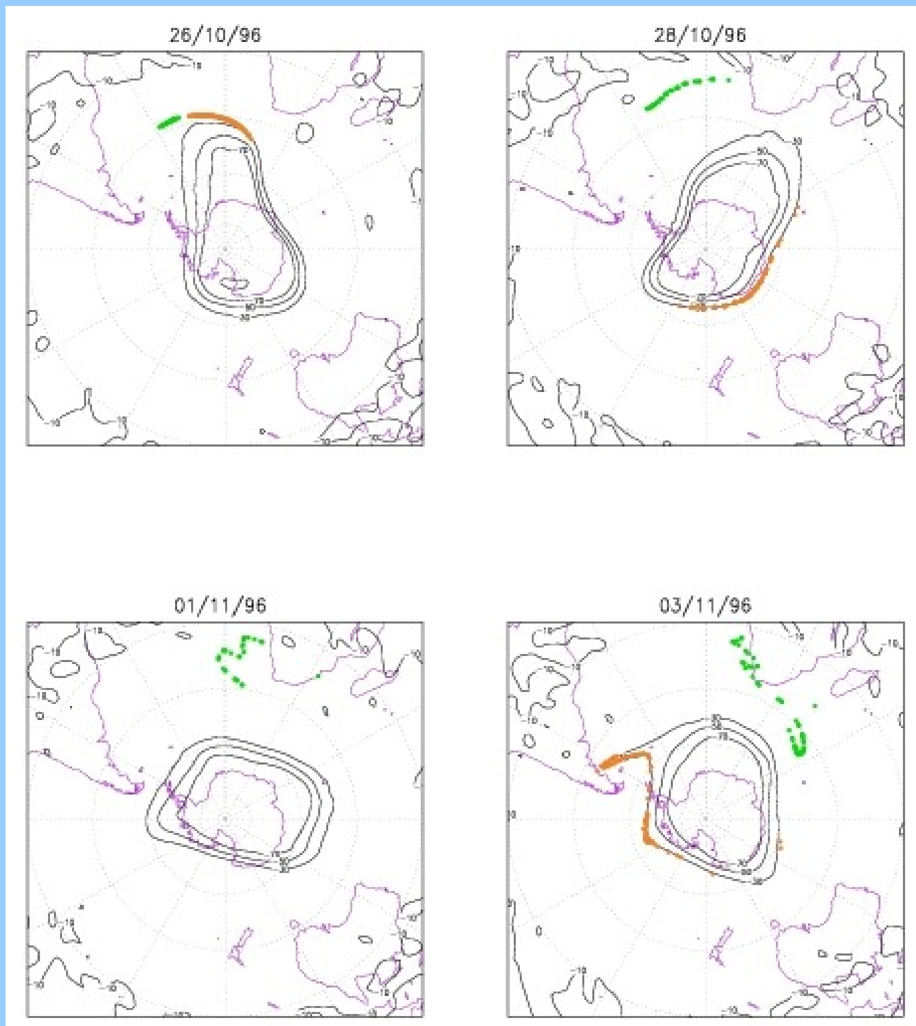

forward integration

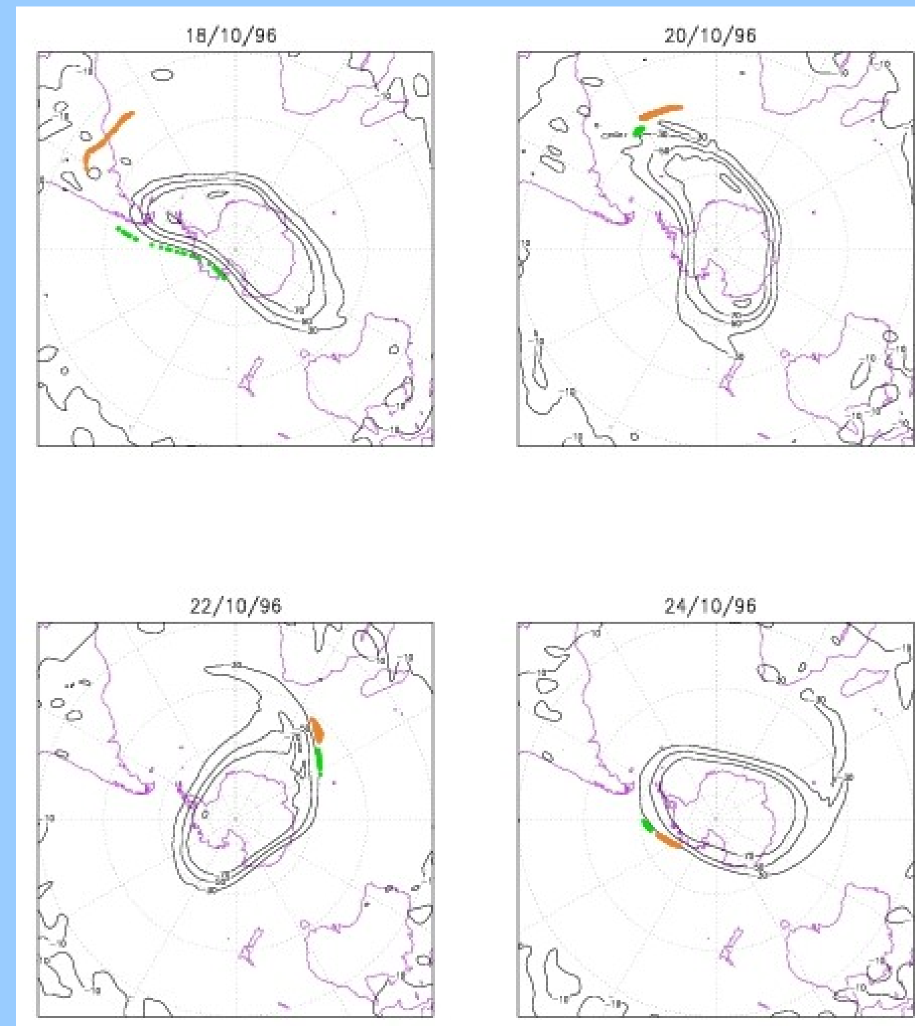

backward integration

Lobes can be detected and followed in aperiodic flows and induced transport can be calculated.
However, the turnstile mechanism applies only when relevant boundaries are hyperbolic lines. It cannot be used for transport barriers created by KAM invariant tori.
In the case of the stratospheric polar vortex, lobe dynamics explains the exchanges between the mixing zone surrounding the vortex and the extra-tropics.

Koh and Plumb, 2000,
Phys. Fluids, 13, pp. 1518-1528

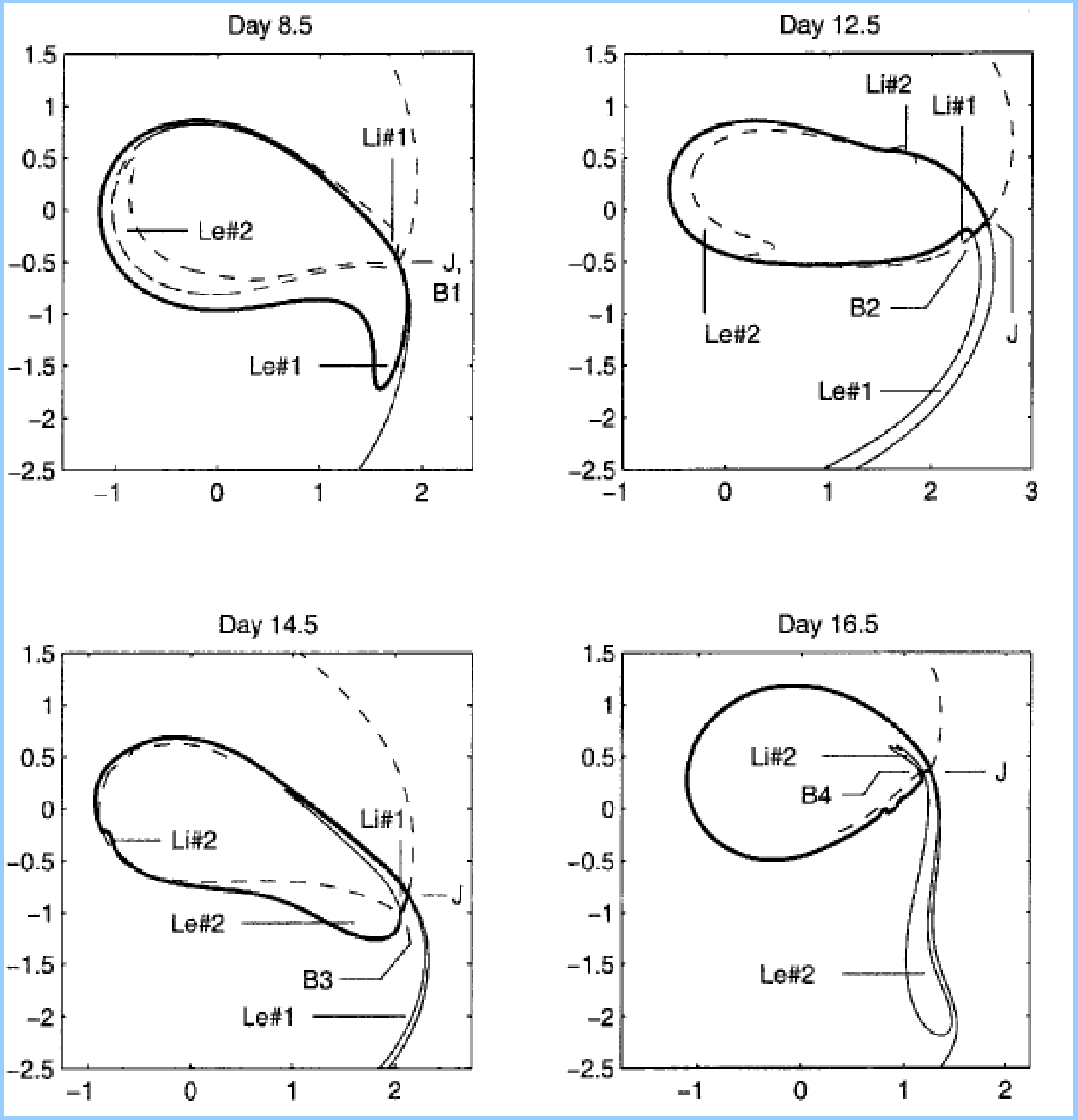

Effective diffusivity

- detection of barriers
- estimation of cross-contour mixing

Finite-size Lyapounov exponents

- detection of the hyperbolic structure
- local stirring times

IV.B.1 Effective diffusivity

Tracer-based coordinate system

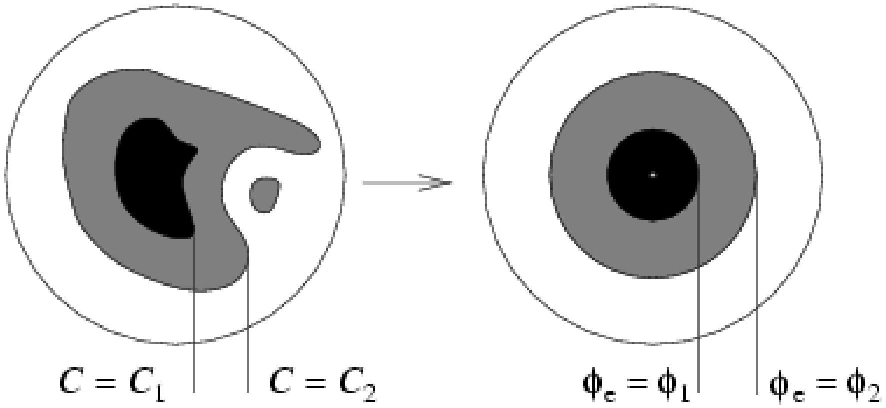

$$\langle \chi \rangle = \frac{\partial}{\partial A} \iint_{c \le C} \chi \, dA = \left(\oint \chi \frac{dl}{|\nabla c|} \right) \left(\oint \frac{dl}{|\nabla c|} \right)^{-1}$$

Equivalent latitude $A = 2\pi r^2 (1 - \sin \phi_e)$

Advection-Diffusion

$$\frac{\partial c}{\partial t} + \mathbf{u} \cdot \nabla c = \nabla \cdot (\kappa \nabla c)$$

Transformation to tracer-based coordinates:

(a) change in area within a tracer contour

$$\frac{\partial A(C,t)}{\partial t} = \oint_{\gamma(C,t)} \mathbf{u}^C \cdot \frac{\nabla c}{|\nabla c|}\, dl = - \oint_{\gamma(C,t)} \frac{\partial c}{\partial t} \frac{dl}{|\nabla c|}$$

$$\frac{\partial A(C,t)}{\partial t} = -\frac{\partial}{\partial C} \oint_{\gamma(C,t)} \kappa |\nabla c|\, dl$$

(b) convert to expression for $\partial C / \partial t$,

$$\frac{\partial C(A,t)}{\partial t} = \frac{\partial}{\partial A}\left(K_{\text{eff}}(A,t) \frac{\partial C(A,t)}{\partial A} \right) ,$$

where

$$K_{\text{eff}}(A,t) = \frac{\partial A}{\partial C} \oint_{\gamma(C,t)} \kappa |\nabla c|\, dl = \frac{\langle \kappa |\nabla c|^2 \rangle}{(\partial C/\partial A)^2}$$

i.e. diffusion-only equation.

Nakamura, JAS, 1996
Haynes & Shuckburgh
JGR, 2000

Equivalent length

For κ constant, $K_{\text{eff}}(A,t) = \kappa L_{\text{eq}}^2(A,t)$.

Under transformation of tracer, $c \mapsto \tilde{c} = f(c)$

$$L_{\text{eq}}^2 \mapsto L_{\text{eq}}^{\tilde{2}} = \oint_\gamma |f'(c)||\nabla c|\, dl \oint_\gamma \frac{dl}{|f'(c)||\nabla c|} = L_{\text{eq}}^2$$

since $f'(c) = f'(C) =$ constant on $\gamma(C,t)$,

equivalent length is invariant.

Equivalent length $\sim$ actual length L of the tracer contour C since

$$L_{\text{eq}}^2 = L^2 \overline{\left|\frac{1}{\nabla c}\right|}\ \overline{|\nabla c|} \ \geq L^2$$

Geometric structure of tracer

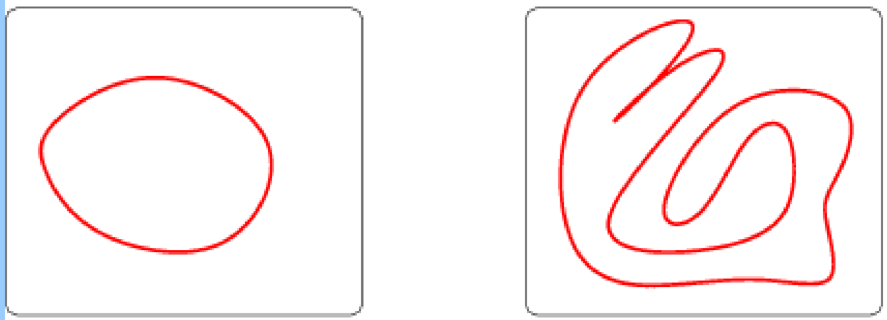

weak mixing

small length

strong mixing

large length

Mixing (barrier) regions $\rightsquigarrow$

complex (simple) tracer geometry.

L_{eq} large (small) in mixing (barrier) regions.

Effective Diffusivity

Flow on a sphere, effective diffusivity

$$\kappa_{\mathrm{eff}}(\phi_{\mathrm{e}}, t) = \frac{\kappa L^2_{\mathrm{eq}}(\phi_{\mathrm{e}}, t)}{(2\pi r \cos\phi_{\mathrm{e}})^2}$$

κ_{eff} $\therefore$ largest where tracer contours most complex.

Mixing ability of a flow = ability to produce complex tracer contours $\therefore$ κ_{eff} = measure of mixing ability.

Hybrid Eulerian-Lagrangian type diagnostic;

c.f. Eulerian effective diffusivities.

IV.B.1 Effective diffusivity in the atmosphere

L_{eq} as a function of log-pressure height and ϕ_e.

Increased mixing in the summer lower stratosphere

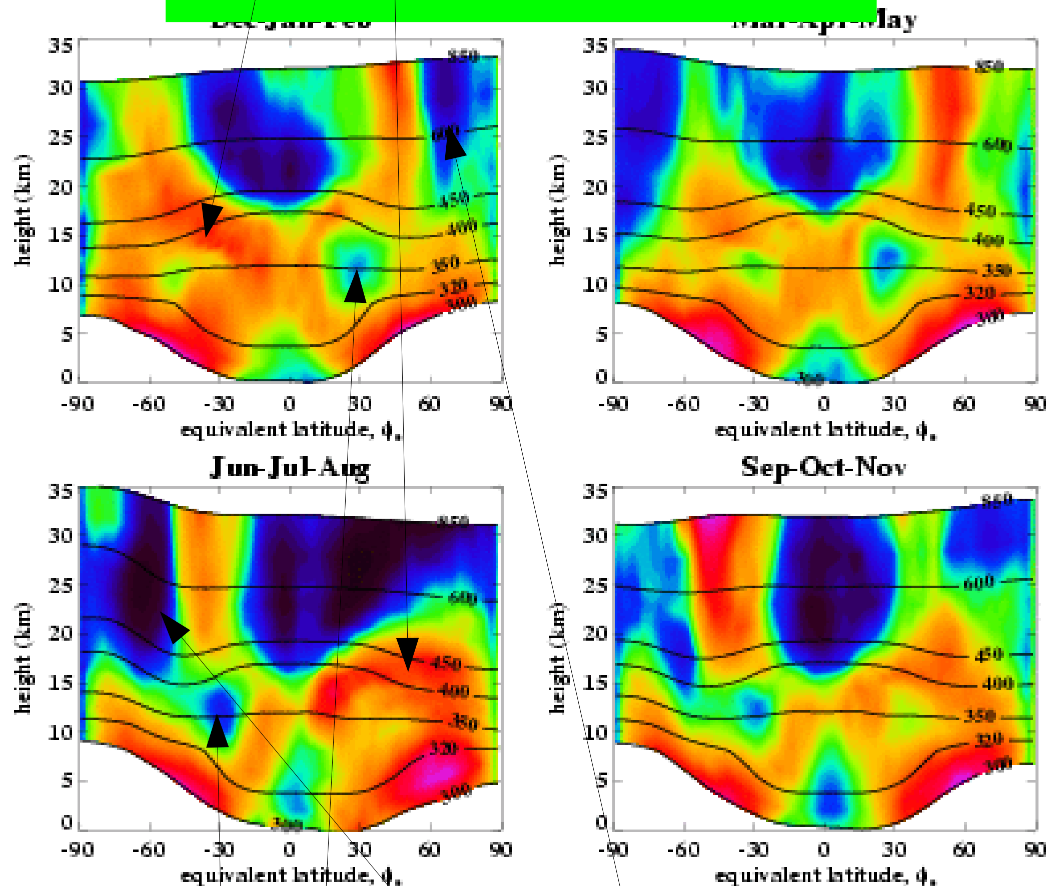

see Haynes and Shuckburgh, 2000, JGR, 105, 22777-22810.

Subtropical jets and polar vortex jets as minima (barriers) in effective diffusivity

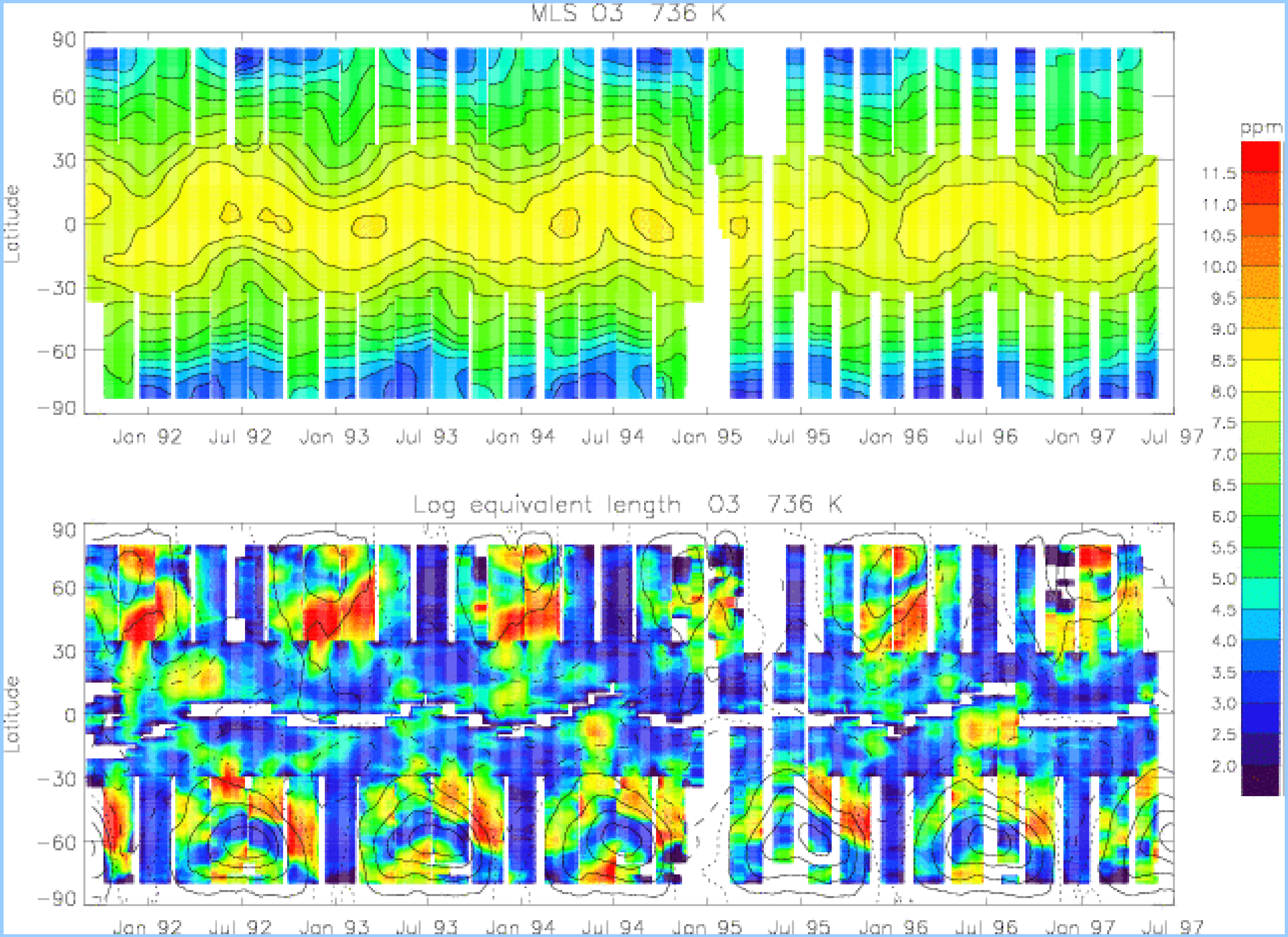
MLS O3 736 K
Latitude
90 60 30 0 −30 −60 −90
Jan 92 Jul 92 Jan 93 Jul 93 Jan 94 Jul 94 Jan 95 Jul 95 Jan 96 Jul 96 Jan 97 Jul 97
ppm
11.5 11.0 10.5 10.0 9.5 9.0 8.5 8.0 7.5 7.0 6.5 6.0 5.5 5.0 4.5 4.0 3.5 3.0 2.5 2.0
Log equivalent length O3 736 K
Latitude
90 60 30 0 −30 −60 −90
Jan 92 Jul 92 Jan 93 Jul 93 Jan 94 Jul 94 Jan 95 Jul 95 Jan 96 Jul 96 Jan 97 Jul 97

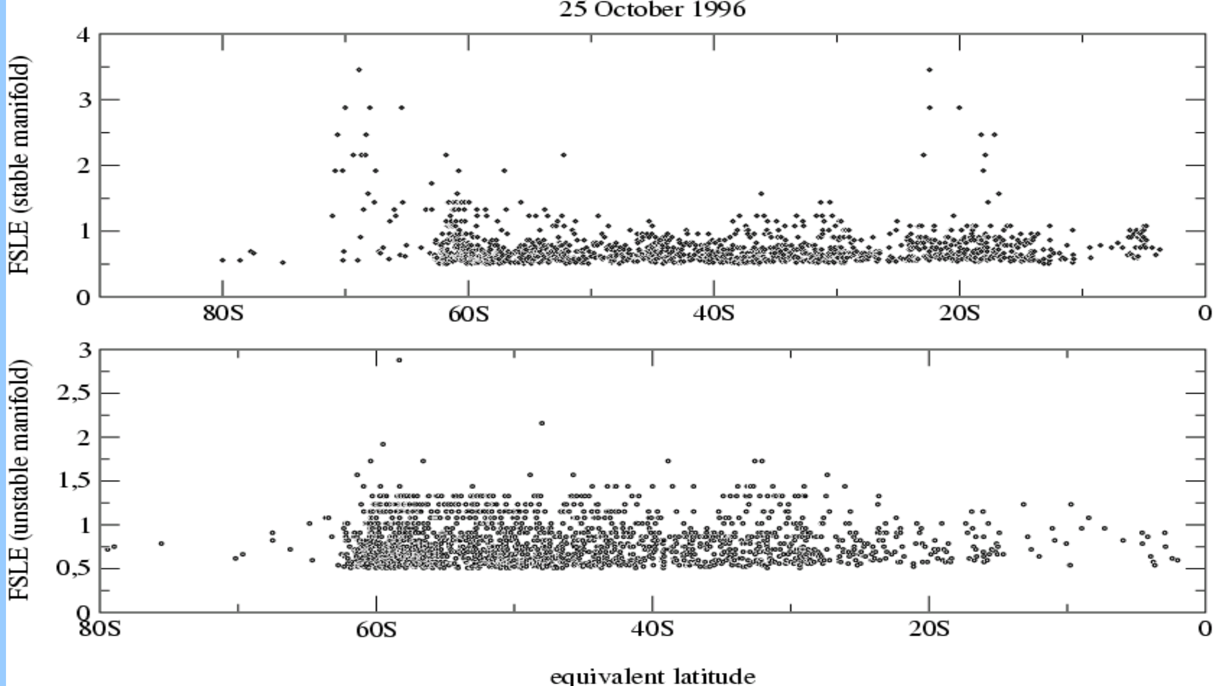

Distribution of the points on the unstable and stable material surfaces as a function of equivalent latitude

Densities *ds* and *du* of the stable and unstable lines versus PV gradient and effective diffusivity.

The stable or unstable material lines are NOT the boundary of the polar vortex.

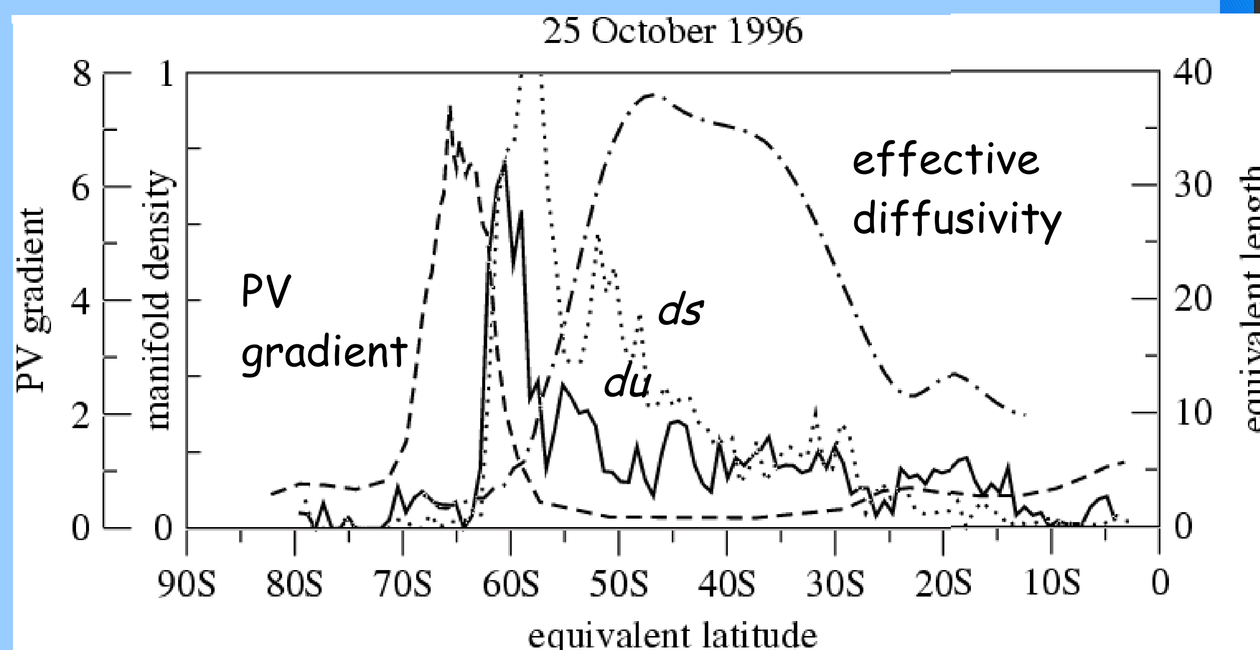

PV & FSLE (+/- 10 d), 350 K, 01/07/1998, r=100

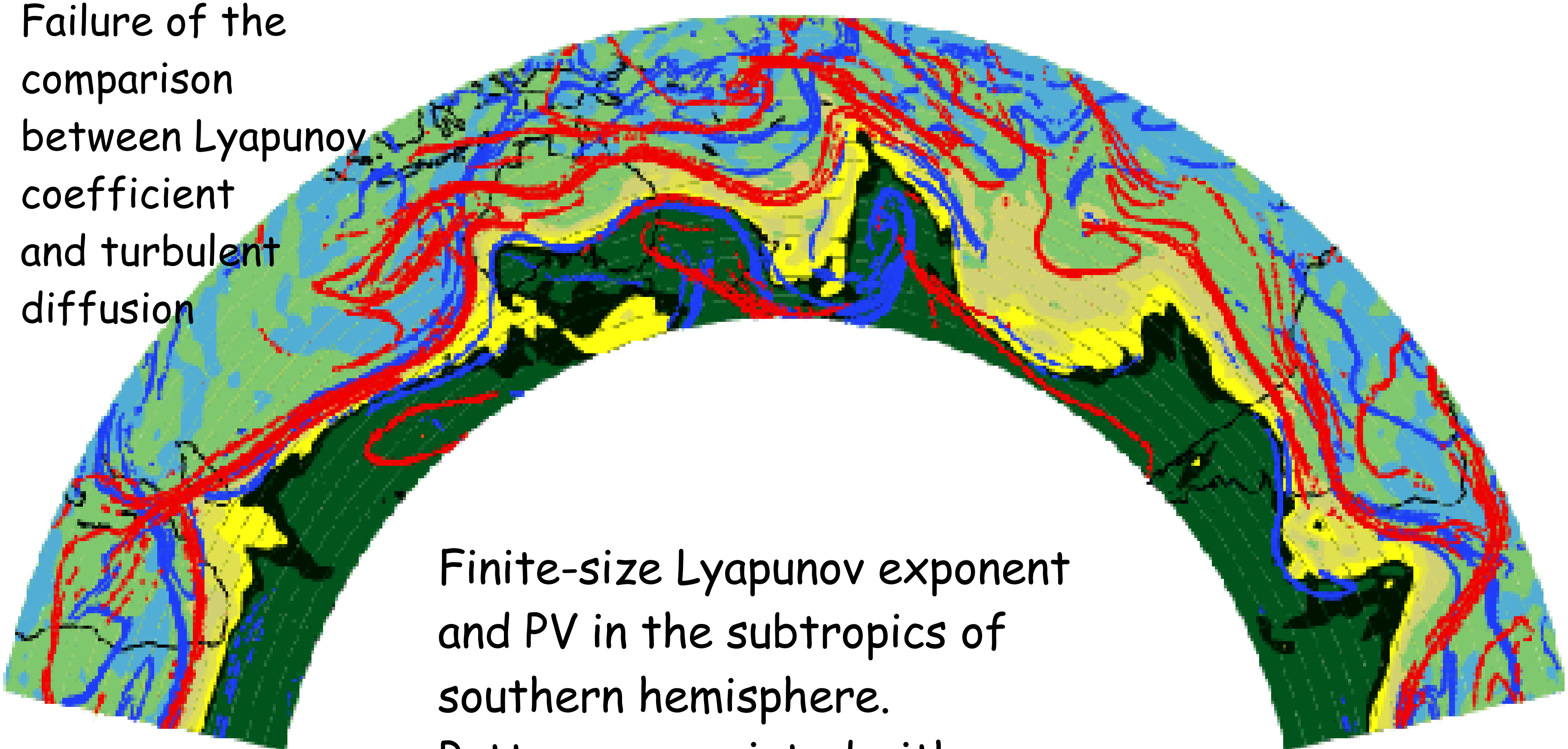

Failure of the comparison between Lyapunov coefficient and turbulent diffusion

Finite-size Lyapunov exponent and PV in the subtropics of southern hemisphere.
Patterns associated with travelling baroclinic perturbations.
Barrier effect?

Red: large forward Lyapunov <=> unstable (past) material line
Blue: large backward Lyapunov <=> stable (future) material line

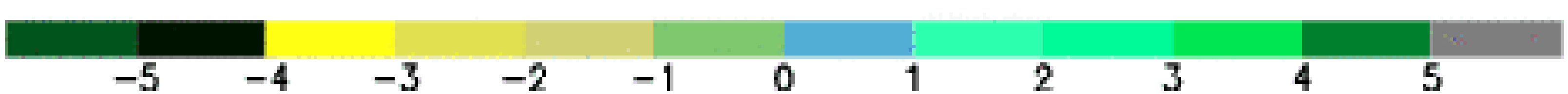

FSLE versus effective diffusivity at 350K

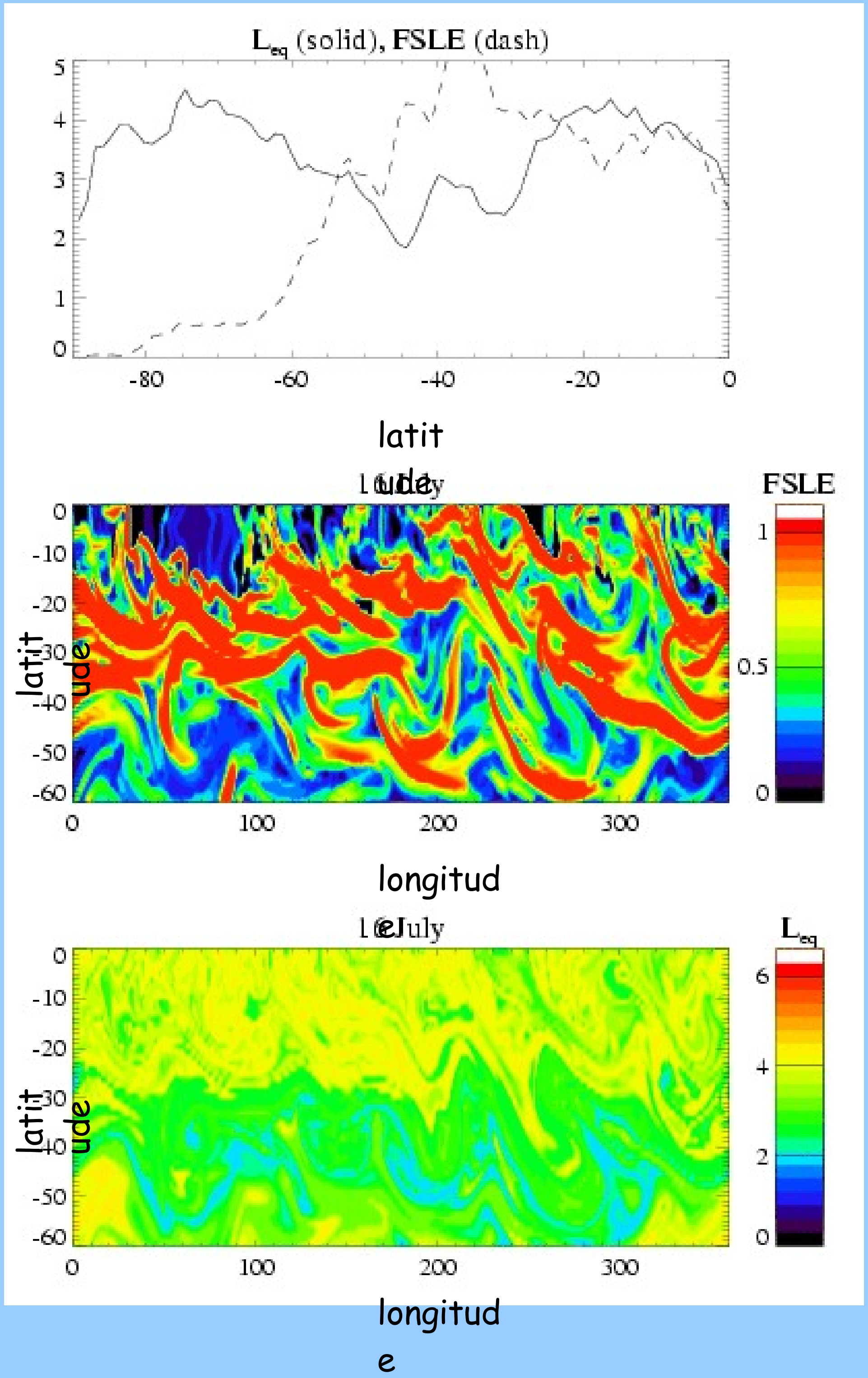

Averaging FSLE along contours leads to the paradoxical conclusion that there is anticorrelation rather than correlation with effective diffusivity.

Anticorrelation of FSLE with effective diffusivity persists even after time averaging.

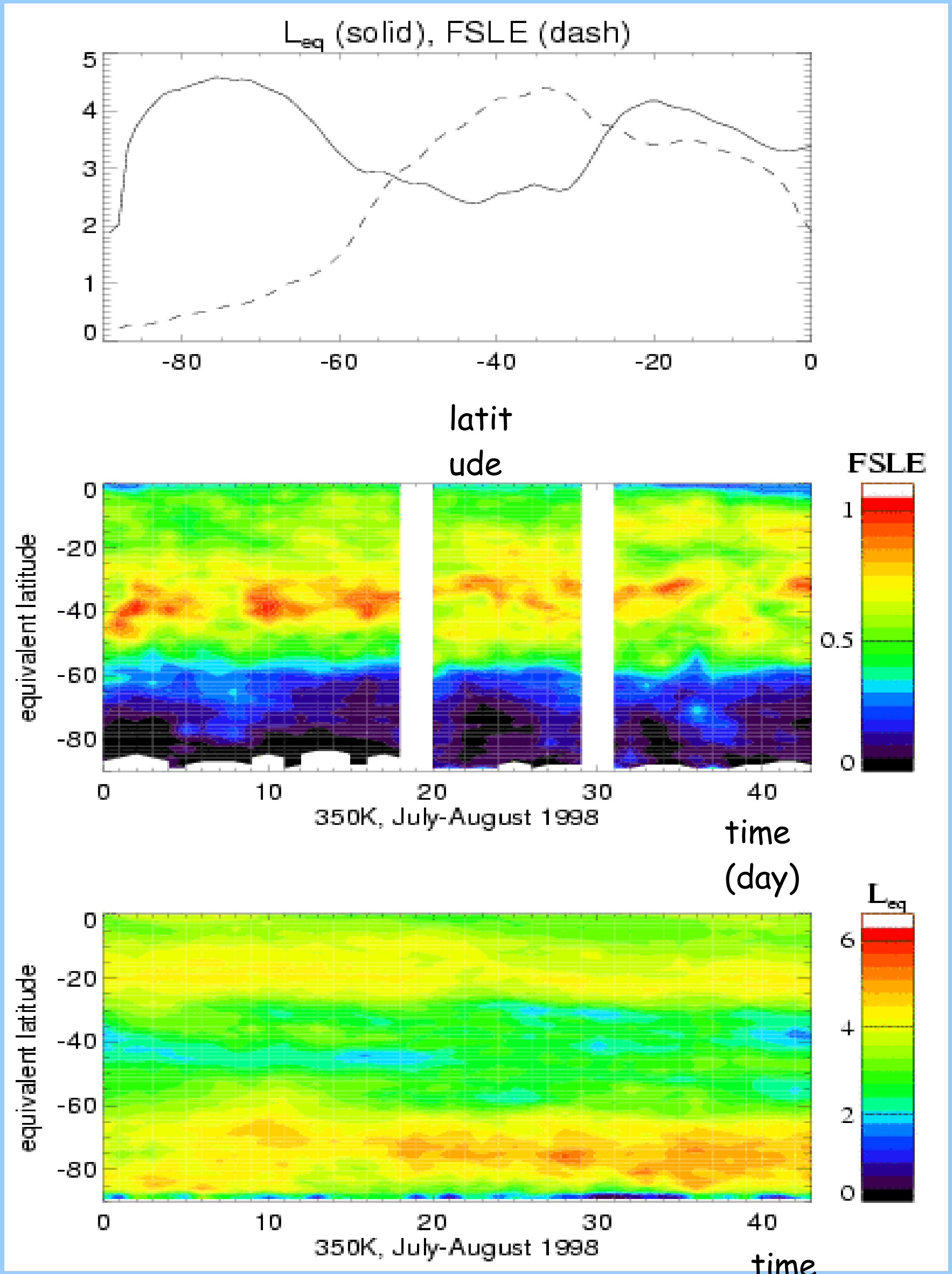

Effective diffusivity in practice

$$K_{\text{eff}}(A,t) = \frac{\partial A}{\partial C} \oint_{\gamma(C,t)} \kappa |\nabla c| \, dl = \frac{\langle \kappa |\nabla c|^2 \rangle}{(\partial C/\partial A)^2}$$

- Keff (Leq) is well defined from contour averaging on isentropic surfaces
- Measures mixing as the amount of foldings beared by a given contour.
- Pro: Is a diffusivity. Easily calculated. Depends weakly on the quantity being contoured. Usable as a turbulent parameterization in 2D vert-lat models.
- Con: Limited to isentropic motion. Does not diagnose variation of diffusion along contours.

L_{eq} as a function of log-pressure height and ϕ_e.

Increased mixing in the summer
lower stratosphere

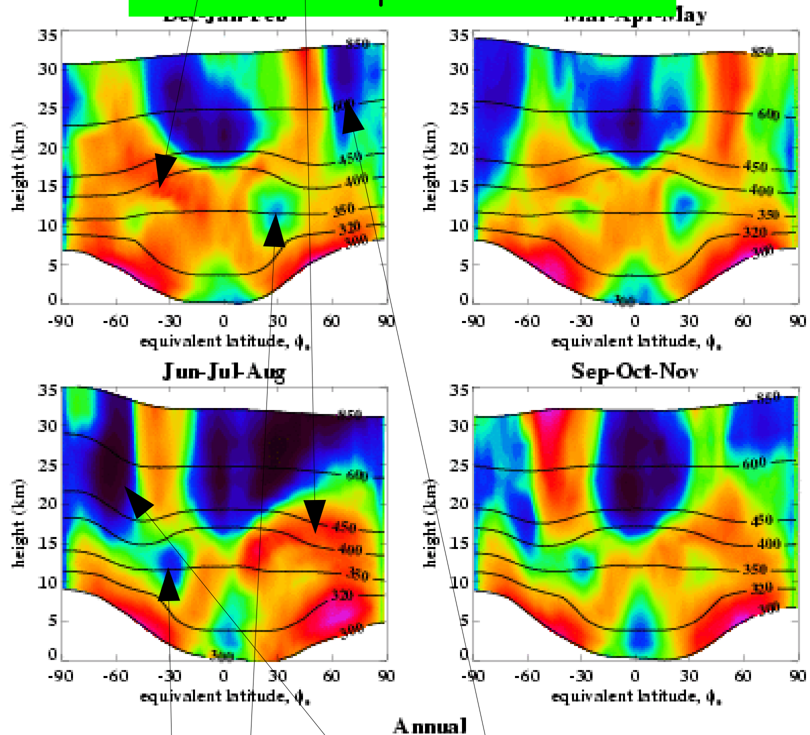

see Haynes and Shuckburgh, 2000, JGR, 105, 22777-22810.

Subtropical jets and polar vortex jets
as minima (barriers) in effective diffusivity

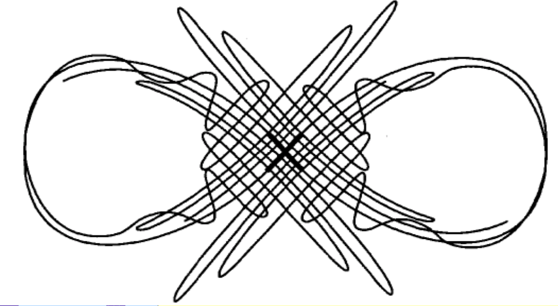

Stretching rate - Lyapunov exponent

Over a time interval $[t_{0,}t_0+\tau]: \delta\mathbf{x}(t_0+\tau)=\mathbf{M}(t_{0,}t_0+\tau)\delta\mathbf{x}(t_0)$ $\nabla\theta(t_0+\tau)=-\mathbf{M}^T(t_{0,}t_0+\tau)\nabla\theta(t_0)$

Finite-time Lyapunov exponent $\lambda(\tau,\mathbf{x}(t_0))=\frac{1}{\tau}\ln\frac{|\mathbf{M}\,\delta\mathbf{x}|}{|\delta\mathbf{x}|}=\frac{1}{\tau}\ln\frac{|\mathbf{M}^T\nabla\theta|}{|\nabla\theta|}$

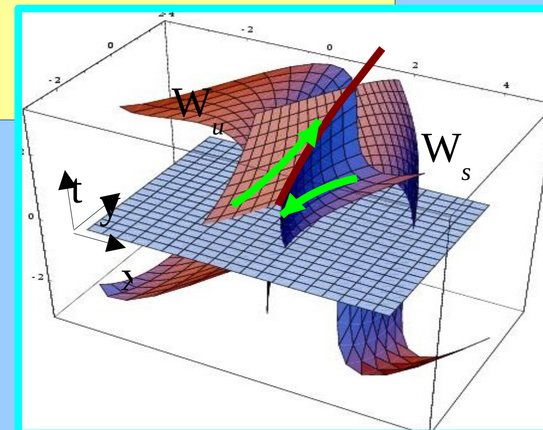

- Finite-time (FTLE) or finite-size (FSLE) Lyapunov exponent measures stretching experienced by a parcel during a time interval.
- Pro: Easily calculated and physically sound. Standard tool in the theory of dynamical systems. Not limited to 2D. Provides maps of dynamical barriers.
- Con: Complicated patterns when short lived structures. Is usually dominated by shear and hence is not a measure of mixing for distributed tracer. Does not correlate with effective diffusivity

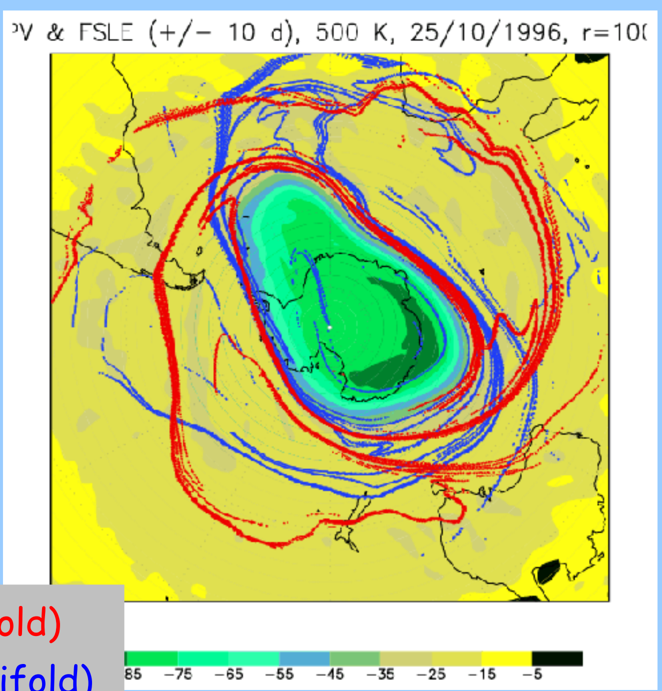

Red: large forward Lyapunov <=> unstable (past) material line (manifold)
Blue: large backward Lyapunov <=> stable (future) material line (manifold)

Gradient amplification

Blob mixing

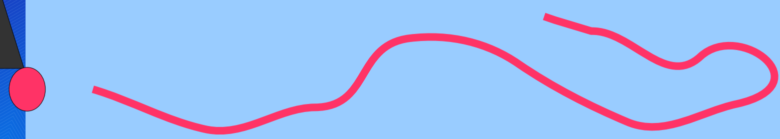

mixing is diagnosed by FTLE/FSLE, either done by

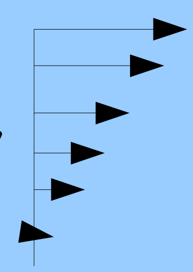

or

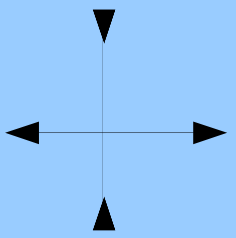

but

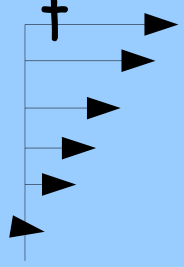

on

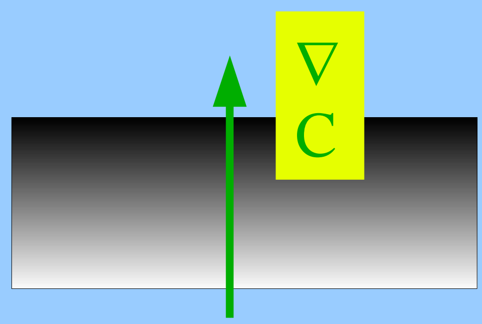

does not change the gradient

Hence, mixing cannot be directly diagnosed by finite-time or finite-size Lyapunov exponent

Assumption: tracer gradient is orthogonal to the local stable material line. (exponential convergence)

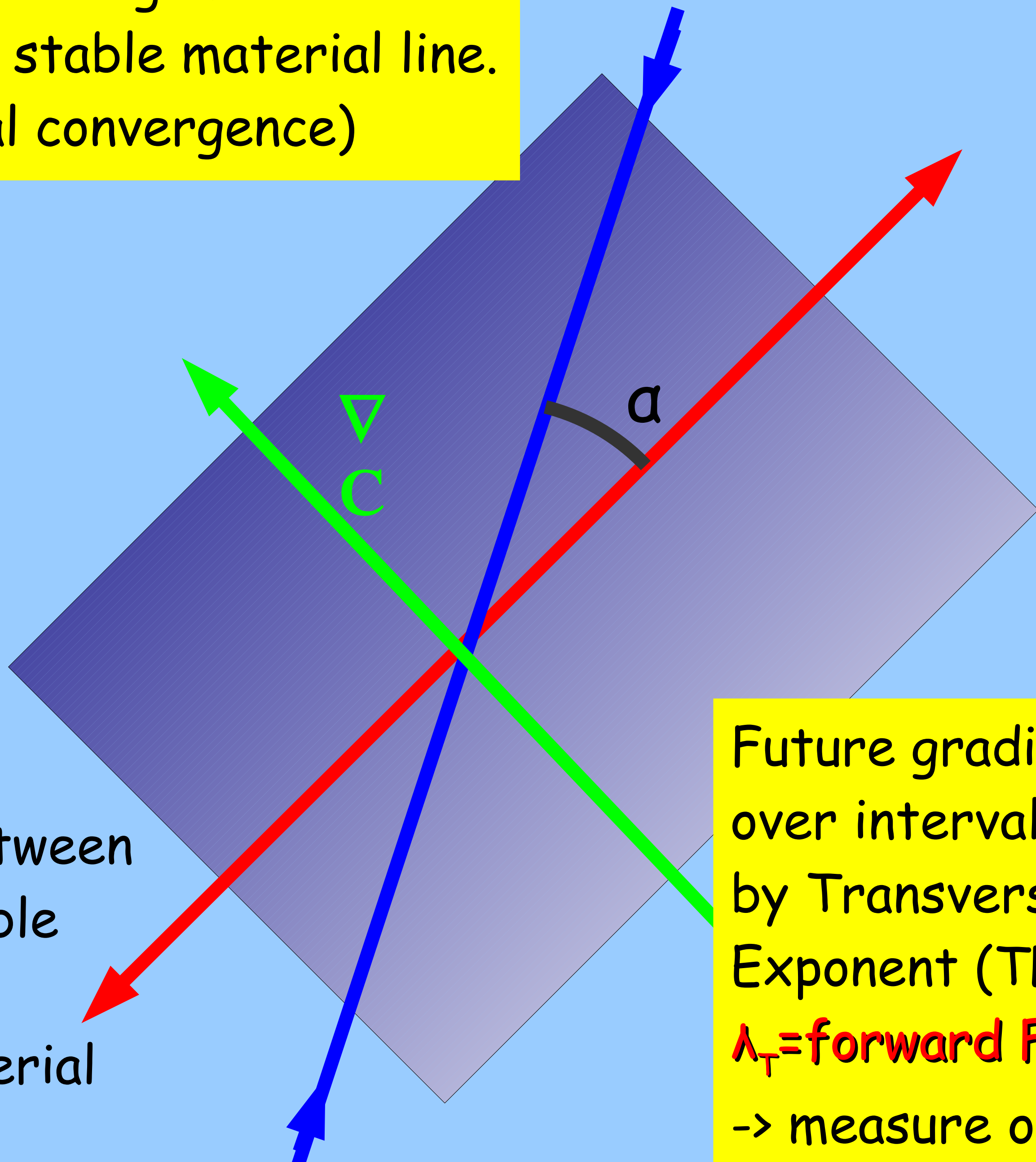

α: angle between local unstable and stable material lines

Future gradient growth over interval t is provided by Transverse Lyapunov Exponent (TLE)

λ_T=forward FTLE x sin(α)

-> measure of mixing (assuming irreversibility)

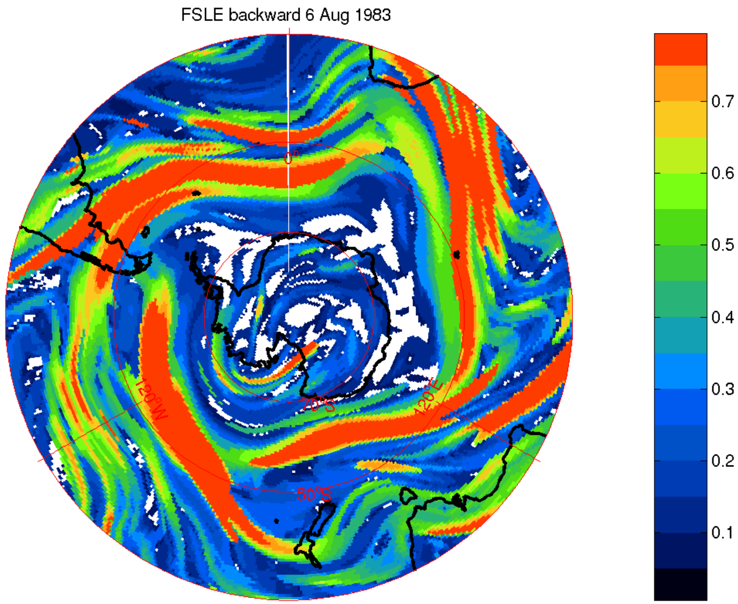

Backward Lyapunov

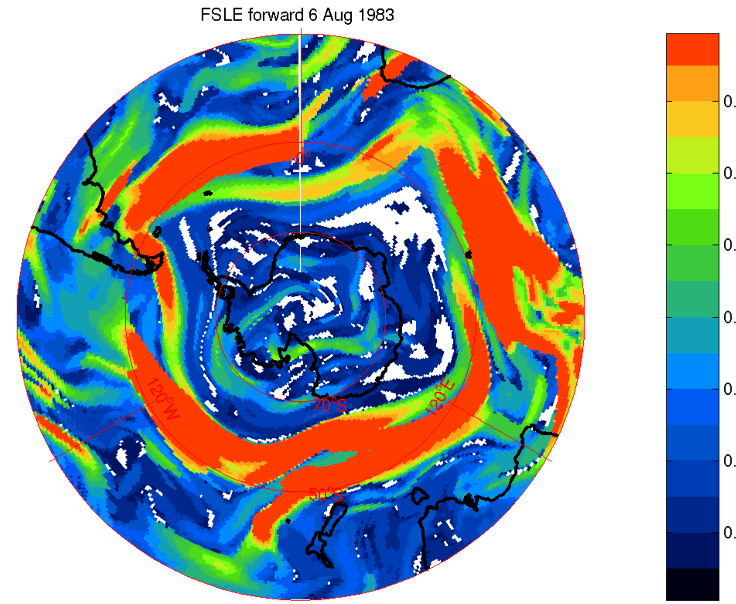

Forward Lyapunov

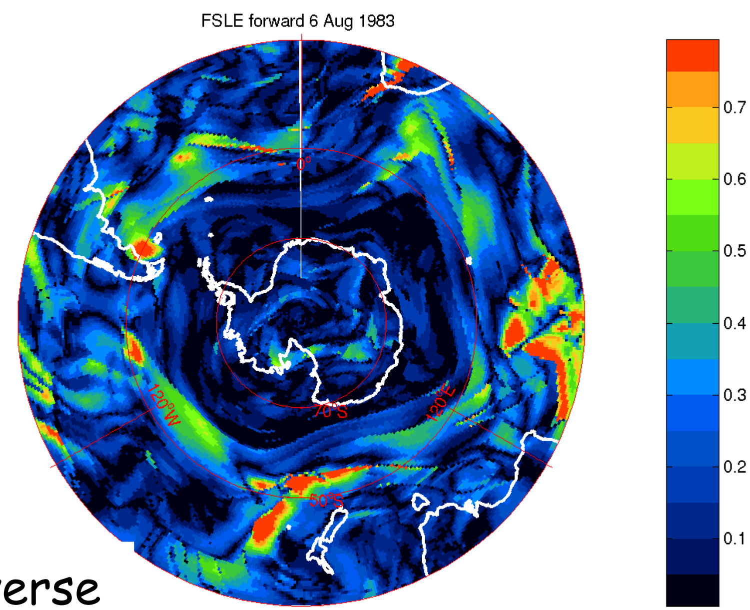

Transverse Lyapunov

Large shear regions where stable and unstable material lines are parallel are expelled from mixing (gradient intensification) which concentrates where stable and unstable material lines are crossing.

Isentropic surface 350K - July 1999

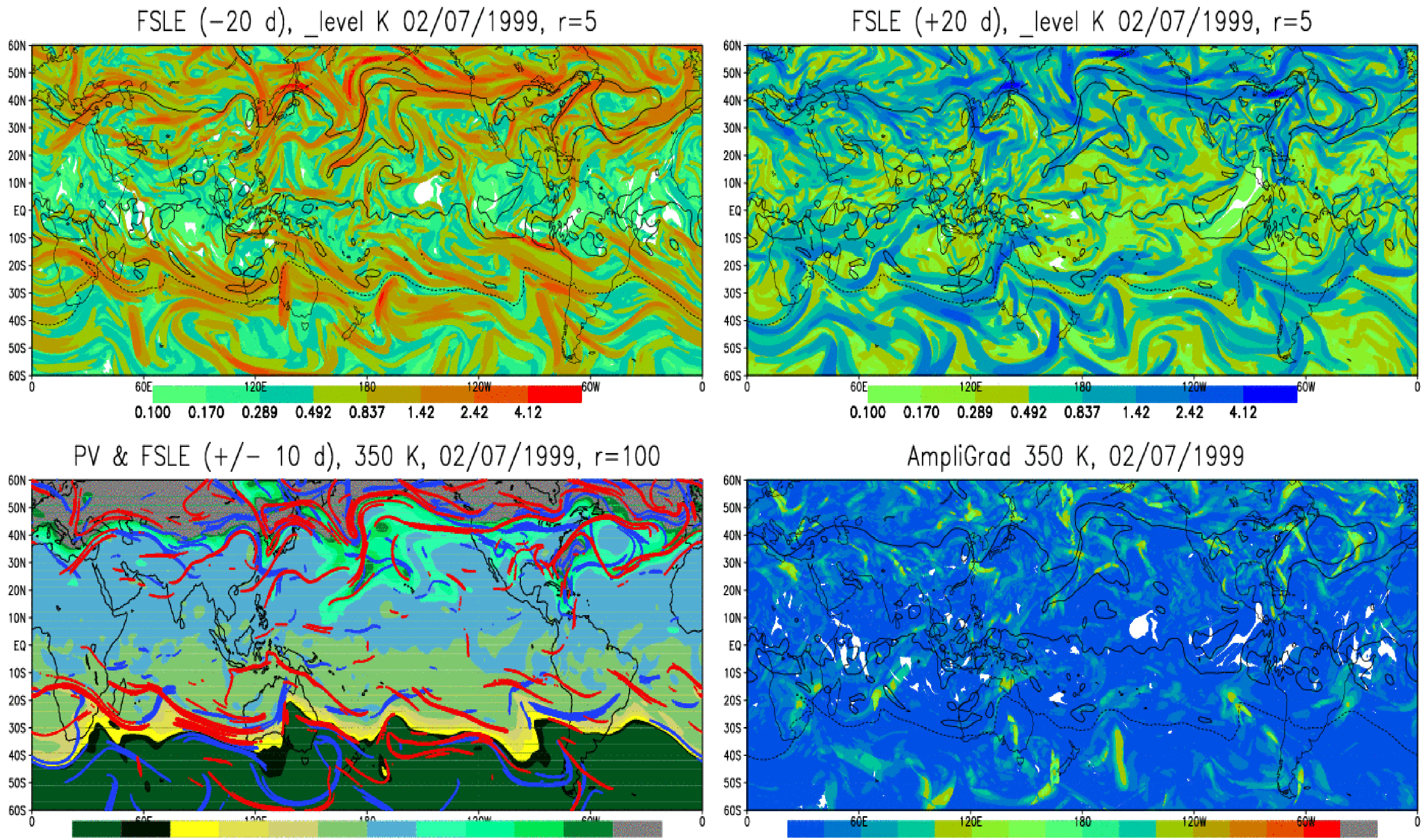

↖ backward Lyapunov exponent (ratio 5) ↗ forward Lyapunov exponent (ratio 5)

↙ backward and forward Lyapunov (ratio 100) + PV ↘ transverse Lyapunov exponent

Isentropic surface 350K: January, average over ERA-40 (1963-2002)

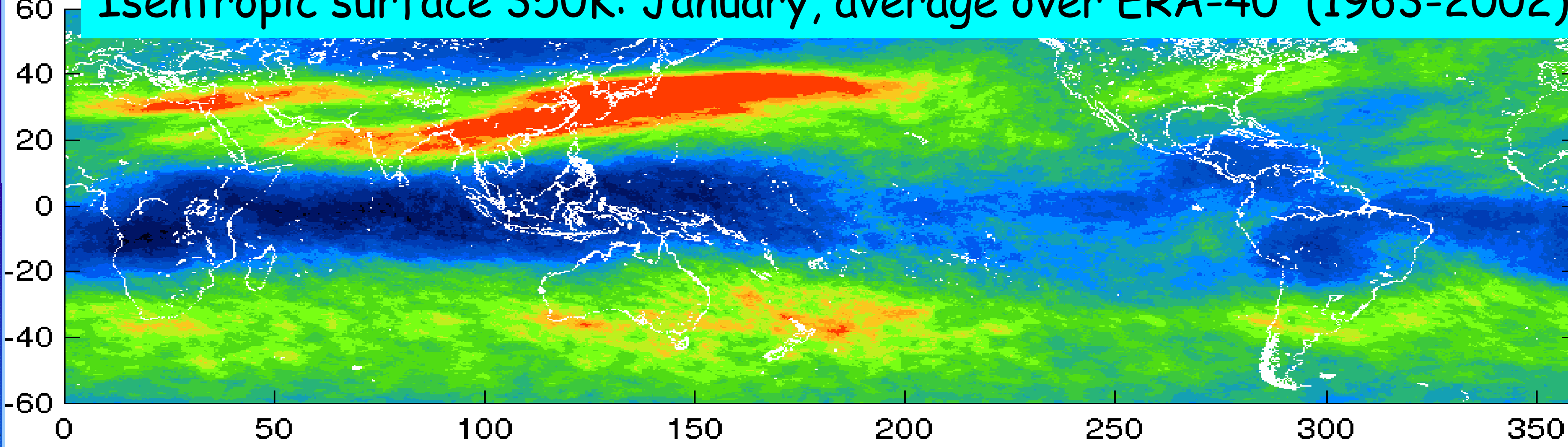

saddle=(forward FSLE x backward FSLE)$^{1/2}$

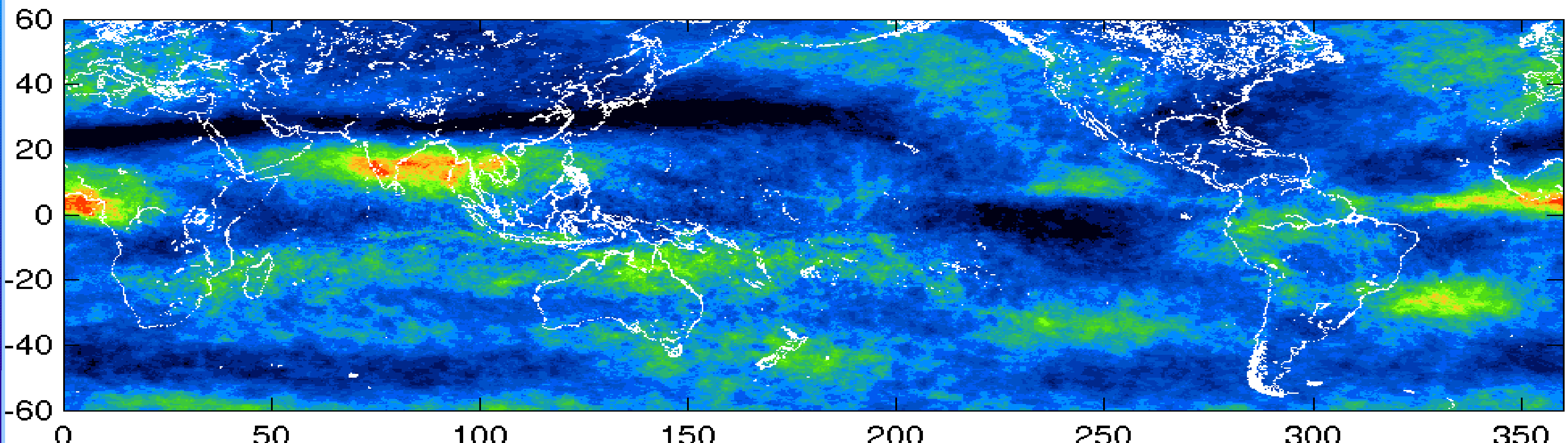

TLE

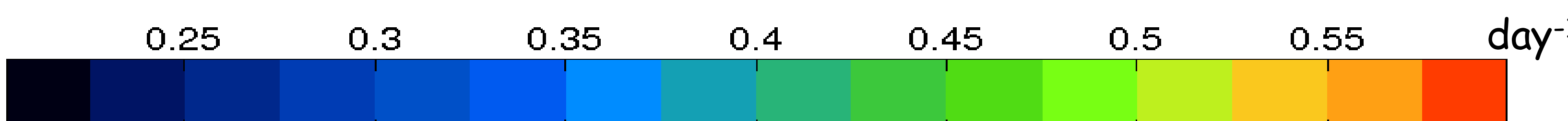

Isentropic surface 350K: January, average over ERA-40 (1963-2002)

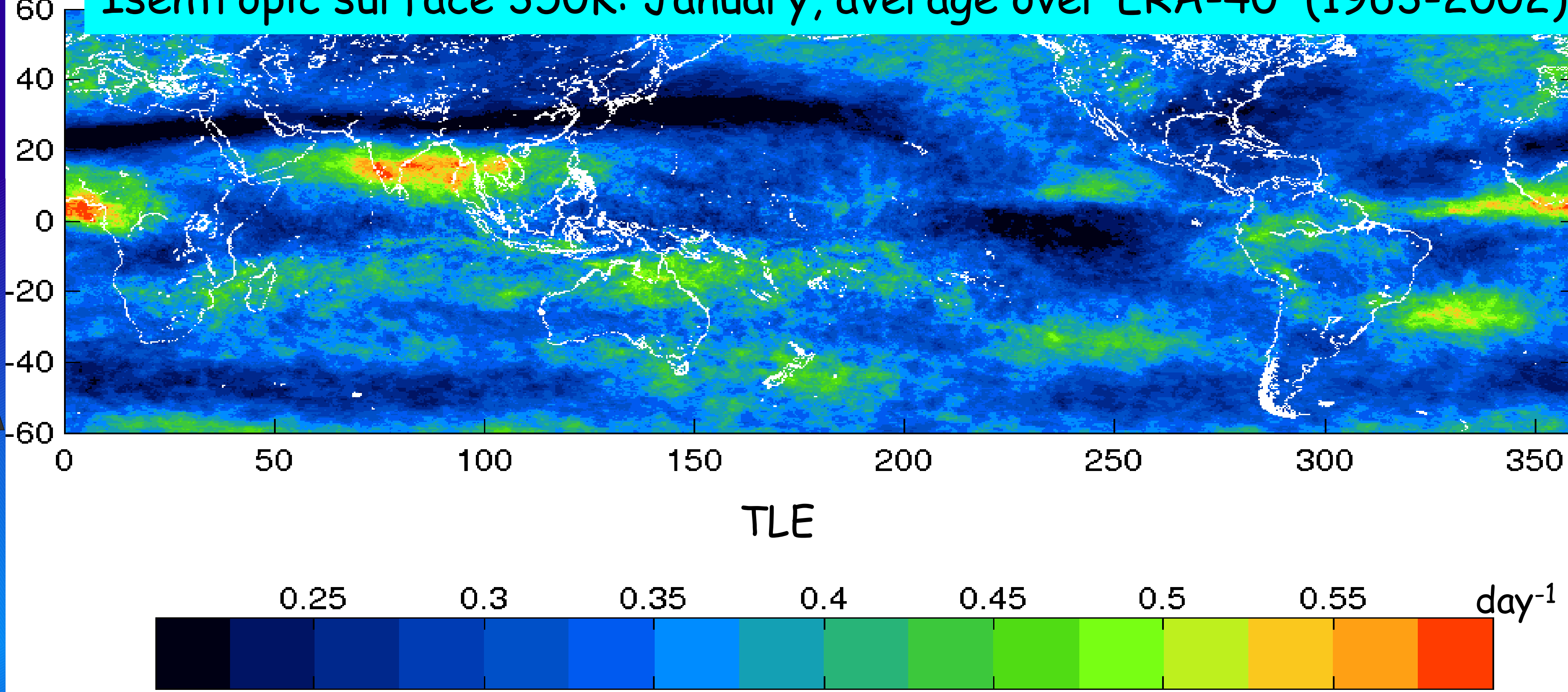

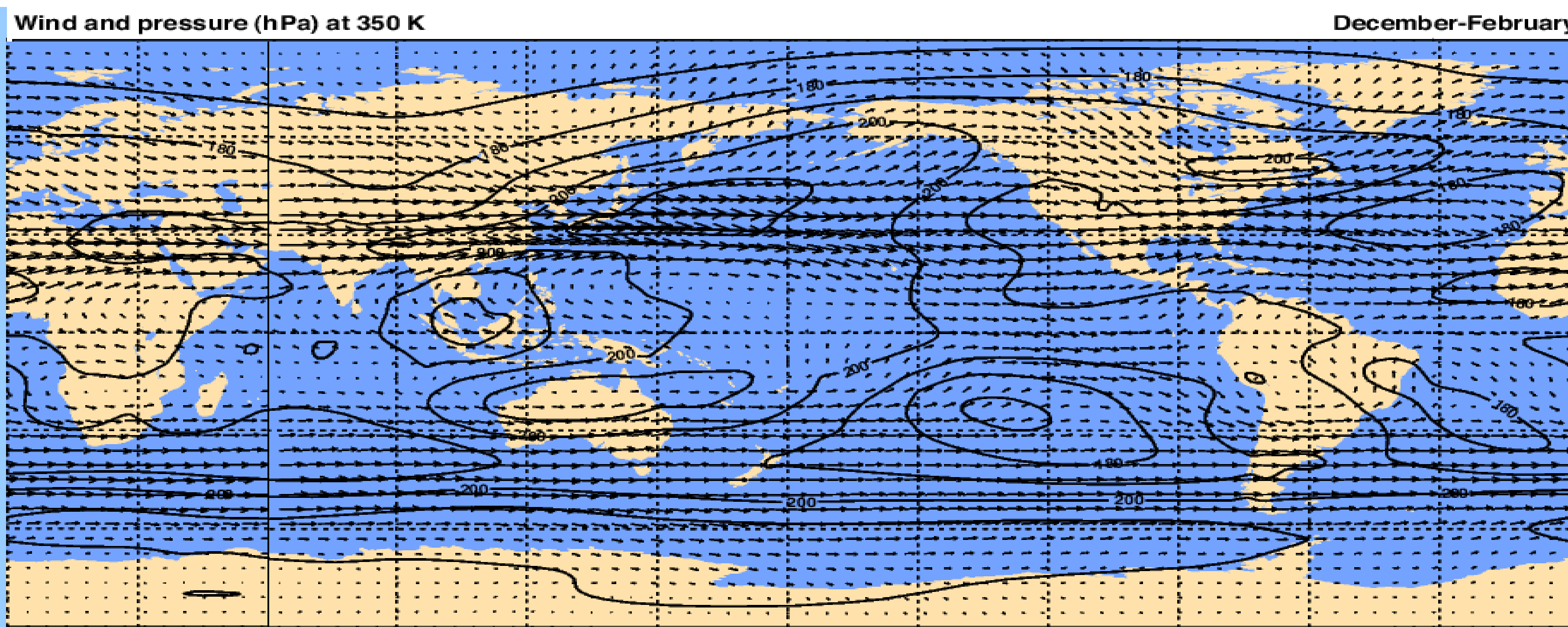

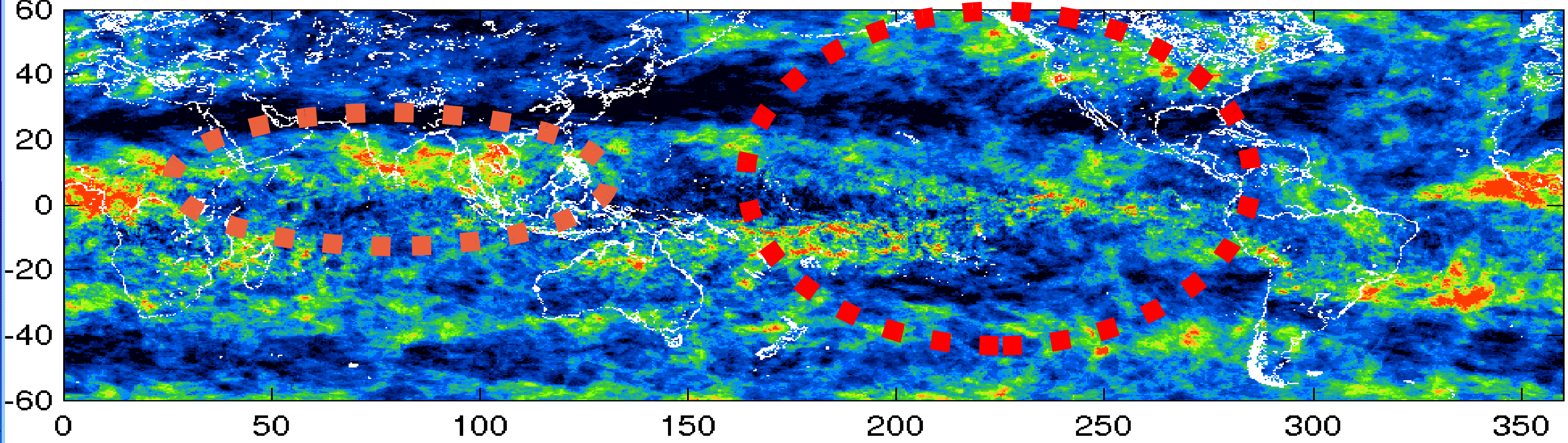

TLE DJF 1997/1998 (El Niño) 350K

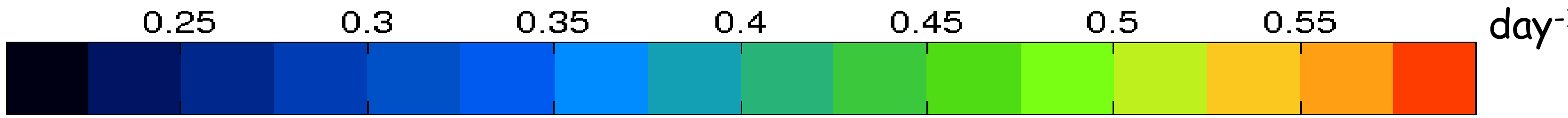

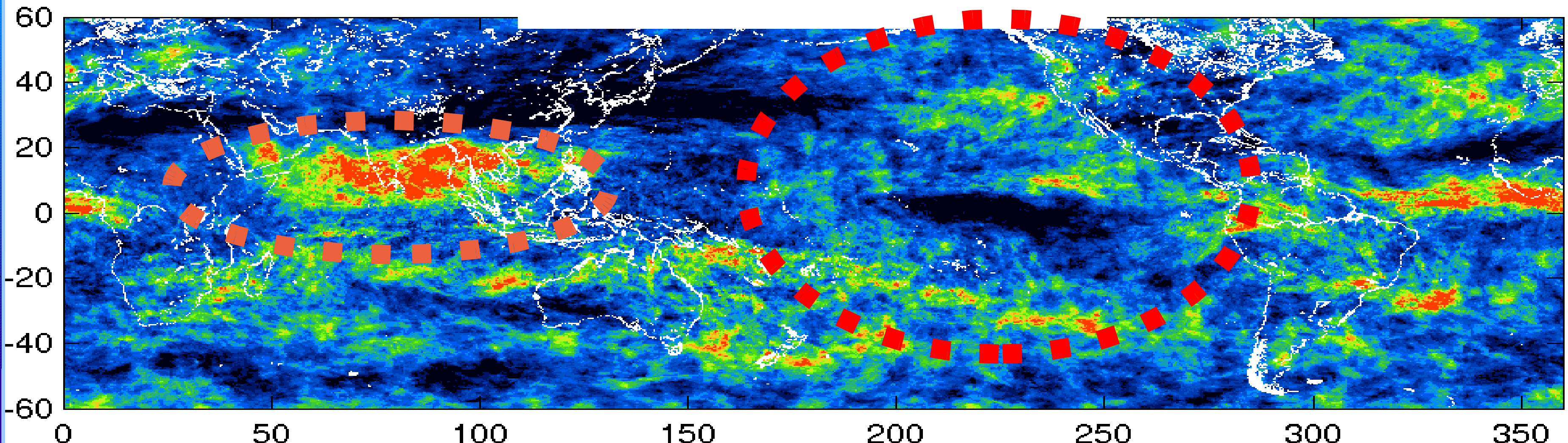

TLE DJF 1998/1999 (normal) 350K

Lyapunov exponent against effective diffusivity

Transverse Lyapunov exponent against effective diffusivity

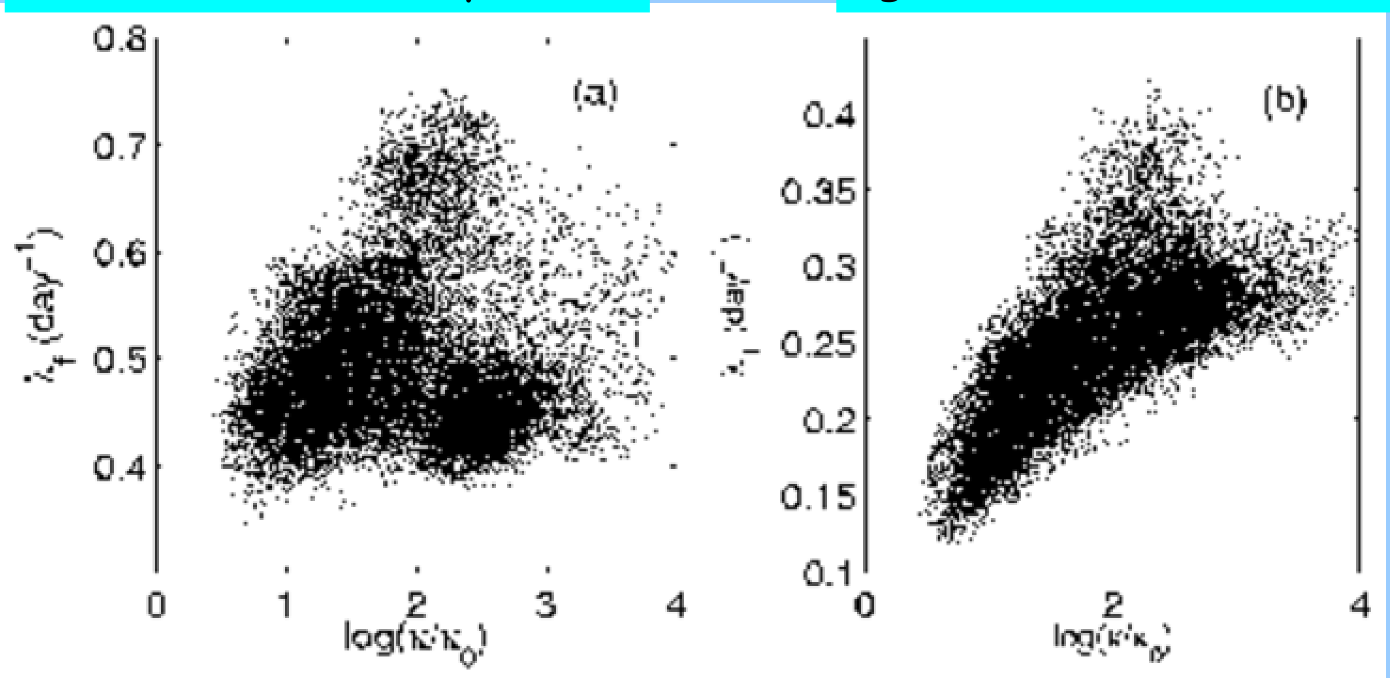

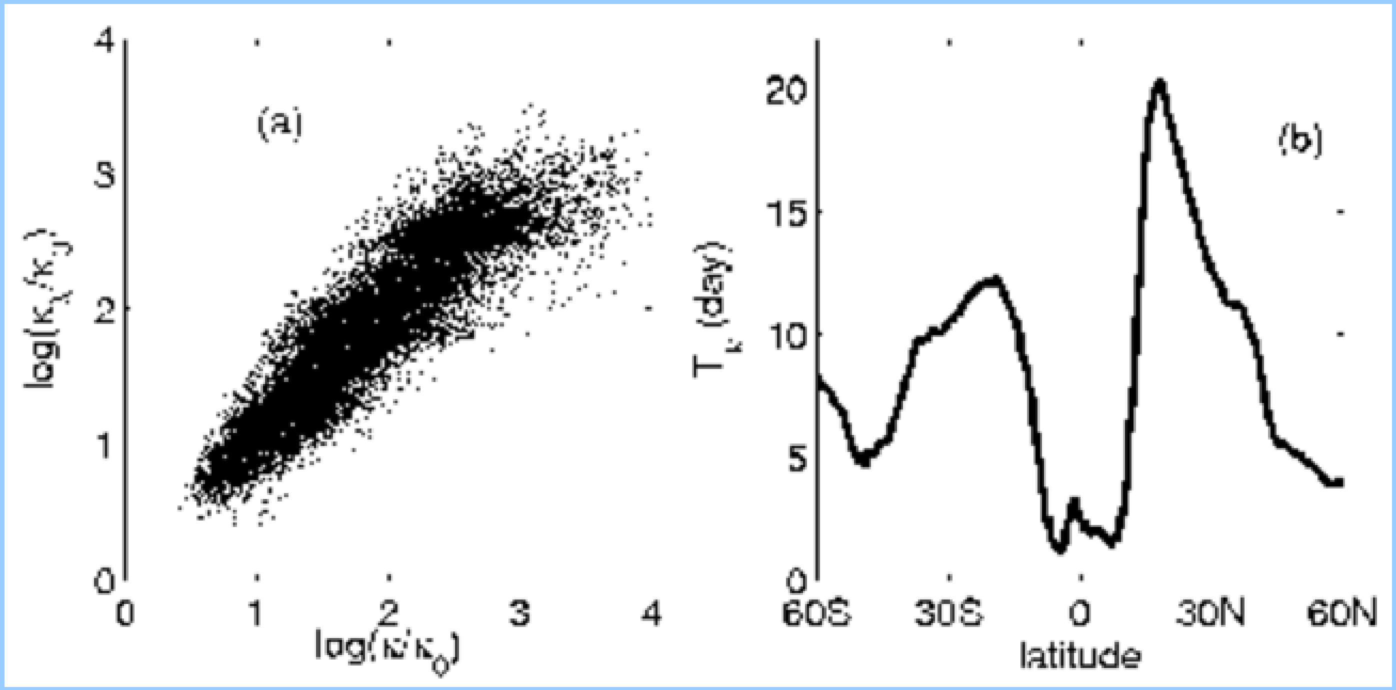

Revised comparison of Lyapunov exponent and effective diffusivity

$$D_{eff} = \kappa_0 \frac{L_{eq}^{\ 2}}{(2\pi a \cos\phi_e)^2}$$

where L_{eq} is approximated by contour length and ϕ_e is the equivalent latitude

$$L_{eq} \approx e^{\lambda_T T_k}$$

where T_k is a characteristic time after which 3-D turbulent diffusion becomes dominant and balances the exponential growth

Hence, the Lyapunov diffusion

$$\log D_\lambda = A + 2 T_k \lambda_T$$

where A and T_k are calculated to match D_{eff}

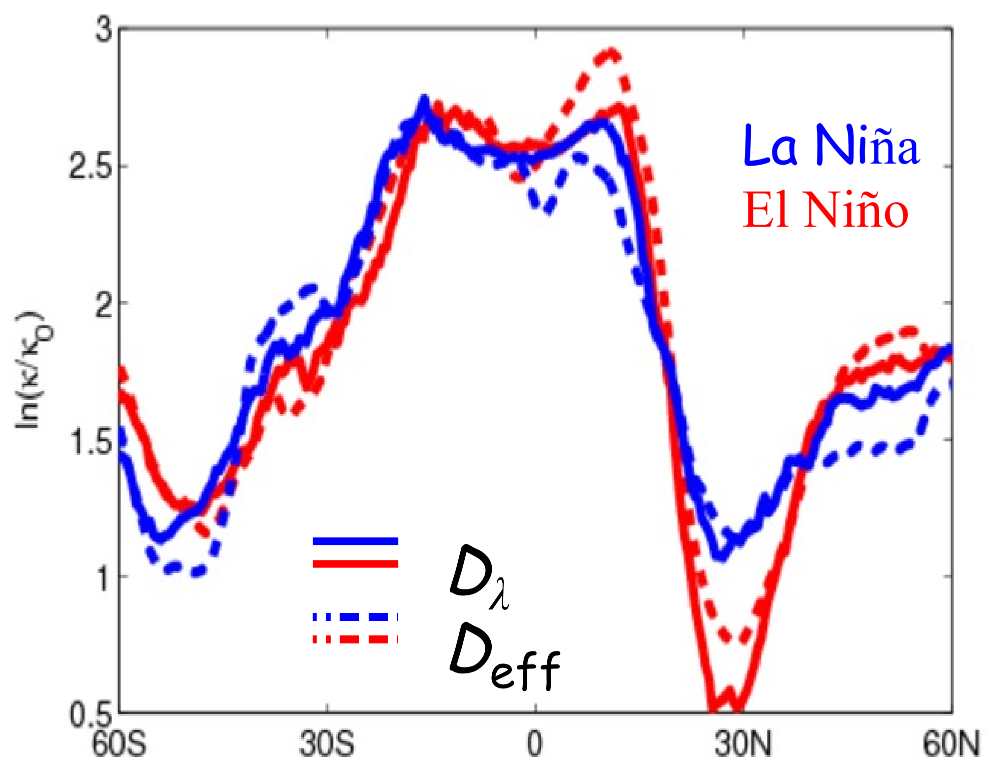

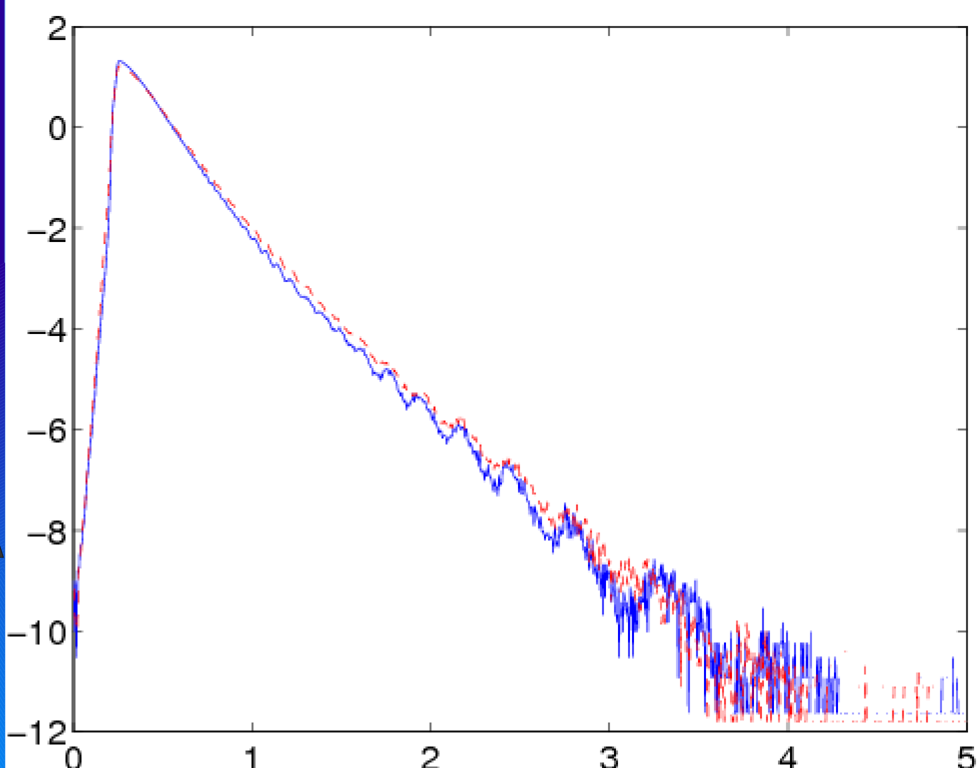

PDF of the FSLE at 350K

Large FSLE are associated
with shear regions that contribute weakly to gradient intensification.

Courtesy of G. Lapeyre

PDF of the angle between the local stable and unstable lines.

Solid blue for all FSLE
Dashed curves for FSLE above a threshold (largest for black curve)

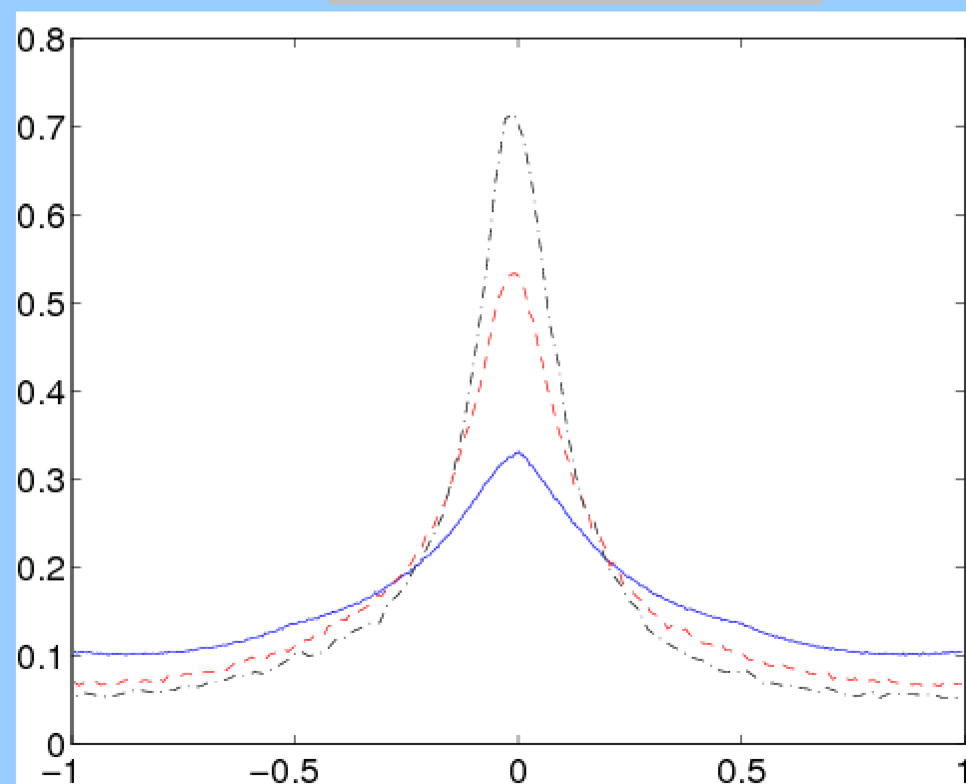

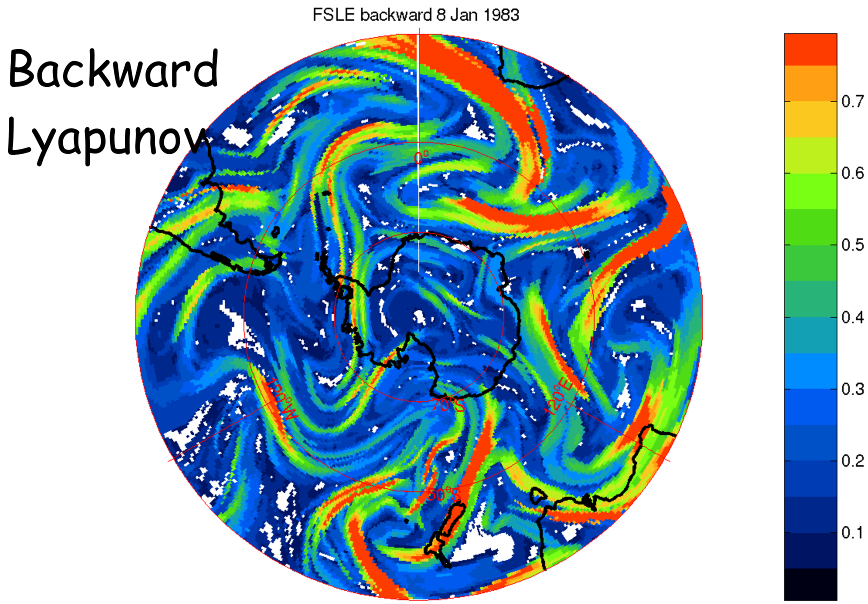

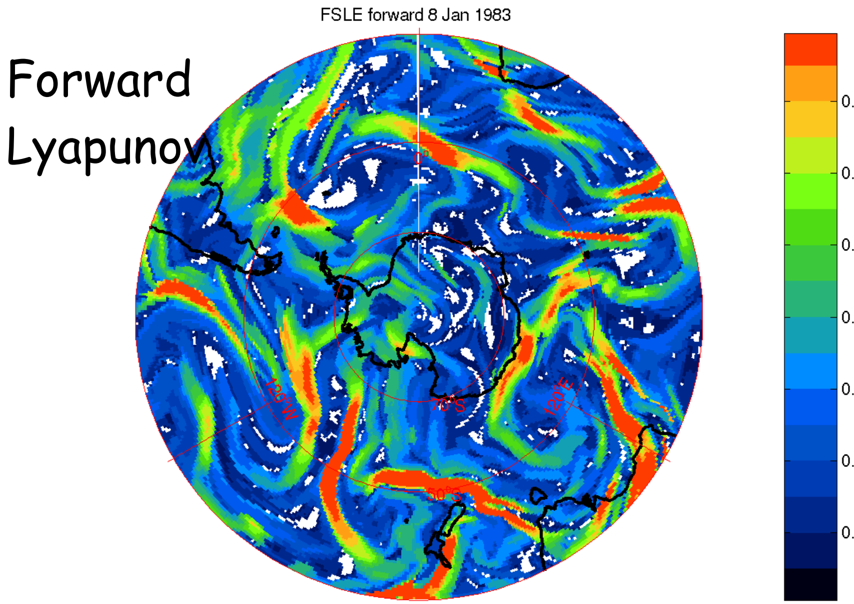

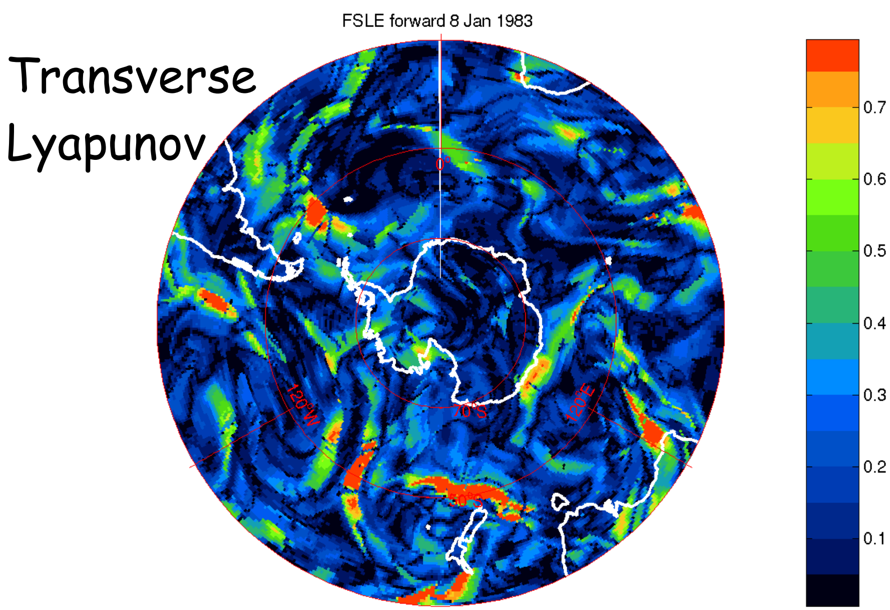

Summer stratospheric mixing in southern hemisphere at 430K

Distance between the stable manifold and the unstable manifold at time τ

$$\Delta\Psi = \underbrace{\int_{-\infty}^{\tau} \epsilon\, g(X_S(t), t-\tau) \times f(X_S(t))\, dt}_{\text{distance } W_U \text{ / separatrix}} - \underbrace{\int_{\infty}^{\tau} \epsilon\, g(X_S(t), t-\tau) \times f(X_S(t))\, dt}_{\text{distance } W_S \text{ / separatrix}}$$

$$\Delta\Psi = \epsilon \int_{-\infty}^{\infty} g(X_S(t), t-\tau) \times f(X_S(t))\, dt$$

The metric distance $M = \dfrac{\Delta\Psi}{\left|\dfrac{\partial\Psi}{\partial n}\right|} = \dfrac{\Delta\Psi}{|f(X_S(\tau))|}$

$M(\tau)=0 \Leftrightarrow X(\tau)$ homoclinic point

width of the stochasticband $\bar{M}$ or $\overline{\Delta\Psi}$

Poincaré map

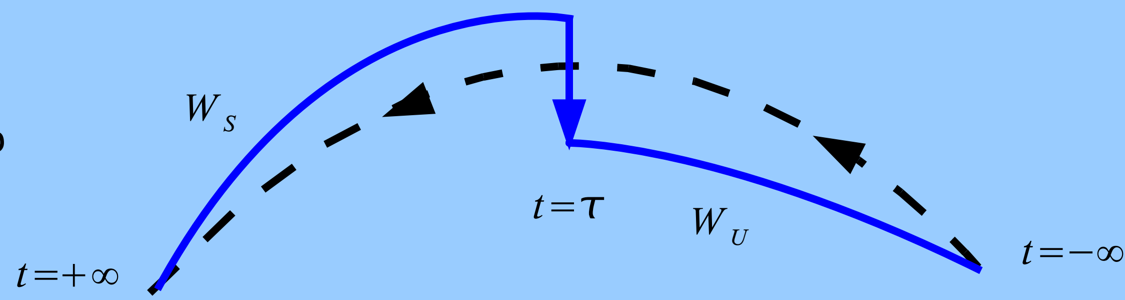

Distance between the stable manifold and the unstable maifold at time τ

$$\Delta\Psi = \underbrace{\int_{-\infty}^{\tau} \epsilon\, g(X_S(t), t-\tau) \times f(X_S(t))\, dt}_{\text{distance } W_U \text{ / separatrix}} - \underbrace{\int_{\infty}^{\tau} \epsilon\, g(X_S(t), t-\tau) \times f(X_S(t))\, dt}_{\text{distance } W_S \text{ / separatrix}}$$

$$\Delta\Psi = \epsilon \int_{-\infty}^{\infty} g(X_S(t), t-\tau) \times f(X_S(t))\, dt$$

The metric distance $M = \dfrac{\Delta\Psi}{\left|\dfrac{\partial\Psi}{\partial n}\right|} = \dfrac{\Delta\Psi}{|f(X_S(\tau))|}$

$M(\tau)=0 \Leftrightarrow X(\tau)$ homoclinic point

width of the stochastic band $\bar{M}$ or $\overline{\Delta\Psi}$